

71 10404  
CR 111097

J-910900-5

Analytical Studies of Start-Up and  
Dynamic Response Characteristics  
of the Nuclear Light Bulb Engine

NASA Contract No. SNPC-70



**CASE FILE**  
**COPY**

**United Aircraft Research Laboratories**

EAST HARTFORD, CONNECTICUT

# United Aircraft Research Laboratories



UNITED AIRCRAFT CORPORATION

EAST HARTFORD, CONNECTICUT

J-910900-5

Analytical Studies of Start-Up and  
Dynamic Response Characteristics  
of the Nuclear Light Bulb Engine

NASA Contract No. SNPC-70

REPORTED BY

Harold E. Bauer  
Harold E. Bauer

Richard J. Rodgers  
Richard J. Rodgers

Thomas S. Latham  
Thomas S. Latham

APPROVED BY

James W. Clark  
James W. Clark, Chief  
Fluid and Systems Dynamics

DATE September 1970

NO. OF PAGES 117

COPY NO. 27



## FOREWORD

An exploratory experimental and theoretical investigation of gaseous nuclear rocket technology is being conducted by the United Aircraft Research Laboratories under Contract SNPC-70 with the joint AEC-NASA Space Nuclear Propulsion Office. The Technical Supervisor of the Contract for NASA is Captain C. E. Franklin (USAF). Results of portions of the investigation conducted during the period between September 16, 1969 and September 15, 1970 are described in the following eight reports (including the present report) which comprise the required first Interim Summary Technical Report under the Contract:

1. Klein, J. F. and W. C. Roman: Results of Experiments to Simulate Radiant Heating of Propellant in a Nuclear Light Bulb Engine Using a D-C Arc Radiant Energy Source. United Aircraft Research Laboratories Report J-910900-1, September 1970.
2. Jaminet, J. F. and A. E. Mensing: Experimental Investigation of Simulated-Fuel Containment in R-F Heated and Unheated Two-Component Vortexes. United Aircraft Research Laboratories Report J-910900-2, September 1970.
3. Vogt, P. G.: Development and Tests of Small Fused Silica Models of Transparent Walls for the Nuclear Light Bulb Engine. United Aircraft Research Laboratories Report J-910900-3, September 1970.
4. Roman, W. C.: Experimental Investigation of a High-Intensity R-F Radiant Energy Source to Simulate the Thermal Environment in a Nuclear Light Bulb Engine. United Aircraft Research Laboratories Report J-910900-4, September 1970.
5. Bauer, H. E., R. J. Rodgers and T. S. Latham: Analytical Studies of Start-Up and Dynamic Response Characteristics of the Nuclear Light Bulb Engine. United Aircraft Research Laboratories Report J-910900-5, September 1970. (present report)
6. Latham, T. S. and H. E. Bauer: Analytical Studies of In-Reactor Tests of a Nuclear Light Bulb Unit Cell. United Aircraft Research Laboratories Report J-910900-6, September 1970.
7. Palma, G. E. and R. M. Gagosz: Optical Absorption in Transparent Materials During 1.5 Mev Electron Irradiation. United Aircraft Research Laboratories Report J-990929-1, September 1970.
8. Krascella, N. L.: Analytical Study of the Spectral Radiant Flux Emitted from the Fuel Region of a Nuclear Light Bulb Engine. United Aircraft Research Laboratories Report J-910904-1, September 1970.

Report J-910900-5

Analytical Studies of Start-Up and Dynamic Response

Characteristics of the Nuclear Light Bulb Engine

TABLE OF CONTENTS

	<u>Page</u>
SUMMARY. . . . .	1
RESULTS AND CONCLUSIONS. . . . .	3
INTRODUCTION . . . . .	6
NUCLEAR LIGHT BULB ENGINE DESIGN . . . . .	7
Basic Reference Engine. . . . .	7
Modifications to Reference Engine . . . . .	9
ENGINE START-UP INVESTIGATION. . . . .	10
Modifications to Start-Up Simulation Model. . . . .	10
Start-Up Control System Concept . . . . .	12
Start-Up Characteristics Assuming Ideal Control System. . . . .	16
Pressure, Temperature, Propellant Flow Rate, and Nozzle Area Profiles. . . . .	16
Nuclear Characteristics. . . . .	17
Expected Dynamic Behavior During Start-Up with Control System . . . . .	19
Fuel Injection System . . . . .	20
ENGINE DYNAMICS INVESTIGATION. . . . .	21
Engine Dynamics Simulation Models . . . . .	21
Thermal and Fluid Dynamics Model . . . . .	21
Neutron Kinetics Model . . . . .	29
Dynamic Characteristics of Uncontrolled Engine. . . . .	31
Effects of Changes in Fuel Injection Area and Pressure Differential. . . . .	32
Effects of Changes in Average Fuel Residence Time. . . . .	33
Effects of Changes in Acoustic Lag Time in Fuel Cycle Circuit. . . . .	33

## TABLE OF CONTENTS (Continued)

Page

Control Methods Investigated. . . . .	34
Reactor Period Control . . . . .	35
Neutron Flux Level Control . . . . .	35
Transfer Volume Pressure Balance Control . . . . .	36
Secondary Control System . . . . .	36
Scram Mechanisms . . . . .	37
Dynamic Characteristics of Controlled Engine. . . . .	37
Effects of Positive Step Changes in Imposed Reactivity and Fuel Control Valve Area . . . . .	37
Effects of Negative Step Changes in Imposed Reactivity and Fuel Control Valve Area . . . . .	40
Effects of Perturbations in Turbopump Wheel Speed, Fuel Region Radius and Exhaust Nozzle Area . . . . .	40
Effects of Changes in Control System Parameters. . . . .	41
Response of Engine to Activated Scram . . . . .	41
Transfer Volume Requirements. . . . .	41
Analysis of Possible Variations in Steady-State Operating Temperatures. .	43
REFERENCES . . . . .	46
LIST OF SYMBOLS. . . . .	49
APPENDIX A - COMPARISON OF CALCULATED CRITICAL MASSES WITH RESULTS OF GE-IDAHO EXPERIMENTS. . . . .	55
APPENDIX B - SPACE RADIATOR PARAMETRIC STUDIES . . . . .	57
APPENDIX C - ALTERNATE CONFIGURATION FOR NUCLEAR LIGHT BULB ENGINE . . . . .	59
TABLES . . . . .	61
FIGURES. . . . .	76

Analytical Studies of Start-Up and Dynamic Response

Characteristics of the Nuclear Light Bulb Engine

SUMMARY

Analytical studies were conducted to evaluate systems for control of the reference nuclear light bulb engine during start-up and at nominal full-power operating conditions. Analytical models of the control systems were incorporated in the digital computer simulation programs developed previously to determine operating conditions of the reference engine during start-up and the transient response of the engine to various perturbations at the nominal full-power operating level.

Additional analyses were conducted (1) to determine the effects of off-design flow fluctuations and fabrication tolerances on the operating conditions of the reference engine, (2) to compare critical mass calculations with results of experiments on a seven-module cavity reactor, (3) to determine the design parameters such as radiator materials and operating temperatures and pressures for a space radiator to reject a portion of the moderator heat load, and (4) to investigate the design characteristics and performance of an alternate nuclear light bulb engine configuration employing unit cells of smaller diameter than those envisioned for the reference engine.

Start-up is divided into two phases. The first phase requires about 80 sec (1) to bring the turbopump up to operating speed, (2) to pressurize the engine to an initial condition required to achieve containment of a critical mass (20 atm or greater), (3) to initiate flow in all circuits, (4) to start fuel injection to obtain cold critical mass, and (5) to stabilize engine at 0.1 percent of full power. The second phase consists of a start-up ramp in power from 0.1 to 100 percent of full-power operation. In studies to date, no limitation has been found which would prevent the use of start-up times for the second phase as short as 6 sec using a linear ramp in fuel temperature. Neutron detectors are employed to sense absolute power level and the rate-of-change of power level during both phases of start-up. Control signals from the neutron sensors are used to adjust fuel injection rate such that the desired start-up power profile is produced. During the second phase of start-up,

propellant, coolant, and buffer gas flow rates and exhaust nozzle flow area are also controlled by signals from the neutron detectors which measure absolute power level. The variation of the exhaust nozzle flow area is the primary means of establishing the desired pressure profile during start-up. Small pressure differentials within the engine are controlled by transfer chambers which allow rapid transfer of gases between regions of slightly different pressures.

The UNIVAC 1108 digital computer simulation program for the reference engine, which includes analytical models of the thermal and flow dynamics of the nuclear fuel, buffer gas, coolant, and propellant loops and their coupling to the neutron kinetics equations, was expanded (1) to include simulation of systems for controlling the engine during perturbations near full-power operating conditions and (2) to incorporate the simulation of transfer chambers added to the reference engine design to minimize pressure differentials across the transparent structure during power perturbations. Control of the engine was achieved by varying fuel injection control valve area (hence, fuel injection rate) based upon signals from neutron detectors which sense absolute power level and the rate-of-change of power level. It was concluded that satisfactory control of the engine can be achieved during full-power operation on the basis of calculated responses of the controlled engine to perturbations in reactivity, fuel injection rate, exhaust nozzle flow area, turbopump wheel speed, and fuel region radius. Pressure differentials across the transparent structure for the power perturbations analyzed were limited to less than 1 lb/in.<sup>2</sup> by the transfer chamber pressure equalization system.

The study also indicated the desirability of additional work in certain areas. Continued analysis of the start-up characteristics should be made to incorporate the variations in reactivity coefficients and evaluate engine stability during start-up. Further analysis should also be directed toward determining the factors which impose an absolute lower limit on the time required for both phases of start-up. The sensitivity of engine response to variations in fuel injection system acoustic lags and pressure fluctuations indicates that the design and response characteristics of the fuel injection system should be analyzed in greater detail and the results incorporated in the dynamics simulation program. In addition, engine shutdown should be investigated to determine the engine performance and control requirements during both a slow shutdown and an emergency shutdown. Analyses of shutdown procedures should be extended to include investigations of afterheat removal requirements and activity levels in the engine after shutdown. The activation analysis could be used to determine the reusability of the engine by determining the accessibility of the engine after shutdown.

## RESULTS AND CONCLUSIONS

1. A start-up mode which provides a linear change in average fuel temperature with time reduces the maximum rate of increase in temperature and pressure during start-up relative to linear power start-up ramps. The rate of change of average fuel temperature for a 6-sec linear fuel temperature ramp is 7500 deg R/sec compared with a maximum value of 10,000 deg R/sec for a 60-sec linear power start-up ramp.

2. Pressure differentials across the transparent walls may be minimized by use of a transfer volume connected to the propellant and vortex regions. Pressure differences between these regions displace a diaphragm in the transfer volume and cancel any pressure differential by transferring the required volume of gas from the high-pressure region to the low-pressure region. The diaphragm provides a positive barrier to eliminate the possibility of fuel leaving the vortex region and entering the propellant region.

3. The maximum rate of change of pressure during start-up for which pressure equalization across the transparent walls could be maintained for a transfer volume of 4.5 ft<sup>3</sup> was calculated to be 100 atm/sec. The rate of change of pressure for a 6-sec linear fuel temperature start-up ramp is below this limit.

4. It was determined that the form of fuel most desirable for injection into the vortex region during start-up and full-power operation would be uranium dust transported by a carrier gas unless, during start-up, it is impossible to prevent centrifuging of particles or liquid droplets to the transparent walls during the time required to vaporize the nuclear fuel. In that case, UF<sub>6</sub> should be employed during phase I and the initial part of phase II of start-up. During full-power operation, buffer-gas bypass flow which serves to cool the spent fuel and vortex buffer gas as it enters the thru-flow ports should be regulated to cool the uranium rapidly to temperatures well below its melting point of 2600 R. Investigation of the thru-flow duct wall geometry and selection of flow conditions required to minimize deposition of condensed fuel on the duct walls should be the objective of an experimental test program.

5. The critical mass of U-233 varies during linear fuel temperature start-up ramps from 27.1 lb at zero-power conditions to peak values of 37.1 and 34.2 lb at the end of the 6-sec and 60-sec start-up ramps, respectively. After reaching the peak values, the critical mass requirements decrease slowly to the full-power value of 30.9 lb when the bulk moderator materials (BeO and graphite) reach their full-power operating temperatures about 200-300 sec after initiation of the start-up ramps. Critical mass of U-233 during the 60-sec linear power start-up ramp varies from 18.6 lb at zero power conditions to 28.2 lb at the end of the start-up ramp, and then

approaches 30.9 lb asymptotically as the bulk moderator materials heat up. The peaking of critical mass during linear fuel temperature start-ups causes the reference design fuel containment limits to be exceeded. These peaks can be eliminated by lowering the initial-condition pressure for phase II of start-up to a value approaching the 20 atm employed for the 60-sec linear power start-up ramp.

6. Satisfactory control of the engine can be achieved by varying fuel injection control valve area (hence, fuel injection rate) based upon signals from neutron detectors which sense absolute power level and rate-of-change of power level. Typical responses of the controlled engine to various perturbations in reactivity, fuel injection rate, thrust nozzle flow area, turbopump wheel speed, and fuel region radius are in the form of rapid oscillations in power which are rapidly damped and either converge to a new steady state value or vary, with a long period, between the control limits.

7. Pressure differentials across the transparent structure for the power perturbations analyzed were limited to less than 1 psi by a transfer chamber pressure equalization system of 7.6 ft<sup>3</sup> in volume employing a diaphragm 0.005 in. in thickness.

8. The analysis of temperature variations from the nominal design values due to local variations in heat deposition, coolant flow rates and dimensional tolerances indicated that it may be necessary to reduce the nominal operating temperatures in some components in order to reduce the probability of exceeding the maximum allowable temperature in the components. In particular, the nominal value of the peak temperature in the transparent structure is calculated to be 2490 R which is only 80 R below the maximum allowable material temperature of 2570 R. The statistical analysis of the assumed variations in nominal operating temperatures indicates that the probability of exceeding 2570 R in this component is approximately 50 percent. This probability of exceeding the maximum allowable temperature of 2570 R may be reduced to the order of 0.0001 by either reducing the nominal operating temperature to 2250 R or by reducing the possible variations in temperature by improving the tolerances on structural dimensions.

9. Critical masses were calculated which were 11 to 16 percent less than values measured in GE-Idaho experiments with a seven-module cavity reactor fueled with U-233 and employing heavy-water moderator material. Fuel and hydrogen reactivity worths for the seven-module reactor were also calculated to within 15 to 20 percent of the measured values. The calculations were made using a one-dimensional neutron transport theory analysis in spherical geometry.

10. Studies of weight-optimized space radiators indicated that the total radiator weight required to reject a given amount of heat from the engine varies considerably with the operating temperature levels in the radiator. Minimum radiator weights were obtained for tungsten radiators operating between 2000 and 3500 R, with estimates of a 1000 lb radiator weight to reject 1 percent of the total engine power (i.e., to reject 46 megw).

11. Preliminary analysis indicated that an alternate nuclear light bulb engine configuration in which the diameter of the unit cell was reduced (hence, the number of cells per engine was increased) would have the advantages of higher allowable bursting and collapsing pressures across the transparent walls and of being of a size which might be more easily tested full-scale in a nuclear reactor. These advantages would result with a slight reduction in engine performance. For example, an engine employing 37 unit cells, 7.4 in. in average diameter, would have a specific impulse of 1760 sec and allowable bursting and collapsing pressures across the transparent walls of 6.9 and 7.4 atm, respectively, compared with values of 1870 sec, and 1.0 and 0.1 atm for the reference engine. However, since the transfer volume in the reference engine appears to limit the pressure differences to acceptable values, a change in the reference engine to a 37-cell configuration is not recommended at the present time.



## INTRODUCTION

Investigations of various phases of gaseous nuclear rocket technology are being conducted at the United Aircraft Research Laboratories under Contract SNPC-70 administered by the joint AEC-NASA Space Nuclear Propulsion Office. Previous investigations were conducted under NASA Contracts NASw-847, NASw-768, and NAS3-3382; under Air Force Contracts AF 04(611)-7448 and AF 04(611)-8189; and under Corporate sponsorship.

The principal research effort is presently directed toward the closed-cycle, vortex-stabilized nuclear light bulb engine. As discussed subsequently, this engine concept is based on the transfer of energy by thermal radiation from gaseous fissioning uranium, through a transparent wall, to hydrogen propellant. The basic design of this engine is described in detail in Ref. 1. Subsequent investigations which were performed to supplement and investigate the basic design and to investigate other phases of nuclear light bulb engine component development are reported in Refs. 2 through 9. Reference 10 includes a summary of pertinent nuclear light bulb research conducted through November 1969.

The majority of work performed prior to 1969 was concerned with the design and operating characteristics of the nuclear light bulb engine operating at full-power, steady-state conditions. During the 1969 contract period, a digital computer simulation model was formulated for the purpose of investigating the transient response of the reference engine to perturbations about the full-power, steady-state design condition. This engine dynamics model is described in detail in Ref. 2. In addition to the dynamic response studies, preliminary investigations of engine start-up procedures and operating conditions during start-up were performed. These investigations were all based on the reference engine design described in Ref. 1 with modifications which evolved subsequently.

The objectives of the research described in the present report were (1) to investigate further the transient operating conditions during reactor start-up, with particular emphasis on determining the form of fuel most appropriate for start-up and on formulating a control system concept that could be employed, (2) to refine the engine dynamics simulation program to include the most recent modifications to the reference design and to investigate the effects of various types of control systems on the dynamic response of the engine, and (3) to conduct preliminary studies of the effects of off-design performance of engine components and design tolerances on engine dynamic characteristics.

## NUCLEAR LIGHT BULB ENGINE DESIGN

### Basic Reference Engine

The reference nuclear light bulb engine design which has resulted from previous studies has the following characteristics:

1. Cavity configuration --- seven separate, 6-ft-long cavities having a total overall volume of 170 ft<sup>3</sup>.
2. Cavity pressure --- 500 atm.
3. Specific impulse --- 1870 sec.
4. Total propellant flow (including seed and nozzle transpiration coolant flow) --- 49.3 lb/sec.
5. Thrust --- 92,000 lb.
6. Engine power --- 4600 megw.
7. Engine weight --- 70,000 lb.
8. Ratio of average density in fuel-containment region to neon density at edge of fuel --- 0.7.
9. Equivalent axial-flow Reynolds number in neon vortex --- 5500.

The reference engine offers the potential of a specific impulse more than twice that of solid-core nuclear rockets and more than four times that of chemical rockets. Studies are underway to determine whether still higher specific impulses are obtainable with the nuclear light bulb type of engine.

Sketches illustrating the principle of operation of the engine are shown in Fig. 1. Energy is transferred by thermal radiation from gaseous nuclear fuel contained in a neon vortex (Fig. 1(b)) to hydrogen propellant seeded with tungsten particles to increase its opacity. The vortex and propellant regions are separated by an internally cooled fused silica transparent wall. A seven-cavity configuration (Fig. 1(a)) is employed in the reference engine, rather than one large single cavity, to increase the total surface radiating area at the edge of the fuel for a given total cavity volume.

A schematic diagram of the current engine flow circuits is shown in Fig. 2. Neon is injected from the transparent wall to drive the vortex, passes axially toward the end walls, and is removed through ports at the center of one or both end walls (Fig. 1(b)). The neon discharging from the cavity, along with any entrained fuel and fission products, is cooled in the fuel cycle circuit (Fig. 2) by mixing with low-temperature neon, thus causing condensation of the nuclear fuel to liquid or solid form. The condensed fuel is centrifugally separated from the neon and pumped back to the vortex region through the fuel injection circuit. The neon is further cooled by rejecting heat to the primary hydrogen propellant, and is then pumped back to drive the vortex. The temperatures at key points in the flow circuits are shown in parentheses in Fig. 2.

The seven cavities are surrounded by a beryllium oxide moderator region (Fig. 1(a)) which fills the interstitial regions. The beryllium oxide region is surrounded by an annular graphite moderator region. These two axial moderator regions are separated by an internally cooled beryllium flow divider which separates the flow in the two regions. The moderator is supported by 24 beryllium tie rods which pass through the moderator regions. In addition to the axial moderator regions, there are upper and lower end-moderator regions which form the ends of the cavity. These end-moderator regions consist of a beryllium oxide region, which is adjacent to the cavity end walls, and a graphite region. The heat deposited in the moderator by neutron and gamma ray heating and the heat transferred to the moderator and structure by conduction, convection, and radiation is also transferred to the primary hydrogen propellant before it enters the cavity (see primary and secondary hydrogen circuits in Fig. 2).

The heat deposition rates in the engine components are shown in Table I. The percentage of the total energy which is deposited in the moderator and structure is 12.15 percent. The energy loss from the engine due to neutron and gamma ray leakage is on the order of 0.5 percent. The remaining energy (87.35 percent) is transferred to the hydrogen propellant stream by direct thermal radiation from gaseous nuclear fuel in the cavity.

The temperature, enthalpy, and pressure levels in the primary hydrogen propellant circuit and the secondary hydrogen circuit are summarized in Tables II and III, respectively. The temperatures and enthalpy levels in the neon and fuel cycle circuit are given in Table IV. Pressure levels in the neon and fuel cycle circuit were not calculated since detailed design studies of certain components, such as the separator, have not been made.

## Modifications to Reference Engine

Three modifications were made to the basic reference design described in Refs. 1 and 2. These are (1) inclusion of a transfer volume connecting the vortex region and the propellant region to minimize pressure differentials across the transparent structure, (2) modification of the fuel injection circuit model to simulate a closed circuit (see fuel return loop in fuel cycle circuit --- Fig. 2), and (3) reduction in fuel residence time from 20 sec to 4 sec to reflect the results of recent fuel containment tests (Ref. 5). None of these modifications cause any major change in the steady-state operating conditions of the reference engine, but they do affect the transient response to various perturbations. In addition to the modifications listed above, various control mechanisms were investigated for start-up and transient operation. The primary means of control considered were variations in the turbine control valve, fuel control valve, and exit nozzle throat areas.

## ENGINE START-UP INVESTIGATION

Analyses of the start-up characteristics of the nuclear light bulb engine were continued (1) to investigate modes of start-up other than the linear power ramp, and also shorter start-up times, (2) to determine the form of fuel most appropriate for start-up, and (3) to arrive at a control system concept for the start-up process. A mathematical model of the engine was derived and programmed for digital computer solution.

The start-up studies described in Ref. 2 were limited to linear power start-up ramps. In this start-up mode, extremely rapid increases in average fuel temperature and pressure occur during the early phases of start-up due to the poor efficiency of heat transfer from the cavity region when the principal heat transfer mechanisms are conduction and convection. With the linear power start-up ramps, it appeared that start-up times of less than 60 sec would produce temperature and pressure variations during start-up which would be prohibitively large. It was also determined that short start-up times were desirable for minimizing the amount of propellant expended during the start-up period.

## Modifications to Start-Up Simulation Model

The basic model used for simulation of the start-up characteristics is described in Ref. 2. The two major modifications to the basic start-up simulation model were (1) inclusion of equations to calculate the local temperature and pressure levels so that the pressure differential across the transparent structure could be determined and (2) modification of the existing equations to permit the investigation of linear average fuel temperature start-up ramps.

Since the coolant passages in the engine are fixed volumes, a general or local temperature variation will cause transient variations in pressure. The three coolant circuits (primary, propellant, secondary hydrogen, and fuel cycle circuits) are not interconnected; hence, temperature variations in the engine will cause pressure variations between the circuits. The most critical region in the reactor, from the standpoint of pressure differential, is the transparent structure which separates the primary propellant from the fuel cavity region. During start-up and transient variations near steady-state operation, pressure differentials would exist across the transparent walls due to temperature variations in the propellant and fuel cycle circuits. These variations in pressure must be determined so that appropriate changes in the primary flow rate or exit nozzle area may be included in the start-up schedule to minimize the pressure difference. The modified start-up equations included calculations of local temperatures throughout the engine and the resulting pressure levels in the three coolant circuits.

The differential equation used to determine the average fuel temperature profile during start-up for linear power ramps is (from Ref. 2)

$$\frac{dT_F}{dt} = B_1 t - B_2 T_F - B_3 T_F^4 \quad (1)$$

where  $T_F$  = average fuel temperature in deg R,  $t$  = total elapsed time since initiation of start-up in sec, and the constant  $B_1$  varies with the slope of the power ramp. This equation may be written in the form

$$\frac{dT_F}{dt} = Q - B_2 T_F - B_3 T_F^4 \quad (2)$$

where  $Q$  = time-dependent power level. If it is assumed that the power level variation with time ( $Q$ ) is such that the average fuel temperature follows a linear ramp from 600 R (initial conditions) to 45,000 R (design fuel temperature), then

$$\frac{dT_F}{dt} = \text{CONSTANT} = B_4 \quad (3)$$

and

$$T_F = 600 + B_4 t \quad (4)$$

After substituting Eqs. (3) and (4), Eq. (2) may be used to determine how the power level must vary with time to produce a linear temperature ramp. The general form of the time-dependent power level equation will be

$$Q = -B_4 + B_2(600 + B_4 t) + B_3(600 + B_4 t)^4 \quad (5)$$

The required power variations for 6-sec and 60-sec start-up times are shown in Fig. 3. The power variation for a 60-sec linear power ramp is also shown for comparison. Considering the two 60-sec ramps, the power level required for a linear temperature start-up ramp is considerably lower during the early phases of start-up and rises very sharply toward the end of the start-up period. Thus, power is maintained at a lower level during the period when conduction and convection heat transfer are dominant in the fuel region; when radiation heat transfer becomes the major means of heat loss from the fuel ( $T_F > 15,000$  R), power is increased much more rapidly without causing as rapid a rise in temperature.

The preceding discussion pertains to the changes that were made to the start-up model. The resulting start-up profiles of fuel injection weight flow, fuel control valve area, propellant exhaust nozzle area, average fuel temperature, cavity pressure, average BeO temperature, average graphite temperature and propellant exit temperature are discussed subsequently in the section entitled Start-Up Characteristics Assuming Ideal Control System.

Considerations of the procedures required during the approach to criticality and the increase of the power from the range of 1 watt to an initial condition of 4.6 megawatt have indicated that it may be necessary to employ very small power ramps during this period and to remain at low power levels for relatively long periods of time. The neutron level sensing devices which would be used during this period would have to be much more sensitive than those used at full power since the neutron flux levels are as much as nine orders of magnitude lower than the full-power values. Provision must be made for switching the control response between neutron flux level sensors of different sensitivity and insuring continuity of the control responses. In order to fully investigate these problems, the start-up simulation model must be further modified to permit a calculation of the engine operating conditions if the power level ramps are interrupted for finite time periods during start-up and to permit more detailed calculations of the engine conditions for very low power levels.

#### Start-Up Control System Concept

The calculations of the operating conditions during start-up which were reported in Ref. 2 are based on the assumption of an ideal control system which is capable of monitoring and adjusting fuel injection flow rates, hydrogen coolant flow rates, neon buffer gas and bypass flow rates, and exhaust nozzle areas to conform to a predetermined schedule. A preliminary start-up control system concept was devised to determine the number and type of sensors, comparators, and valves which would be necessary to achieve the desired control and to provide a basis for future studies of the effects of control response time on the operating conditions during the start-up transient.

The basic elements of the start-up control system concept\* are:

<u>Parameter</u>	<u>Schedule or Control</u>
Neutron Flux**	Scheduled vs time
Fuel Flow Rate	Scheduled vs Neutron flux and Rate of Change of Neutron Flux
Primary Propellant Flow Rate	Scheduled vs Neutron Flux
Neon Flow Rate	Scheduled vs Neutron Flux
Secondary Coolant Flow Rate	Scheduled vs Neutron Flux
Propellant Exhaust Nozzle Area	Scheduled vs Neutron Flux
Pressure Differential Across Transparent Wall	Controlled by Transfer Volume

Each of these flow systems contains its own proportional feedback circuit to insure that the flow rate follows the commanded (scheduled) value. In the case of fuel flow rate, the feedback circuit would include both proportional and rate feedback --- i.e., both neutron flux and rate of change of flux --- to insure that the fuel flow rate followed the schedule closely. The transfer volume system for equalizing the pressure on opposite sides of the wall would incorporate a diaphragm displacement sensor and a neon make-up system for insuring that the diaphragm remains close to the null position. Further discussion of these basic control elements follows.

The sequence of events during start-up are listed in Table V. A number of preliminary operations, referred to as phase I of start-up, are performed prior to the initiation of the start-up power ramp as shown in Table V. After these operations are performed, phase II of start-up is initiated. At the beginning of phase II, the engine is operating at 0.1 percent of the design power level at 600 R. In both the linear power ramp and the linear average fuel temperature ramp the principal means of raising power is to increase the contained mass in the engine from the level required at the initial condition (0.1 percent power, 600 R) to the value required at the full-power operating condition. This increase in contained fuel mass is achieved by varying the fuel injection rate. Once the desired power level schedule is specified, the required fuel injection flow rate to produce such a variation in power may be calculated. The temperature variation in the fuel and heat deposition in the various coolant circuits may be calculated and the coolant flow rates required to maintain reasonable temperature levels throughout the engine may be determined.

---

\* There would be additional sensors and controls to initiate scram mechanisms.

\*\*Power is proportional to neutron flux.



Once the power and flow rates have been established, local temperatures and pressures throughout the system may be calculated. The basic control method follows this calculational sequence in that the control of the fuel injection rate determines the power profile and the absolute value of power, together with the local temperature restraints, determines the coolant flow rates.

A conceptual control schematic is shown in Fig. 4. After the engine is brought to 0.1 percent of full power by the sequence described in Table V, the fuel injection flow rate is increased to produce the power variation shown in Fig. 3. The increase in flow rate required is shown in Fig. 5. This variation is made by the input of a predetermined signal to the control which varies the area of the fuel control valve  $V_1$ . Since the pressure level is changing throughout the start-up ramp, the required area variation of the fuel injection control valve is described by an equation of the form

$$A_F / (A_F)_0 = K \sqrt{\frac{W_F^2}{P_C}} \quad (6)$$

where  $K$  is a function of  $(\Delta P_F)_0$ ,  $(W_F)_0$ , and  $(P_C)_0$ . The variations of  $A_F / (A_F)_0$  during start-up are shown in Fig. 6. Signals from the neutron level sensor,  $S_1$ , and from the neutron flux rate-of-change sensor,  $S_2$ , would continuously compare the measured values of neutron level and neutron flux rate of change to the desired value and correct the flow area to obtain the desired power variation.

The flow rates of hydrogen and neon are increased linearly with time from 1 percent of their full-power value. Input signals to the flow rate sensors,  $S_3$ ,  $S_4$ , and  $S_5$  cause the respective control valves to open according to a schedule derived from equations similar to Eq. (6). Actual flow rates are compared with the desired values. In addition to the sensing of actual flow rates, the flow rate controls are also influenced by the magnitude of the neutron flux. The absolute neutron flux level is directly proportional to the power level, and for a given power level there is a required value of hydrogen or neon flow to avoid exceeding component temperature levels. The required flow rate associated with a given neutron flux level or power level is continuously compared to the actual values measured by the flowmeters.

The pressure in the engine increases from an initial pressure of 71 atm to the steady-state operating condition of 500 atm. During start-up, pressure is controlled by varying the area of the exhaust nozzle,  $V_6$ . The desired area variation as shown in Fig. 7 is achieved by means of varying the exhaust nozzle area in a predetermined relationship to the measured neutron flux level. A pressure sensor,  $S_6$ , measures and compares pressure to the desired level and adjusts the exhaust nozzle area accordingly.

The entire control system, therefore, consists of a series of closed-loop control circuits which continuously compare the actual values of the parameters to be controlled with either a predetermined value of that parameter or with a measured value of a parameter to which it must be proportional. The rate of change of neutron flux level and the absolute value of neutron flux level, which are directly proportional to the rate of change of power and the absolute power level, respectively, are specified for the start-up period and input signals to control circuits governing these parameters cause the fuel control valve to open to produce the power profile shown in Fig. 3. If the measured value of neutron flux rate of change or absolute neutron flux level deviates from the desired input schedule, a feedback signal will cause an appropriate change in the fuel control valve area.

As previously mentioned, to insure that the maximum temperature levels in the various engine components are not exceeded during the start-up schedule, it is necessary to insure that coolant be circulated in the engine at appropriate flow rates. The required values of flow rate may be calculated if the power level is known. Since the power level is proportional to the neutron flux level, the required flow rates are also uniquely proportional to the neutron flux level. Therefore, the flow rates of propellant, secondary coolant, bypass flow and buffer flow may be controlled, in a closed-loop circuit, by continuously comparing the measured value of the particular flow rate to the absolute neutron flux level.

In a similar manner, there is a particular value of exhaust nozzle area associated with the absolute neutron flux level. A comparison of actual pressure with the required pressure based on the flux level may be used in a closed-loop circuit to maintain the proper valve setting. The combination of neutron flux level (i.e., power level), exhaust nozzle area, and primary propellant flow rate establishes the current operating pressure level of the engine. Any local variations in pressure are equalized by the transfer volume system described below.

The propellant region and the vortex region are interconnected by means of a fixed volume containing a movable diaphragm which is referred to in Fig. 4 as a transfer volume. The action of the transfer volume is to provide a response time for the various controls without imposing large pressure differentials across the transparent structure. The diaphragm displacement sensor,  $S_7$ , measures the transfer volume diaphragm position and sends control signals to the neon make-up system to insure that the diaphragm remains close to the null position. As an example, the maximum value of pressure rise during a 6-sec start-up is on the order of 100 atm/sec. If some signal error caused this pressure ramp to exist in only the propellant circuit, while the neon pressure remained constant, the pressure difference across the transparent structure would increase as shown in Fig. 8. With a transfer volume, the pressure differentials will cause a displacement of the diaphragm and a given volumetric flow rate of gas through the transfer volume will occur. For a finite

transfer volume there will be a finite time before the diaphragm reaches the limiting displacement. It may be seen that a transfer volume of  $4.5 \text{ ft}^3$  will provide a 0.1-sec lag time for the correction of the error causing the pressure ramp. A total transfer volume of approximately  $8 \text{ ft}^3$  ( $4 \text{ ft}^3$  in either direction) is the size required to equalize the pressure variations encountered in the most severe perturbations from steady state. This size of transfer volume results in a response time of 0.09 sec which is sufficiently large to assure that the error may be sensed and corrected by the control system.

#### Start-Up Characteristics Assuming Ideal Control System

The calculations of the engine characteristics during phase II of start-up that are discussed in this section were based on the assumptions that the fuel injection flow rate would be controlled to produce the power variations shown in Fig. 3 and that the area of the propellant exhaust nozzles could be varied to match the pressure level in the propellant region to that of the vortex. The temperature levels throughout the engine were calculated for all three power ramps assuming linear variations in propellant flow rate during the ramps. The variation of pressure in each circuit was calculated based on the volume of coolant in each circuit and the initial pressure level. The results of these calculations were used to determine the desired values of initial conditions and the engine responses during the start-up ramps.

The sequence of events during both phases of start-up is shown in Table V. Initial values of all major parameters during phase II can be seen in Figs. 9 through 14. Although the sequence is similar to that of Ref. 2, the initial values of flow rates and pressure are different for the linear temperature ramps from those of the linear power ramps. Based on the volume of gas in the propellant and fuel cycle circuits and the temperature variations in the circuits, an initial pressure of 71 atm at zero power conditions will result in 500 atm pressure in both circuits at the end of the linear temperature ramps. Due to the lower values of power level during the initial phases of a linear temperature start-up, initial values of the flow rates in the primary and secondary coolant circuits are reduced to 1 percent of the steady-state values ( $0.42 \text{ lb/sec}$ ). The schedule for the flow rate of neon buffer gas is unchanged.

#### Pressure, Temperature, Propellant Flow Rate, and Nozzle Area Profiles

The variations of average fuel temperature with time during start-up are shown in Fig. 9 for two linear average fuel temperature start-up ramps (6 sec and 60 sec) and one linear power start-up ramp (60 sec). It may be seen by comparing the two 60-sec start-up ramps that the very rapid rise in average fuel temperature which occurs in the linear power start-up mode does not occur in the linear-temperature

mode, and the temperature rise during the latter stages of the start-up is increased. As a result, the maximum rates of increase in pressure tend to be less severe and it is possible to consider short start-up times. In the case of a linear power start-up ramp of 60-sec duration, the maximum rate of change of average fuel temperature was on the order of 10,000 deg R/sec whereas a linear temperature start-up ramp of only 6 sec results in a maximum rate of change in average fuel temperature of only 7500 deg R/sec. Short start-up ramps on the order of 6 sec are necessary in the case of a linear temperature start-up ramps to insure vaporization of the fuel as rapidly as when a 60-sec linear power ramp is employed. Rapid vaporization is desirable to prevent centrifuging of fuel particles or droplets to the transparent wall.

The cavity pressure variations during start-up are shown in Fig. 10. The maximum rate of change of pressure for the 60-sec linear temperature ramp is about one-half of that predicted for the 60-sec linear power ramp. The maximum value of the pressure variation for the 6-sec linear temperature ramp is approximately 100 atm/sec.

The variations of average BeO temperature and average graphite temperature are shown in Figs. 11 and 12, respectively. These temperatures do not vary appreciably with the type of start-up profile since they are primarily dependent upon the heat capacity of the moderator material and the length of the start-up ramp. The time to reach full-power operating temperatures in the moderator is on the order of 200-300 sec, regardless of the mode of start-up for short (less than 60 sec) start-up ramps.

The variation of propellant exit temperature during start-up is shown in Fig. 13.

### Nuclear Characteristics

The bulk moderator regions heat up relatively sluggishly during start-up due to their large mass and heat capacity. There is a unique critical mass of U-233 nuclear fuel and a corresponding U-233 reactivity worth for each set of operating conditions during the start-up ramp. These critical mass requirements and nuclear fuel reactivity worths were calculated so that fuel injection rate schedules could be established which would keep the engine on the start-up power profiles shown in Fig. 3.

#### Critical Mass Profiles

U-233 critical mass requirements were calculated for the 6-sec and 60-sec linear average fuel temperature start-up ramps and the 60-sec linear power ramp. Conditions of pressure and temperature in the major regions of the engine at various times after start-up were taken from Figs. 9 through 13. A one-dimensional, spherical,

homogenized-core model of the full-scale engine similar to that employed for the analysis of the seven-module reactor experiment described in APPENDIX A was used for the criticality calculations. The cross section energy group structure and nuclear codes employed in the analysis were the same as those used in Ref. 3.

The results of the critical mass calculations are shown in Fig. 14. In all cases, the duration of the start-up ramp is short (6 and 60 sec) relative to the moderator heating time (200 to 300 sec). The lag in bulk moderator temperatures reaching their asymptotic values gives rise to the lag in critical masses reaching their steady-state, full-power value of 30.9 lb. In the case of linear fuel temperature start-up ramps, critical mass reached peak values of 37.1 and 34.2 lb when full power was reached for the 6-sec and 60-sec start-up ramps, respectively. The peaking of the critical masses was found to be coincident with the peaking of hydrogen coolant density (hence, neutron absorption by the hydrogen) in the moderator regions which occurred when the full operating pressure of 500 atm was reached. In the case of the 60-sec linear power start-up, the coolant density reaches its peak value relatively early in the start-up ramp ( $\sim 5 - 10$  sec) and hence critical mass requirements are dictated by other more dominant factors such as propellant density and temperature and bulk moderator temperature.

The peaking of critical mass during linear fuel temperature start-ups causes the reference design fuel containment limits (i.e., the fuel-to-buffer-gas density ratio limits as presently envisioned based on fluid mechanics tests) to be exceeded. These peaks can be eliminated by lowering the initial-condition pressure for phase II of start-up to a value approaching the 20 atm employed for the 60-sec linear power start-up ramp.

#### Fuel Flow Rate Profiles

Fuel weight flow requirements during start-up were calculated using the results of the criticality calculations in the neutron kinetics equations assuming that (1) the power level per unit fuel mass was directly proportional to the neutron level and (2) the average fuel residence time of 4 sec (i.e.,  $\lambda_F = 0.25 \text{ sec}^{-1}$ ) was constant throughout start-up. Under these assumptions, the neutron level equation can be written at any point in time during the start-up ramp as

$$\delta k = \ell^* \left( \frac{1}{N} \frac{dN}{dt} \right) + \sum_{i=1}^6 \frac{\beta_i}{1 + \frac{\lambda_i}{\frac{1}{N} \frac{dN}{dt}}} \quad (7)$$

Equation (7) was solved for  $\delta k$  for appropriate values of the rate-of-change of power level,  $dQ/dt$ . The amount of excess fuel loading required to provide the necessary excess reactivity was obtained from the calculated values of  $(\delta k/k)/(\Delta M/M_c)$ . The fuel weight flow profiles required to maintain the critical mass and power profiles corresponding to the assumed linear temperature and power start-up ramps are shown in Fig. 5. The excess fuel weight flow required to sustain the assumed power profiles were less than 0.2 percent of the total weight flows shown in Fig. 5. The maximum value of excess fuel weight flow was equivalent to an excess reactivity of 0.0017 during the 6-sec linear fuel temperature start-up, the steepest start-up power ramp considered.

#### Expected Dynamic Behavior During Start-Up with Control System

The results of the start-up studies have indicated that a start-up schedule which produces a linear variation in average fuel temperature is preferable to a linear increase in power since it permits short start-up times with a reduction in the maximum rate of change of pressure and temperature during the start-up ramp. Brief calculations indicate that it is possible to inject fuel, coolant and buffer gas to control pressures according to the required schedules. Use of the start-up control system with the transfer volume (Figs. 4 and 8) to minimize the pressure differential across the transparent structure should allow sufficient response time to correct any variation from the scheduled start-up sequence.

The engine dynamics program was used to calculate the controlled response of the engine to the conditions which exist at the end of the start-up sequence. In this case, it was assumed that the power ramp shown in Fig. 3 for the 6-sec linear temperature ramp and the fuel flow rate ramp shown in Fig. 5 at the completion of the start-up sequence ( $t = 6$  sec) were applied as input perturbations to the engine at the full-power operating condition. The full-power control system (see later discussion of Fig. 20 in section entitled ENGINE DYNAMICS INVESTIGATION) was used to stabilize the engine. The results of this analysis indicated that there is no appreciable overshoot in the power response, and the full-power control system is capable of stabilizing the engine as it approaches the full-power operating level.

Further studies are necessary to evaluate the dynamic behavior during start-up and to assure that the system would be stable at all conditions. These studies would probably show that gain programming of the feedback would be necessary. However, the development of such a control system should be feasible.

### Fuel Injection System

Three forms of nuclear fuel were considered: uranium or uranium oxide particles,  $\text{UF}_6$  gas, and liquid  $\text{UF}_6$  or molten uranium. All of the fuel forms have physical and chemical properties which must be considered over the ranges of operating conditions in the nuclear light bulb engine. Only the physical properties were investigated in this study; the influence of chemical properties should be the subject of further experimental investigations.

It was concluded that the preferable system for fuel injection and circulation would be a uranium metal dust transported by a carrier gas.  $\text{UF}_6$  and  $\text{UO}_2$  were considered less preferable because their dissociation in the fuel region would add significantly to the total operating pressure of the engine. Since molten uranium is more likely to plate on the recirculation system duct walls than would a cooler, condensed uranium, it was also considered desirable to regulate the buffer-gas bypass flow which serves to cool the spent fuel and vortex buffer gas as it enters the thru-flow port to cool the uranium rapidly to temperatures well below its melting point. Extrapolations of expressions for uranium vapor pressure near one atm from Ref. 11 indicate that the boiling point of uranium might be about 12,000 R for fuel partial pressures of 200 atm (the average fuel partial pressure in the nuclear light bulb engine is estimated to be 175 to 200 atm in Ref. 3). This means that, in quenching the spent nuclear fuel upon entry into the thru-flow ports, there is a temperature range from about 12,000 R to 2500 R (melting point) during which the uranium is condensed in a liquid form. To prevent the liquid uranium from plating on the thru-flow duct walls during this period, cold neon bypass flow must be introduced continuously to maintain a steep temperature gradient and to essentially blow the fuel droplets and/or crystals away from the walls. Plating of solid fuel in the wall could be avoided by keeping the wall temperature above 2500 R. Investigation of the thru-flow duct wall geometry and selection of flow conditions required to minimize deposition of condensed fuel on the duct walls should be the objective of an experimental test program.

During phase I and the initial part of phase II of start-up, it may not be possible to prevent particles or droplets from centrifuging to the transparent walls during the time required to vaporize the nuclear fuel. If that should in fact occur,  $\text{UF}_6$  should be employed during phase I and the initial part of phase II with a transition to the particle-carrier gas system at about one-third of full-power operating conditions.

## ENGINE DYNAMICS INVESTIGATION

Analyses were conducted of the dynamic response of the engine at full-power conditions to perturbations of various parameters such as reactivity, fuel weight flow, turbopump wheel speed, propellant exhaust nozzle throat area, and fuel region radius. Emphasis was placed on (1) refining the UNIVAC 1108 digital computer simulation program to provide more detailed local temperature and pressure calculations, (2) equalization of pressure differences throughout the engine (in particular, across the transparent wall), (3) conceptual design of an engine control system, and (4) calculation of the dynamic response of the controlled engine to various perturbations in the system.

## Engine Dynamics Simulation Models

In this section, the thermal and fluid dynamics model and the neutron kinetics model are described. Modifications made to these models are discussed. In addition, several aspects of the dynamic response which were considered but which did not lead to model changes are also discussed.

Thermal and Fluid Dynamics Model

The thermal and fluid dynamics model used to calculate the transient response of the engine at full-power is described in Ref. 2. Modifications to the model made to reflect changes in the basic reference design are described below. The assumptions employed in the engine dynamics simulation program are listed in Table VI. The dynamic simulation program flow diagram is shown in Fig. 15.

The specific modifications to the basic model were (1) separate calculation of vortex and propellant pressures, (2) inclusion of a transfer volume for pressure equalization between the propellant and cavity regions, (3) modification of the fuel recycle system model to simulate a closed circuit system, (4) consideration of acoustic velocities in the engine components and the time lags associated with pressure variations, and (5) calculation of local temperature effects on engine pressures. In addition to these modifications, calculations were made to determine the dynamic pressures in the boundary layers adjacent to the transparent walls to predict local pressure variations which might occur in these regions. The cooling sequence, component heat loads and the general calculational procedure are described in Ref. 2.



Separate Calculation of Vortex and Propellant Pressures

In the thermal and fluid dynamics model described in Ref. 2, the engine pressure level was determined by the nozzle outflow conditions according to the equation

$$P_c = \frac{W_p \sqrt{T_p}}{K_p A^*} \quad (8)$$

where  $P_c$  = engine pressure level,  $W_p$  = primary propellant flow rate,  $T_p$  = primary propellant temperature at nozzle,  $A^*$  = nozzle throat area (see Ref. 12), and  $K_p$  = throat flow parameter (see Ref. 12). It was assumed that this pressure would be maintained throughout the engine by internal controls.

Modifications were made to the model to include (1) a more detailed calculation of the turbopump characteristics and their effects on pressure and flow conditions, (2) expressions for calculating turbine control valve effects, and (3) separate calculations of vortex region and propellant region pressures to include the effects of local temperature variations during engine transients.

The effects of finite control valve flow area and turbine nozzle area and the conditions of choked flow in the exhaust nozzle (Eq. (8)) were combined to establish the effects of turbopump wheel speed during transient operation. The flows in the turbine and control valve are assumed to be subsonic and the pressure loss in these components may be expressed as

$$\Delta P = \frac{W^2}{2g\rho A^2} \quad (9)$$

where  $\Delta P$  = pressure loss,  $W$  = flow rate,  $\rho$  = density,  $g$  = gravitational acceleration constant, and  $A$  = flow area of component. If the frictional losses in the coolant circuits are small relative to the pressure losses in the turbine and valve, the turbine pressure ratio may be expressed as

$$PR = \frac{P_c + \Delta P_t}{P_c} \quad (10)$$

where  $P_c$  = cavity pressure and  $\Delta P_T$  = pressure loss in turbine. The total head rise in the primary pump, assuming 1-atm tank pressure, may be expressed

$$\Delta P_{pp} = P_c + \Delta P_T + \Delta P_V - 1 \quad (11)$$

where  $\Delta P_{pp}$  = pressure rise required in primary pump and  $\Delta P_V$  = pressure loss in valve. The total power produced by the turbine may be expressed as

$$Q_T = \eta_T C_p W T_{IN} \left[ 1 - \left( \frac{1}{PR} \right)^{0.26} \right] \quad (12)$$

where  $Q_T$  = power produced by turbine,  $\eta_T$  = turbine efficiency,  $C_p$  = specific heat of primary coolant at turbine conditions, and  $T_{IN}$  = inlet temperature to turbine. The total power required by the pumps was assumed to be 1.1 times the power required for the primary propellant pump, or

$$\sum Q_P = 1.1 \left[ \frac{W \Delta P_{pp}}{\eta_P \rho_P} \right] \quad (13)$$

At steady-state operating conditions,

$$Q_T = \sum Q_P \quad (14)$$

and during transient operating conditions, the variation in turbopump wheel speed is governed by

$$\frac{dV^2}{dt} = \frac{2}{I} \{ Q_T - \sum Q_P \} \quad (15)$$

where  $\nu$  = turbopump wheel speed and  $I$  = moment of inertia of turbopump. The turbine nozzle area required at steady-state operation may be calculated by solving Eq. (10) for  $\Delta P_T$  at the desired value of pressure ratio, PR, and solving Eq. (9) for the area  $A$ . The turbine valve area required at steady-state operation may then be calculated from a combination of Eqs. (9), (11), (12), (13), and (14) using steady-state values of flow rate,  $W$ , turbine inlet temperature,  $T_{IN}$ , specific heat and the desired turbine pressure ratio.

The same equations may then be applied to (1) transient conditions using fixed nozzle and valve areas, (2) prediction of transient conditions which arise from valve area changes, and (3) determination of the required valve changes to produce a desired pressure level.

The variations in propellant and vortex pressure which are caused by local changes in temperature are estimated by assuming a constant-volume heating of the circuit components, so that

$$P = P_0 \left\{ \frac{1}{V_T} \sum_{i=1}^n V_i \frac{T_i}{(T_i)_0} \right\} \quad (16)$$

where  $P$  = pressure,  $V_T$  = total volume of circuit,  $V_i$  = volume of  $i$ th region of circuit,  $T_i$  = average temperature in  $i$ th region of circuit, and the  $0$  subscript refers to steady-state conditions. In the dynamic model, the fuel cycle circuit was divided into two regions (the vortex region and the external region) and the primary propellant was divided into three regions ((1) the piping, heat exchanger and manifold region, (2) the moderator region, and (3) the cavity region).

The equations described above were incorporated into the engine dynamics model and used to predict the pressure differentials which would occur across the transparent structure during various perturbations to the steady-state in an uncontrolled engine (i.e., fixed valve areas). It was determined that the pressure differentials were considerably larger than the allowable values of 1 atm bursting and 0.1 atm collapsing. Attempts to match the propellant circuit pressure to the vortex pressure by adjusting the turbine valve or the exhaust nozzle area introduced instabilities in the dynamic response of the engine even with no lag time associated with the valve adjustment. These results led to the inclusion of a transfer volume, as described below, to minimize the pressure differential.

Transfer Volume Equalization of Pressure Differences

To minimize the pressure differential across the transparent structure, it was proposed to include a transfer volume which interconnects the vortex region and the duct region of the primary propellant circuit as shown schematically in Figs. 4 and 8. If a pressure difference exists between the two regions, volume will be transferred from the region of high pressure to the region of low pressure, through the transfer volume, until the pressure is equalized. The purpose of the transfer volume itself is to provide separation of the two circuits by means of a movable or deformable diaphragm so that there can be no loss of fuel to the propellant stream or injection of hydrogen into the fuel cycle circuit, and to provide a buffer volume of gas similar to that in the adjacent circuit which may be transferred.

If the pressure is to be equalized by increasing the volume of the high pressure region and decreasing the volume of the low pressure region, then, for  $P_1 > P_2$ ,

$$P_1 \left( \frac{V_1 - \Delta V}{V_1} \right) = P_2 \left( \frac{V_2 + \Delta V}{V_2} \right) \quad (17)$$

where  $P$  = pressure,  $V$  = volume of region, and  $\Delta V$  = volume transferred. Solving Eq. (17) for  $\Delta V$ ,

$$\Delta V = \left( \frac{P_1}{P_2} - 1 \right) / \left( \frac{1}{V_2} + \frac{P_1}{P_2} \frac{1}{V_1} \right) \quad (18)$$

The corrected or balanced pressure in the circuits may be expressed as

$$P_{\text{CORR}} = P_1 \left( \frac{V_1 - \Delta V}{V_1} \right) = P_2 \left( \frac{V_2 + \Delta V}{V_2} \right) \quad (19)$$

The rate of volume transfer is  $\Delta V / \Delta t$  and the rate of change of the pressure differential which would exist if no interconnection were used is  $(P_1 - P_2) / \Delta t$ . The required velocity of the diaphragm and the gas in the transfer chamber will be

$$v_D = \left( \frac{l}{A_D} \right) \left( \frac{\Delta V}{\Delta t} \right) \quad (20)$$

where  $A_D$  = cross-sectional area of the transfer chamber diaphragm. If the allowable pressure differential across the transparent structure is  $\Delta P_w$ , then the diaphragm and the gas in the transfer chamber must reach the velocity given by Eq. (20) in a time period less than or equal to

$$\tau_D = \Delta P_w / \left( \frac{P_1 - P_2}{\Delta t} \right) \quad (21)$$

The minimum average acceleration required is

$$a_D = v_D / 32.2 \tau_D \quad (22)$$

The total mass of the gas which must be accelerated is

$$(\rho_H + \rho_{Ne}) \frac{\Delta V}{\Delta t} \tau_D \quad (23)$$

where  $\rho_H$  = density of hydrogen and  $\rho_{Ne}$  = density of neon. The total mass of the diaphragm is

$$\rho_D A_D \Delta x_D \quad (24)$$

where  $\rho_D$  = density of the diaphragm material and  $\Delta x_D$  = thickness of diaphragm. The force required to accelerate the gases and the diaphragm at the acceleration given by Eq. (22) is

$$F = \left\{ (\rho_H + \rho_{NE}) \frac{\Delta V}{\Delta t} \tau_D + \rho_D A_D \Delta x_D \right\} \frac{v_D}{32.2 \tau_D} \quad (25)$$

Since the pressure required for accelerating the gas and diaphragm ( $F/A_D$ ) must be equal to the allowable pressure difference across the transparent structure ( $\Delta P_w$ ), Eqs. (25) and (21) may be combined to obtain

$$\Delta P_w = \frac{1}{32.2 A_D^2 \tau_D} \frac{\Delta V}{\Delta t} \left\{ (\rho_H + \rho_{NE}) \frac{\Delta V}{\Delta t} \tau_D + \rho_D A_D \Delta x_D \right\} \quad (26)$$

Solving Eq. (25) for the diaphragm thickness,

$$\Delta x_D = \frac{32.2 A_D^2 \tau_D \Delta P_w}{\rho_D \frac{\Delta V}{\Delta t}} - \frac{(\rho_H + \rho_{NE}) \frac{\Delta V}{\Delta t} \tau_D}{\rho_D A_D} \quad (27)$$

It may be noted from Eq. (27) that the force required to accelerate the gases (second term on right hand side of Eq. (27)) causes a reduction in allowable diaphragm thickness and in some cases there will be a minimum allowable value of  $A_D$  associated with a given diaphragm thickness.

#### Boundary Layer Pressure Fluctuations

In addition to pressure differentials between the vortex and propellant regions, the flow of the propellant and buffer-gas-boundary layers over the two sides of the transparent walls can give rise to fluctuating pressure fields. The rms pressure fluctuations at subsonic speeds have been observed experimentally to be given by

$$\Delta P' = (1.5 \times 10^{-3} \text{ to } 1.2 \times 10^{-2}) q_0 \quad (28)$$

where  $q_0$  is the dynamic pressure of the free stream (Ref. 13). For the reference nuclear light bulb engine, the neon buffer gas dynamic pressure is  $q_0 = 0.075$  psi. and the propellant dynamic pressure is about  $q_0 = 0.050$  psi. Thus, the rms pressure fluctuations associated with the flow of buffer gas and propellant over the

transparent walls should fall within the range of  $\Delta p' = 7.5 \times 10^{-5}$  to  $9.0 \times 10^{-4}$  psi. This level of pressure fluctuation is insignificant relative to the allowable local bursting or collapsing loads on the transparent structure of 1.0 and 0.1 atm, respectively. Further calculations of the spectral distribution of wall-pressure fluctuations induced by the buffer gas and propellant flows indicate that the peak intensities occur at about 50 cps. It is not anticipated that the pressure fluctuations at that frequency, about  $10^{-5}$  psi, will lead to strength degradation of the transparent walls due to cycle fatigue.

### Fuel Injection System

In the dynamics model described in Ref. 2, the variation in fuel injection rate during transient operating was calculated from the equation

$$W_F = K_F A_F \left( \frac{P_F - P_C}{P_F - (P_C)_0} \right)^{1/2} \quad (29)$$

where  $W_F$  = fuel injection rate,  $K_F$  = proportionality constant,  $A_F$  = area of fuel injection control valve,  $P_F$  = pressure of fuel upstream of control valve,  $P_C$  = vortex pressure, and  $(P_C)_0$  = vortex pressure at steady-state. In Eq. (29),  $P_F$  is assumed to be a constant value. This is representative of a system with a constant delivery pressure which would be unaffected by any engine perturbation.

A series of perturbations were investigated using the model which included the transfer volume described above and it was determined that the fuel injection model described by Eq. (29) causes unstable responses. Inclusion of the transfer volume introduces a lag in the pressure response of the engine. This pressure lag, coupled with the fixed fuel injection pressure, results in a tendency to over-correct the fuel flow rate and thereby introduce oscillations of increasing amplitude. Values of fuel injection pressure were varied from 20 atm to 0.25 atm and, although the period of the oscillations could be changed, they could not be damped.

If it is assumed that the fuel cycle circuit is a closed system with a constant-head pump, any pressure change in the vortex region will be transmitted to the inlet of the pump with a finite delay time equal to the acoustic delay time of that portion of the circuit between the vortex and pump inlet. The difference in response of the open- and closed-cycle systems is best illustrated by assuming a sustained step increase in vortex pressure. In the open-cycle system the pressure change will result in a sustained decrease in fuel injection rate. In the closed-cycle system the same magnitude change in flow rate will occur initially but it will only be sustained for a period of time equal to the acoustic transit time between the vortex region and the pump inlet.

The equation describing the fuel injection rate becomes:

$$W_F = K_F A_F \left( \frac{P_c(t - \tau) - P_c(t)}{P_F - (P_c)_0} \right)^{1/2} \quad (30)$$

where  $P_c(t)$  = vortex pressure at time  $t$  and  $P_c(t - \tau)$  = vortex pressure  $\tau$  sec before time  $t$ .

The acoustic delay time calculated for the region between the vortex and the fuel pump inlet is 0.008 sec. The modified equation for fuel injection rate (Eq. (30)) was incorporated in the dynamics model and it was determined that the oscillatory response previously encountered was eliminated.

The engine has been shown to be very sensitive to fuel injection flow rate. This flow rate is in turn sensitive to the magnitude of the pressure drop across the injectors and the response characteristics of the fuel injection system to pressure fluctuations. Equation (30) is a simplified analytical model employed to explore engine response for various ranges of fuel injection pressure drop, average fuel residence time, and acoustic lag. Further analytical and experimental studies of the fuel injection system should be made to determine the model which most accurately represents the characteristics of the system. These studies should include detailed design of the fuel injection system and investigation of the properties of particle-carrier gas mixture flowing through the circuit.

#### Acoustic Velocities During Pressure Transients

Pressure transients which occur during perturbations will be transmitted throughout the engine according to the sonic velocity in the gases in each component. To introduce the proper response times in the simulation program, the acoustic velocities and characteristic times for the various components in the primary propellant and fuel and neon circuits were calculated. The estimated volumes, average gas densities, sonic velocities, and characteristic times for the primary propellant and neon and fuel circuits used in the dynamics model are listed in Table VII.

#### Neutron Kinetics Model

The principal unusual feature in the kinetic behavior of a nuclear light bulb engine is that the nuclear fuel is injected continuously into the active core volume. Recent experimental results (Ref. 5) indicate that the average residence time of nuclear fuel in a full-scale engine would probably be on the order of 4 sec (reduced from an average fuel residence time of 20 sec employed in the engine dynamics



studies of Ref. 2). Delayed neutron precursors which emit delayed neutrons at time periods greater than 4 sec after the fission event would contribute essentially no neutrons to the active volume of the reactor core. This problem is quite similar to that for circulating-fuel reactors; the important difference is that compressible gases are employed in a nuclear light bulb engine, whereas in the circulating-fuel reactors, the fuel solution is an incompressible liquid. Due to compressibility, it is possible to have fluctuations in total fuel loadings which result from fluid dynamic fluctuations in the fuel residence time. Thus, both the fraction of delayed neutrons which are lost from the active core and the total mass of nuclear fuel within the active core will vary with time. These are primary considerations in the overall control of the engine. The neutron kinetics equations employed in these studies which include the effects of variable fuel loading and delayed neutron fraction are described in Ref. 2.

#### Reevaluation of Reactivity Coefficients

Principal reactivity coefficients employed in the dynamic simulation program were reevaluated using the homogenized-core spherical model similar to that employed for the calculations of the seven-module reactor experiment (see APPENDIX A). In evaluating the reactivity coefficients, it was assumed that they were linear over the range of interest for the dynamic simulation studies and that they were independent of one another. The reactivity coefficients evaluated were those associated with hydrogen propellant density, hydrogen propellant temperature, hydrogen coolant density, BeO moderator temperature, U-233 nuclear fuel, and the fuel region radius.

The values of the calculated reactivity coefficients are contained in Table VI. The reactivity associated with changes in moderator temperature, hydrogen propellant density and temperature, and nuclear fuel loading are of the same sign as those used previously from Ref. 3. Differences in the magnitude of these values are attributable to the use of a different calculational model. The reactivity coefficient associated with the density of hydrogen coolant in the moderator regions alone was not separated out in previous calculations. Its negative value relative to total positive hydrogen density worth calculated in Ref. 3 can be explained by its relative magnitude. In the calculations of Ref. 3, all hydrogen density in all regions was changed simultaneously, and the worth of hydrogen in the propellant and nozzle regions dominated the total material worth. In the present case, the hydrogen worth in the moderator was calculated independently and it might be expected that its principal effect would be to add to the absorption in the moderator regions and thereby decrease reactivity.

The change in the sign of the reactivity coefficient associated with a change in the fuel region radius must be attributed to the different calculational model also. In Ref. 3, the model was a finite cylinder with equal-volume annular regions representing the seven unit cells. This model placed the fuel of the six outer cells

in a narrow annular region such that a change in fuel region radius resulted in a rather modest change in the thickness of the annulus representing the six outermost cells. This meant that in 6/7ths of the fuel regions, the self-shielding was relatively unchanged and, therefore, the presence of a slightly thicker propellant region caused a small rise in reactivity. It is felt that the model currently employed is more valid with respect to geometric changes within the unit cell, and this is verified by the comparisons of radius effects in the seven-module experiment discussed in APPENDIX A.

#### Nuclear Fuel Loading Equations

The equation describing the variations of nuclear fuel mass stored in the active core of the nuclear light bulb engine are given in Ref. 2. Results of recent containment measurement (Ref. 5) have indicated that the fuel decay constant,  $\lambda_F$ , (the inverse of the average fuel residence time) varies approximately as follows:

$$\lambda_F \propto \frac{1}{\rho_{B_6}} \left( \frac{W_B}{W_L} \right)^{1.0} \quad (31)$$

where  $\rho_{B_6}$  is the buffer gas density at the nominal edge of the fuel cloud,  $W_B$  is the buffer-gas weight flow, and  $W_L$  is the fuel weight flow out of the vortex region. In the previous studies of Ref. 2, the exponent of the buffer-gas-to-fuel weight flow ratio was assumed to be 1.2. Calculations of dynamic responses of the uncontrolled engine have shown the system to be relatively insensitive to changes in the exponent between 1.2 and 0.9.

The fuel injection weight flow,  $W_F$ , and the equations governing its variation with cavity pressure level has been described previously.

#### Dynamic Characteristics of Uncontrolled Engine

A series of dynamic responses to step changes in imposed reactivity of a magnitude which would cause the reactor to become prompt critical and to positive step changes in fuel injection rate of 10 percent of the full-power value were calculated using the new model of the engine with no control mechanisms. In these cases, the fuel injection pressure differential and the average fuel residence time were varied to determine their effects on engine response and to select the most desirable value of fuel injection pressure differential.

### Effects of Changes in Fuel Injection Area and Pressure Differential

The dynamic response of the engine for three different fuel injection pressure differentials (1.0, 0.5, and 0.25 atm) was investigated at a fuel residence time of 4 sec. The power response to a step change in imposed reactivity is shown in Fig. 16. Although the responses are similar (i.e., initial oscillations which are damped well within 1.0 sec), the magnitude and frequency of the oscillations vary. The lower values of fuel injection pressure differential result in higher frequency oscillations with a lower amplitude (e.g., Fig. 16(a)). Based on rough calculating it was estimated that 0.25 atm is the minimum value of the pressure differential which may be used to provide sufficient pressure to overcome frictional losses in the piping and to provide the required injection velocities.

Power responses to step changes in fuel injection area (and, hence, initial step changes in flow rate) are shown in Fig. 17. Unlike the responses to reactivity perturbations, these responses have initial oscillations followed by a linear power ramp. This power ramp is a result of cavity pressure feedback through the closed-cycle fuel injection system (see Fig. 2 for flow diagram). If the change in fuel injection rate is assumed to be the result of a change in the control valve area, an increase in this area will cause an increase in fuel injection rate. The increased fuel injection rate will cause an initial rise in pressure which will tend to retard the fuel injection rate but, after a period of time equal to the acoustic lag between the vortex region and the fuel pump inlet, this pressure rise will be felt at the pump inlet. If the pressure rise in the pump is constant, the initial pressure rise in the vortex region will be transmitted throughout the fuel injection circuit and the retardation in flow will no longer be present.

This effect is best described by observing the variation of the fuel injection pressure differential ( $P_F - P_C$ ) as shown in Fig. 18. In the case of a step change in imposed reactivity, the fuel control valve area is constant and the fuel injection pressure differential varies as shown in Fig. 18(a). The large fluctuations in fuel injection pressure differential gradually damp out to the design value of 0.25 atm so that the engine returns to steady state operating condition. In the case of a step increase in fuel injection area, the fluctuations in pressure differential ( $P_F - P_C$ ) are much smaller, but the new final value is 0.21 atm. The equation governing the fuel injection flow rate is

$$W_F = K_F A_F \left[ \frac{P_F - P_C}{0.25} \right]^{1/2} \quad (32)$$

The decrease in the pressure differential,  $P_F - P_C$ , does not compensate for the increase in the valve area and the calculated value of  $W_F/(W_F)_0$  from Eq. (32) for  $A_F = 1.1 (A_F)_0$  and  $(P_F - P_C) = 0.21$  atm is 1.008. This increase in fuel injection

flow rate causes the power ramps seen in Fig. 17. The curves in Fig. 17 indicate that, as in the case of a change in imposed reactivity, the magnitude of the perturbation is least at the lowest initial injection pressure differential, and the frequency of the initial oscillations is greatest. The power ramps in the case of a step increase in fuel injection area (initial step change in flow rate) vary from 15 percent per sec with a 1.0-atm pressure differential to 5 percent per sec with a 0.25-atm pressure differential.

As a result of these cases, it was concluded that the lowest usable pressure differential, estimated to be 0.25 atm, is the most desirable value to minimize the magnitude of the perturbations in power during transient operation. The total reactivity responses of the uncontrolled engine to step increases in imposed reactivity and fuel control valve area with this differential of 0.25 atm are shown in Fig. 19.

#### Effects of Changes in Average Fuel Residence Time

Calculations were made to determine the dynamic response of the engine to step increases in imposed reactivity and fuel injection control valve area with average fuel residence times of 4, 10, and 20 sec, using a 0.25-atm fuel injection pressure differential. The fuel injection flow rate varies inversely with fuel residence time from a value of 7.5 lb/sec for a 4-sec residence time to a value 1.5 lb/sec for a 20-sec residence time. The lower fuel injection flow rates (longer residence times) result in smaller reductions in contained mass for a given increase in cavity pressure. If the cavity pressure is increased to a value which completely stops fuel injection, the fuel outflow will remain essentially constant and the stored mass will decrease. The rate of decrease in stored mass will be 7.5 lb/sec for a 4-sec fuel residence time, but only 1.5 lb/sec for a 20-sec residence time. The natural pressure control in the fuel cycle system is, therefore, more sensitive for shorter residence times. As a result, the response of the engine for long residence times will have lower frequencies and higher amplitudes.

The 4-sec fuel residence time was used in all subsequent dynamics cases. The response of the engine to longer residence times indicated that the engine is stable and controllable for any residence time in the range investigated.

#### Effects of Changes in Acoustic Lag Time in Fuel Cycle Circuit

The estimated value of the characteristic sound velocity in the region between the cavity and the fuel pump inlet is 8.02 msec (Fig. 2). This value may vary due to the design of the fuel separator and associated piping. Calculations were made to determine the dynamic response of the engine to step increases in imposed reactivity and fuel injection control valve area with acoustic lag times of 5, 10, and 15 msec using a fuel injection pressure differential of 0.25 atm and a fuel

residence time of 4 sec. A variation in this lag will affect the total length of time the fuel injection flow rate will be influenced by changes in vortex pressure. For longer lag times, the total decrease in contained mass which will result from a given pressure rise will become greater. It was determined that the engine response for short lag times (5 msec) showed lower magnitude, higher frequency responses since there was less of a tendency for overcorrection. At the long lag times (15 msec), the engine response was a sustained oscillation which was not damped.

The time increment used in the calculation of the dynamic response of the engine was varied between 0.5 and 5 msec. It was found that the accuracy of the calculation was essentially unchanged by using the highest time increment of 5 msec while calculation time was reduced substantially. The actual acoustic lag in the fuel injection system was approximated by a 10-msec time lag.

As mentioned previously, the engine has been shown to be very sensitive to fuel injection flow rate and further analytical and experimental studies of the fuel injection system should be made to determine the model which most accurately represents the characteristics of the system including detailed design of the fuel injection system and investigation of the properties of particle-carrier gas mixtures flowing through the circuit.

#### Control Methods Investigated

The results of the dynamics studies of the uncontrolled engine indicated a requirement for some type of control to eliminate the continuous power ramps which occur with a step change in fuel injection control valve area. Investigations were made of the possibility of eliminating the pressure differential across the transparent structure by using the turbine control valve or the variable-area propellant exit nozzle, but these control methods were not as satisfactory as the transfer volume concept previously described.

The majority of nuclear reactors have primary control systems based on the continuous measurement of the neutron flux level and the rate of change of the neutron flux level. The latter measurement is used to determine the reactor period, which is defined as the time required for the neutron flux to increase by a factor of  $e$ . Thus, a short reactor period is associated with a large value of the neutron level rate of change,  $dN/dt$ .

In the majority of solid-fueled reactors, control is achieved by removal of neutron absorbing materials from the active core region. In a gaseous nuclear rocket engine the most effective control method is the variation in contained mass in the vortex region by controlling the fuel injection rate. With a 4-sec fuel residence time, the fuel injection rate is 7.5 lb/sec, and rapid changes in contained mass can be achieved by controlling fuel injection rate.

The final full-power control selected (discussed below) was based on a combination of neutron flux rate of change (or reactor period control) and absolute neutron flux level. If it is assumed that there is some finite level of the rate of change of neutron flux which cannot be sensed by a period meter, it is possible for the power level to increase or decrease on a very shallow ramp, and the absolute level of neutron flux measurement can be used to initiate a control input to correct this condition when a given deviation from the operating power level is reached. Both of the controls were assumed to operate on the fuel injection control valve.

A schematic diagram of the control circuit is shown in Fig. 20. This circuit utilizes sensors  $S_1$  and  $S_2$  in Fig. 4 only, since during perturbations from full-power operation there is no necessity to vary the coolant flow rates or the propellant exhaust nozzle flow area.

### Reactor Period Control

The sensitivities and control gains for the initial investigations of the controlled reactor were chosen by calculating the controlled response for a number of reactor periods and control response times. The reactor period meter was assumed to monitor the neutron flux level continuously and to calculate the average normalized value of the rate of change of neutron flux  $(1/N)(dN/dt)$  over a 0.2-sec time period. The use of an averaged value over a relatively long time tends to make the control insensitive to high frequency oscillations and promoted damping of the perturbation. The normalized value was used so that the engine could stabilize at some power level other than the design steady-state value since a requirement to stabilize at the design steady-state value could initiate an oscillatory response in the control circuit. Further investigations will be made to determine the effect of a control without the normalization factor. The reactor period selected for the initial controlled response cases was approximately 60 sec. This value corresponds to a normalized slope of 5 percent as shown by the control limits in Fig. 20. The control gain selected was a change in fuel control valve area equal to 0.002 times the normalized value of the slope.

### Neutron Flux Level Control

The reactor period control described above tends to damp out the short reactor periods (high rate of change of neutron flux) but does allow values of reactor period greater than 60 sec. If the response results in a constant ramp too small to be corrected by the reactor period meter, a maximum and minimum value of the absolute neutron flux level may be sensed and used to activate a second type of control (Fig. 20). The variation in absolute neutron flux level selected was  $\pm 5$  percent, and the control gain for an absolute flux level outside the limits was a 20 percent change in fuel control valve area per sec which continues as long as the absolute value of neutron flux exceeds the limits specified.

There must be some response time included in the control system simulation to approximate the delay between the sensors and the resulting change in fuel control valve area. The averaging which occurs in the reactor period meter tends to slow the response of this sensor, particularly with respect to initial oscillations. It was also assumed that there would be a 0.050-sec delay time between the sensor and the valve response due to combined delays in the sensing instrument and valve. There were no terms included to approximate the inertia of the control valve since the variations are relatively small. It was assumed that a time delay, rather than a time-varying lag, would be sufficient to approximate the actual response with the small time-step employed in the dynamics calculations.

#### Transfer Volume Pressure Balance Control

The transfer volume must be made large enough to equalize pressures between the vortex and propellant regions for the worst case which can occur. In addition, the design of the movable diaphragm in the transfer volume is dependent upon the rate of volume transfer required during a perturbation, and it must be sized so that the pressure differential across the transparent structure does not exceed the allowable limits (1 atm bursting, 0.1 atm collapsing for the reference engine design). An alternate configuration employing a larger number of unit cavities (hence, smaller cell diameters) was investigated in APPENDIX C. The allowable limits of bursting and collapsing pressures for the alternate configuration were 6.9 and 7.4 atm, respectively. It is necessary to insure that at the end of any perturbation the diaphragm in the transfer volume be returned to a central position. This requirement makes it necessary to determine when steady-state operation has been achieved and to activate the neon make-up system in accordance with a diaphragm position sensor to return the diaphragm to a central position by adding or withdrawing neon from the neon circuit. Detailed analysis of the system required for this operation have not been made, but the total volumes of neon required to reposition the diaphragm are estimated to be small.

#### Secondary Control System

The sensors and controls for coolant flow rate, neon flow rate, and exhaust nozzle flow area would not be designed to respond to small perturbations during steady-state operation, but would be employed during start-up, shutdown, and for large changes in power level ( $\Delta Q/Q > 10$  percent). When used, they would respond to input signals, as they do during start-up, with a feedback signal based on the absolute level of neutron flux level, similar to the operation previously described in the start-up program.

### Scram Mechanisms

The only means available for the rapid shutdown of the engine is a reduction in the contained mass by completely stopping the injection of fuel. The time required to shut down in this manner is dependent upon the fuel residence time. For a 4-sec residence time, complete fuel shutoff is equivalent to insertion of negative reactivity at the rate of about -40 dollars/sec which should reduce power very rapidly. Since an activated shutdown cannot be considered to be a small perturbation, pressure equalization cannot be maintained by means of the transfer volume and the secondary flow and nozzle controls used during start-up must also be used during reactor shutdowns. During shutdown the vortex pressure will drop much more rapidly than the propellant pressure unless some adjustment in neon flow rate is made to keep the neon system at a reasonably high temperature. Control schemes for shutdown in both gradual and emergency modes have not been investigated. However, calculations have been made with the engine dynamics program to indicate how fast the engine power will decrease if fuel injection is interrupted. Further detailed studies of shutdown modes to include the response to an emergency shutdown will be made.

### Dynamic Characteristics of Controlled Engine

The engine dynamics program was used to predict the response of the controlled engine to step changes in imposed reactivity, step changes in fuel control valve area, step changes in exhaust nozzle flow area, and ramp changes in turbopump wheel speed and fuel region radius. The power responses of the engines are presented for all perturbations, and the variations of other important parameters such as reactivity coefficients, pressure, fuel flow rates, transfer volume requirements, total contained mass and local temperatures are shown.

The control methods used for the results presented are those discussed in the preceding section. The preliminary results, which have been obtained with different control gains, are also shown for a fuel control valve area perturbation.

### Effects of Positive Step Changes in Imposed Reactivity and Fuel Control Valve Area

#### Imposed Reactivity

The response of the engine to a positive step change in imposed reactivity is shown in Fig. 21. In these cases, the total reactivity is defined as

$$\delta k = \delta k_0 + \delta k_1 + \delta k_2 \quad (33)$$



where  $\delta k_0$  is the base reactivity required to offset the loss of delayed neutrons (0.001485),  $\delta k_1$  is the imposed change in reactivity (0.000976 for a 4-sec fuel residence time) and  $\delta k_2$  is the feedback in reactivity caused by perturbations from the steady state. At steady-state operation,  $\delta k_1 = \delta k_2 = 0$  and the total reactivity  $\delta k$  is equal to  $\delta k_0$ .

It may be seen from Figs. 21(a) and (b) that the controlled response does not differ greatly from the uncontrolled response (compare with Figs. 19(a) and 16(a), respectively). The reason for the similarity is that the initial oscillations are of relatively high frequency and are damped by the relatively long time used by the control system in calculating the average rate of change of neutron flux level (0.2 sec). None of the oscillations result in a neutron flux level outside the control limits, and the amount of change caused by control system inputs is negligible. The perturbation tends to damp out at the steady-state values of reactivity and power within about 0.3 sec.

The individual values of the reactivity coefficients are shown in Figs. 21(d) through (g). The sum of all of these reactivity coefficients is equal to  $\delta k_2$  in Eq. (33). The mass coefficient (Fig. 21(d)) is the dominant coefficient, and the original imposed step increase in reactivity  $\delta k_1$  is offset by an equal change in  $\delta k_m$  with the remainder of the reactivity coefficients approaching zero as steady-state conditions are approached. Figures 21(h), (i), and (j) show the fuel injection rate, fuel loss rate, and contained fuel mass. They indicate that steady-state operation was achieved by a retardation in fuel injection rate which caused a reduction in the contained fuel mass. This slight reduction in contained fuel mass causes the negative mass reactivity coefficient shown in Fig. 21(d).

Figures 21(k) and (l) show the variation of the fuel surface radiating temperature and the transparent-wall coolant exit temperature, respectively. Figure 21(m) shows the required volume which must be transferred between the vortex and propellant circuits to limit pressure differentials across the transparent structure to less than 0.1 atm. In the calculation of transfer volume requirements, a positive value represents a transfer of volume from the neon circuit to the hydrogen circuit. Although the engine returns to a steady-state operating condition, the diaphragm is displaced from its original centered position ( $V_{TR} \neq 0$ ).

#### Fuel Control Valve Area

The response of the engine to a positive initial step change in fuel control valve area, which causes a positive initial step change in fuel injection flow rate, is shown in Fig. 22. As in the case of an imposed reactivity change, the fuel control valve area is defined as

$$A_F = (A_F)_0 + \delta A_{F_1} + \delta A_{F_2} \quad (34)$$

where  $(A_F)_0$  is the original steady-state value of the area,  $\delta A_{F_1}$ , is the imposed step change in area (equal to  $0.10(A_F)_0$  in these cases) and  $\delta A_{F_2}$  is the time-varying change in area resulting from inputs by the control circuits. The fuel injection rate, fuel loss rate, and contained mass for this perturbation are shown in Figs. 22(d), (e), and (f), respectively. The surface radiating temperature, transparent-wall coolant exit temperature, and transfer volume requirements are shown in Figs. 22(g), (h), and (i).

During the initial part of the perturbation ( $t < 1$  sec), the response does not differ greatly from that of the uncontrolled engine. This is to be expected since the power ramp in the uncontrolled case has a normalized slope of approximately 1.05 and will not cause a large control response. When the power level (and neutron flux level, which is proportional to the power level) reaches a value 5 percent above the steady-state value ( $\Delta Q/Q_0 = 1.05$ ; Fig. 22(b)), the absolute neutron flux level sensor will initiate a control correction. For the low control gain used, the area is reduced to a value which results in a decreasing power and neutron flux ramp. The reactor period control damps the slope of the neutron flux to a level below 1.05 and the power will continue to decrease until the low value of absolute neutron flux level is reached. It may be noted from Fig. 22(d) and (f) that the correction to the fuel control valve area causes a relatively large change in fuel injection rate and contained fuel mass which reverses the direction of the power ramp. This type of correction is necessary to limit the amount of power deviation past the control limit which results from the delay time in the control circuit. Even with this large correction, the power exceeds the limit set by the control for about 0.15 sec. A less severe response would result in a higher power variation for a longer time period.

The forced oscillation in power shown in Fig. 22(b) with an amplitude of  $\pm 0.05 Q_0$  and a frequency of approximately 0.133 cycles per sec is characteristic of those perturbations which are not self-damping. The amplitude and frequency of the oscillation is a function of the control system constants rather than the perturbation itself. Some preliminary results of varying the control constants are discussed in a subsequent section.

### Effects of Negative Step Changes in Imposed Reactivity and Fuel Control Valve Area

The power responses of the engine to a negative step change in imposed reactivity and a negative step change in fuel control valve area are shown in Figs. 23(a) and (b), respectively. The result for the negative step change in fuel control valve area appears to be similar to that for the positive step change (compare Figs. 22(b) and 23(b)). The response for a negative step change in imposed reactivity does not stabilize as did the positive step change (compare Figs. 21(b) and 23(a)), but follows a positive ramp in power which will eventually follow the characteristic control oscillation described above. The explanation for this difference is that an overpressure in the vortex is more effective in changing contained fuel mass than is an underpressure in the vortex. Numerically, an underpressure of 0.25 atm will increase the fuel flow rate by 40 percent while an overpressure of 0.25 atm will reduce the fuel flow rate to zero. This nonlinearity will cause a large control input in the case of an underpressure and cause a positive power ramp.

### Effects of Perturbations in Turbopump Wheel Speed, Fuel Region Radius and Exhaust Nozzle Area

The power response of the engine to terminating ramps in turbopump wheel speed is shown in Fig. 24. In both the positive and negative responses, the initial perturbations are followed by the characteristic controlled response variations.

The power response of the engine to a terminating ramp in fuel region radius is shown in Fig. 25. In these cases, fuel region radius changes were imposed by input parameters. Considerations of variations in fuel region radius due to changes in power or flow conditions or of feedbacks which might tend to restore or damp imposed variations were not included. Development of an analytical model of the dynamics of the fuel region should be the subject of further investigations. The positive and negative perturbations result in power variations that are essentially mirror images; the response is a gradual ramp which will eventually follow the characteristic controlled response oscillation.

The power response of the engine to step changes in propellant exhaust nozzle area are shown in Fig. 26. This type of perturbation was investigated instead of the step change in reactor operating pressure since the general effect is similar (a sudden change in exhaust nozzle area will cause a change in the average propellant pressure and flow rate according to Eq. (8)). Local pressure disturbances due to acoustic lags were not included. Both perturbations cause power ramps which will lead to a characteristic controlled response.

### Effects of Changes in Control System Parameters

Since all of the perturbations, with the exception of the positive step increase in imposed reactivity, eventually result in an oscillation which depends upon the control system parameters, more calculations are needed to determine optimum values for these parameters. It was determined from a survey of reactor control mechanisms that it is possible to measure reactor periods of 600 sec or longer. This would indicate that it is feasible to reduce the minimum measurable slope to the order of 1.005, rather than 1.05 (used in the studies to date). Preliminary calculations of the engine response to a positive initial step change in fuel control valve area were performed for a minimum slope of 1.005 and various values of the gain which determines the area change. The results for three values of the gain are shown in Fig. 27. The basic characteristics of the responses are similar but the frequency of the response may be reduced to on the order of 0.01 cycles per sec. It is also possible to introduce too large a control gain and to impose oscillations of increasing amplitude which finally override the absolute flux limit controls. In these preliminary analyses, no control constant was found which would force the perturbation to a new steady-state value.

A control gain which is good for one particular perturbation may not be the best for all perturbations. Final determination of the optimum control gain will require studies of the response for all perturbations considered.

### Response of Engine to Activated Scram

The response of the engine to an activated scram which is achieved by reducing the fuel injection flow rate to zero is shown in Fig. 28. The rate of power reduction is extremely rapid even though the actual amount of contained mass lost is relatively small. These results indicate that a cutoff of fuel injection is a satisfactory method of shutting down the engine rapidly. Additional investigations of the pressure and flow response must be made to determine an appropriate shutdown method.

### Transfer Volume Requirements

The design of the transfer volume and diaphragm is determined by the most severe operating conditions which occur as a result of the perturbations that will occur. The two factors which must be considered in the transfer volume design are the maximum volume transferred during a given perturbation (both positive and negative) and the diaphragm design necessary to insure that the maximum allowable pressure differential across the transparent structure will not be exceeded. In addition to determining the transfer volume design requirements, it is necessary

to consider the volume flow rates of gas transferred during the various perturbations in order to calculate the effects on the operating conditions in the propellant region and the exhaust nozzles. All of the extreme conditions will not necessarily occur during the same perturbation response.

The diaphragm design is based on a stainless-steel diaphragm with an assumed thickness of 0.005 in. This value of diaphragm thickness,  $\Delta X_D$ , is used in Eq. (27) to determine a minimum allowable value of the diaphragm area,  $A_D$ . A combination of maximum volume transferred and minimum diaphragm area will establish the transfer volume dimensions.

The maximum positive volume displacement (vortex pressure greater than propellant pressure) occurs for the step increase in exhaust nozzle area, and its value is 4.3 ft<sup>3</sup>. The maximum negative volume displacement occurs for the step decrease in exhaust nozzle area, and its value is 3.3 ft<sup>3</sup>. This result is to be expected since this particular perturbation causes an immediate variation in propellant pressure level which must be balanced through the transfer volume. The largest value of diaphragm area necessary to insure that the minimum pressure differential in the transparent will is not exceeded is 2.98 ft<sup>2</sup> and this condition occurs during the perturbation caused by a positive ramp change in turbine wheel speed.

The transfer volume design which results from these limits has a total volume of 7.6 ft<sup>3</sup> and a cross-sectional area of 2.98 ft<sup>2</sup> if a single unit is employed. If the transfer volume is divided into 7 separate units, the dimensions of each unit would be approximately 1.1 ft<sup>3</sup> with a cross-sectional area of 0.44 ft<sup>2</sup>. If seven units are used, they are small enough to be included in the upper or lower end plug regions so that the length of the ducting to the transfer volume could be minimized and a sufficient amount of coolant would be available to maintain moderate temperature levels in the transfer volume. In this region, the cross-sectional area could be increased to on the order of 2 ft<sup>2</sup>, so that only 0.5 ft of length would be required.

The maximum instantaneous values of volumetric flow rate through the transfer volume occur for the step increases in exhaust nozzle area since, as previously mentioned, the pressure variation introduced by this perturbation is large and must be balanced through the transfer volume. The calculated volumetric flow rate is on the order of 50 ft<sup>3</sup>/sec. This is relatively large compared with the volumetric flow rate of coolant at the inlet to the propellant region (125 ft<sup>3</sup>/sec) but less than 10 percent of the volume flow rate through the exhaust nozzle (565 ft<sup>3</sup>/sec). The total duration of the high volumetric flow rate is only 0.025 sec so that the total volume transferred is on the order of 1.25 ft<sup>3</sup>. The total volume of the propellant heating region is 85 ft<sup>3</sup> so that any variations in propellant temperature due to the injection of relatively cold gas from the transfer volume will not cause noticeable changes in the average temperature of the propellant and, therefore, there will be no appreciable change in propellant conditions at the exhaust nozzle.

Any change in the control system gains may affect the response of the engine to the perturbations and, therefore, may change the transfer volume requirements. In general, it would be expected that a tighter control system would result in smaller transfer volumes with smaller cross-sectional areas.

#### Analysis of Possible Variations in Steady-State Operating Temperatures

The present reference design of the nuclear light bulb engine, particularly with regard to the cooling sequence in the internal components and the dimensions of the coolant passages, is based on maintaining certain minimum temperature levels in various components. For example, the temperature levels in the structural components which are made of beryllium (cavity liner tubes, tie rods, and flow-divider) should not exceed 1500 R and the temperature levels in the transparent structure should not exceed 2570 R. The nominal operating conditions of these components are based on calculations involving physical properties of the coolant and structural materials, dimensions of the components and predicted heat loads, all of which are subject to variations from nominal values. These variations can be uniform throughout the reactor, as would occur with a variation in reactor power level, or they may be local variations due to dimensional tolerances in a component. Since it is desirable to operate many of the components as close as possible to their temperature limits to maximize engine performance, the possible variations in temperature levels must be determined. An analysis of the variations in temperature can be used to establish the desired nominal operating temperature, to predict the probability of exceeding a given temperature level, and to identify which of the tolerance variations is most critical in determining the maximum temperature which may be reached.

The analysis of the temperature variations consisted of a determination of the extremes in temperature variation which would be caused by each parameter which was varied and a statistical analysis of the effects of the five largest extreme values to determine the probability of exceeding selected temperature levels.

The procedure employed is similar to that described in Ref. 14. The equations which determine the temperature levels or temperature differences as a function of the physical properties and component dimensions were used to determine the contribution of each variable to the off-design temperature. For example, the temperature rise in a coolant passage may be expressed as

$$\Delta T_c = \frac{Q}{WC_p} \quad (35)$$

where  $\Delta T_c$  = temperature rise in coolant in deg R,  $Q$  = heat input in Btu/sec,  $W$  = mass flow rate in lb/sec, and  $C_p$  = specific heat in Btu/lb-deg R. The effect of varying  $Q$ ,  $W$ , or  $C_p$  may be determined by taking the partial derivative of  $\Delta T_c$  with respect to the appropriate variable, so that

$$\frac{\partial \Delta T_c}{\partial Q} = \frac{1}{WC_p} \quad (36)$$

$$\frac{\partial \Delta T_c}{\partial Q} = \frac{\Delta T_c}{Q} \quad (37)$$

The actual value of the variation in  $\Delta T_c$  due to a variation in  $Q$  of  $\Delta Q$  is equal to

$$\frac{\partial \Delta T_c}{\partial Q} \Delta Q = \frac{\Delta Q}{Q} \Delta T_c \quad (38)$$

where  $Q$  and  $T_c$  in Eq. (38) are nominal values. Similarly, the variations caused by  $W$  and  $C_p$  are

$$\frac{\partial \Delta T_c}{\partial W} = \frac{\Delta W}{W} (-\Delta T_c) \quad (39)$$

$$\frac{\partial \Delta T_c}{\partial C_p} = \frac{\Delta C_p}{C_p} (-\Delta T_c) \quad (40)$$

and the sum of all of the variances is

$$\theta = \sum_{i=1}^n \frac{\partial T}{\partial u_i} \Delta u_i \quad (41)$$

where  $\partial T / \partial u_i$  is evaluated at the mean value of the variables.

It was assumed that each of the variables had a rectangular probability distribution, that is, there is an equal probability of the variable having any value between an upper and lower limit. The variables which were considered and their limits are shown in Table VIII. It may be noted in Table VIII that similar variances in physical properties and temperature levels are employed in all regions but the dimensional tolerances vary depending upon the size of the coolant passage. Allowable wall thickness variations were assumed to be large since there is no simple nondestructive test which could insure close tolerance on wall thicknesses.

The extremes of the temperature variation due to each parameter listed in Table VIII were calculated for the eight regions investigated. The sum of these extremes is the maximum temperature variation which could occur in the region. It is possible to determine a distribution function of the variation from the nominal temperature and to determine the probability of exceeding the nominal temperature by any amount. The method of combining the individual variations is described in Ref. 14 and, to simplify the calculation of the probability of exceeding the nominal temperature by any amount, only the five largest variances were used in the calculation. The maximum variation and the five largest variances are tabulated for each region in Table IX. The probability of exceeding any given value above or below the nominal value is shown in Fig. 29. In Fig. 29, some of the probability functions vary considerably from a normal distribution function. In these cases, one of the variations is much larger than the others and tends to distort the probability function.

Based on the results of this analysis, it is concluded that it may be desirable to reduce the nominal values of the operating temperatures in some of the critical components, such as the transparent structure and the cavity liner, to establish a lower probability of exceeding the maximum allowable temperatures. Further analyses should be conducted before making such changes in the reference engine design.



# REFERENCES

1. McLafferty, G. H. and H. E. Bauer: Studies of Specific Nuclear Light Bulb and Open-Cycle Vortex-Stabilized Gaseous Nuclear Rocket Engines. United Aircraft Research Laboratories Report G-910093-37, prepared under Contract NASw-847, September 1967. Also issued as NASA CR-1030.
2. Latham, T. S., H. E. Bauer, and R. J. Rodgers: Studies of Nuclear Light Bulb Start-Up Conditions and Engine Dynamics. United Aircraft Research Laboratories Report H-910375-4, prepared under Contract NASw-847, September 1969.
3. Latham, T. S.: Nuclear Studies of the Nuclear Light Bulb Rocket Engine. United Aircraft Research Laboratories Report G-910375-3, prepared under Contract NASw-847, September 1968. Also issued as NASA CR-1315.
4. Klein, J. F. and W. C. Roman: Results of Experiments to Simulate the Radiant Heating of the Propellant in a Nuclear Light Bulb Engine Using a D-C Arc Radiant Heat Source. United Aircraft Research Laboratories Report J-910900-1, prepared under Contract SNPC-70, September 1970.
5. Jaminet, J. F. and A. E. Mensing: Experimental Investigations of Simulated Fuel Containment in R-F Heated and Unheated Two-Component Vortexes. United Aircraft Research Laboratories Report J-910900-2, prepared under Contract SNPC-70, September 1970.
6. Vogt, P. G.: Development and Tests of Small Fused Silica Models of Transparent Walls for the Nuclear Light Bulb Engine. United Aircraft Research Laboratories Report J-910900-3, prepared under Contract SNPC-70, September 1970.
7. Roman, W. C.: Experimental Investigations of a High-Intensity R-F Radiant Energy Source to Simulate the Thermal Environment in a Nuclear Light Bulb Reactor. United Aircraft Research Laboratories Report J-910900-4, prepared under Contract SNPC-70, September 1970.
8. Krascella, N. L.: Analytical Study of the Spectral Radiant Flux Emitted from the Fuel Region of a Nuclear Light Bulb Engine. United Aircraft Research Laboratories Report J-910904-1, prepared under Contract SNPC-70, September 1970.
9. Palma, G. E.: Optical Absorption in Transparent Materials During 1.5-Mev Electron Irradiation. United Aircraft Research Laboratories Report J-910929-1, prepared under Contract SNPC-70, September 1970.

## REFERENCES (Continued)

10. McLafferty, G. H.: Investigation of Gaseous Nuclear Rocket Technology - Summary Technical Report. United Aircraft Research Laboratories Report H-910093-46, prepared under Contract NASw-847, November 1969.
11. Nesmeyanov, A. N.: Vapor Pressures of the Chemical Elements. Elsinor Publishing Company, Amsterdam, 1963.
12. Roback, R.: Theoretical Performance of Rocket Engines Using Gaseous Hydrogen in the Ideal State at Stagnation Temperatures up to 200,000 R. United Aircraft Research Laboratories Report E-910093-30, prepared under Contract NASw-847, October 1966. Also issued as NASA CR-696.
13. Richards, E. J. and D. J. Mead: Noise and Acoustic Fatigue in Aeronautics. John Wiley & Sons, Ltd., London, 1968, pp. 169-172.
14. Abernathy, F. H.: The Statistical Aspects of Nuclear Reactor Fuel Element Temperature. Nuclear Science and Engineering, Vol. 11, 1961, pp. 290-297.
15. Kunze, J. F. and P. L. Chase: Critical Experiments on a Modular Cavity Reactor. Idaho Nuclear Corporation Report IN-1376, prepared under Contract C-67747-A, May 1970. Also issued as NASA CR-72681.
16. Engle, W. W.: A Users Manual for ANISN, A One-Dimensional Discrete Ordinates Transport Code with Anisotropic Scattering. Union Carbide Corporation Nuclear Division Report K-1693, March 30, 1967.
17. Joanou, G. D. and J. S. Dudek: GAM-1, A Consistent P-1 Multigroup Code for the Calculation of Fast Neutron Spectra and Multigroup Constants. General Atomics Report GA-1850, June 1961.
18. Shudde, R. H. and J. Dyer: TEMPEST-II, A Neutron Thermalization Code. North American Aviation Report AMTD-111, September 1960.
19. Canfield, E. H., R. N. Stuart, R. P. Freis, and W. H. Collins: SOPHIST-I, An IBM 709/7090 Code which Calculates Multigroup Transfer Coefficients for Gaseous Moderators. University of California, Lawrence Radiation Laboratory Report UCRL-5756, October 1961.
20. Pincock, G. D. and J. F. Kunze: Cavity Reactor Critical Experiment, Volume I. NASA CR-72234, prepared by General Electric Company, Idaho Falls, Idaho, under Contract C-67747-A, September 6, 1967.

REFERENCES (Concluded)

21. Jarvis, G. A.: Cavity Reactor. Proceedings of an Advanced Nuclear Propulsion Symposium, Los Alamos Scientific Laboratory Report LA-3229-MS, p. 344.
22. Thurman, J. L.: Optimization of Steady-State Thermal Design of Space Radiators. Journal of Spacecraft and Rockets, Vol. 6, No. 10, October 1969, pp. 1114-1119.

## LIST OF SYMBOLS

A	Area, $\text{ft}^2$
A*	Nozzle throat area, $\text{ft}^2$
A <sub>D</sub>	Diaphragm cross-sectional area, $\text{ft}^2$
A <sub>F</sub>	Fuel injection control valve flow area, $\text{ft}^2$
a <sub>D</sub>	Diaphragm acceleration, $\text{ft}/\text{sec}^2$
B <sub>j</sub>	Constant
C <sub>p</sub>	Specific heat, Btu/lb-deg R
d <sub>i</sub>	Coolant passage internal diameter, ft
F	Force, lb
g	Acceleration due to gravity, $32.2 \text{ ft}/\text{sec}^2$
I	Moment of inertia of turbopump, $\text{ft-lb-sec}^2$
K <sub>C</sub>	Thermal conductivity of coolant, Btu/ft-sec-deg R
K <sub>F</sub>	Fuel injection flow rate calibration factor, $\text{lb}/\text{sec-ft}^2$
K <sub>m</sub>	Thermal conductivity of structure, Btu/ft-sec-deg R
K <sub>P</sub>	Throat flow parameter, $\text{lb-(deg R)}^{\frac{1}{2}}/\text{sec-ft}^2\text{-atm}$ (see Ref. 12)
k	Effective multiplication factor
L	Coolant passage length, ft
$\ell^*$	Prompt neutron lifetime, sec
M <sub>C</sub>	Critical mass, lb
M <sub>F</sub>	Nuclear fuel loading, gm or lb

## LIST OF SYMBOLS (Continued)

$M_H$	Hydrogen mass, lb
$N$	Neutron density, neutrons/cm <sup>3</sup>
$PR$	Turbine pressure ratio
$P$	Pressure, atm
$P_C$	Total chamber pressure, atm
$P_F$	Fuel injection pressure, atm
$Q$	Power level or heat deposition rate, Btu/sec or megw
$Q_{FP}$	Fission product heating, Btu/sec
$Q_P$	Pump power requirement, Btu/sec
$Q_T$	Turbine power output, Btu/sec
$q_o$	Dynamic pressure, atm
$R_C$	Cavity radius, ft
$R_F$	Fuel region radius, ft
$s$	Coolant hole spacing
$T$	Temperature, deg R
$T^*$	Equivalent black-body radiating temperature, deg R
$T_{BeO}$	Average BeO moderator temperature, deg R
$T_{ci}$	Coolant inlet temperature, deg R
$T_F$	Fuel temperature, deg R
$T_G$	Average graphite moderator temperature, deg R

## LIST OF SYMBOLS (Continued)

$T_{IN}$	Turbine inlet temperature, deg R
$T_M$	Average moderator temperature, deg R
$T_P$	Propellant exit temperature, deg R
$(T_R)_{IN}$	Radiator inlet temperature, deg R
$(T_R)_{OUT}$	Radiator outlet temperature, deg R
$T_W$	Transparent-wall temperature, deg R
$t$	Total elapsed time since initiation of start-up or perturbation, sec
$t_0$	Starting time of perturbation, sec
$u$	Dummy variable
$V$	Volume, ft <sup>3</sup>
$V_T$	Total volume, ft <sup>3</sup>
$V_{TR}$	Required transfer volume, ft <sup>3</sup>
$v_D$	Diaphragm velocity, ft/sec
$W$	Mass flow rate, lb/sec
$W_B$	Buffer gas flow rate, lb/sec
$W_F$	Fuel injection rate, lb/sec
$W_L$	Fuel loss rate, lb/sec
$W_N$	Neon flow rate, lb/sec
$W_P$	Propellant mass flow rate, lb/sec
$(W_T)_{RAD}$	Total radiator weight, lb
$X$	Coolant tube wall thickness, ft

## LIST OF SYMBOLS (Continued)

$\beta_i$	Delayed neutron fraction
$\Delta M$	Change in mass, gm or lb
$\Delta M_F$	Change in fuel mass, lb
$\Delta P$	Pressure differential, atm
$\Delta P'$	Root mean square pressure differential, atm
$\Delta P_F$	Fuel injection pressure differential, atm
$\Delta P_{pp}$	Primary pump pressure, rise, atm
$\Delta P_r$	Pressure loss in radiator, atm
$\Delta P_T$	Turbine pressure drop, atm
$\Delta P_V$	Turbine control valve pressure drop, atm
$\Delta P_w$	Pressure difference across transparent wall, PSF
$\Delta Q$	Power change, Btu/sec
$\Delta R_F$	Change in fuel region radius, cm or in.
$\Delta T_C$	Coolant temperature differential, deg R
$\Delta T_M$	Change in average moderator temperature, deg R
$\Delta T_P$	Change in propellant exit temperature, deg R
$\Delta T_V$	Temperature variation from nominal value, deg R
$(\Delta T_V)_{MAX}$	Maximum temperature variation from nominal value, deg R
$\Delta t$	Time increment, sec
$\Delta V$	Volume differential, ft <sup>3</sup>

## LIST OF SYMBOLS (Continued)

$\Delta X_D$	Diaphragm thickness, ft
$\Delta \rho_H$	Change in hydrogen propellant density, lb/ft <sup>3</sup>
$\delta A_{F1}$	Imposed fuel injection control valve flow area change, ft <sup>2</sup>
$\delta A_{F2}$	Fuel injection control valve flow area change imposed by control system, ft <sup>2</sup>
$\delta k$	Total reactivity change
$\delta k_0$	Reactivity required to compensate for loss of delayed neutrons
$\delta k_1$	Imposed reactivity change
$\delta k_2$	Feedback reactivity change
$\delta K_{CM}$	Moderator coolant reactivity coefficient
$\delta K_M$	Nuclear fuel reactivity coefficient
$\delta K_P$	Propellant temperature and density reactivity coefficient
$\delta K_{TM}$	Moderator temperature reactivity coefficient
$\delta v_1$	Input perturbation of turbine wheel speed, rpm
$\eta_P$	Pump efficiency
$\eta_T$	Turbine efficiency
$\theta$	Total temperature differential, deg R
$\lambda_F$	Fuel decay constant, sec <sup>-1</sup> (reciprocal of fuel residence time)
$\lambda_i$	Neutron precursor decay constants, sec <sup>-1</sup>



## LIST OF SYMBOLS (Concluded)

$\mu$	Fluid viscosity, lb/ft-sec
$\nu$	Turbopump wheel speed, rpm
$\rho$	Density, lb/ft <sup>3</sup>
$\rho_{B6}$	Buffer-gas density at edge of fuel region, lb/ft <sup>3</sup>
$\rho_D$	Diaphragm material density, lb/ft <sup>3</sup>
$\rho_H$	Hydrogen propellant density, lb/ft <sup>3</sup>
$\rho_{Ne}$	Neon density, lb/ft <sup>3</sup>
$\rho_p$	Average fluid density in pump, lb/ft <sup>3</sup>
$\tau$	Acoustic delay time, sec
$\tau_D$	Diaphragm response time, sec
$\tau_V$	Exhaust nozzle valve time lag, sec

Subscripts

j	jth region
o	Denotes reference condition

## APPENDIX A

COMPARISON OF CALCULATED CRITICAL MASSES  
WITH RESULTS OF GE-IDAHO EXPERIMENTS

Calculations of U-235 critical masses for the seven-module cavity reactor experiment carried out by GE-Idaho were performed and the results were compared with the measured critical masses. The seven-module configuration is described in Ref. 15; a schematic diagram of the reactor is shown in Fig. 30. In the experiment, the propellant was simulated by inserting polystyrene (CH) and polyethylene (CH<sub>2</sub>) between the nuclear fuel and the cavity walls.

Previous experience has shown that two-dimensional calculations for cavity reactors with complex geometries are very lengthy. Therefore, it was decided to limit calculation procedures to those for one-dimensional models of the configuration. Two models were chosen: (1) a spherical equal-volume model with fuel, simulated propellant, voids, tank liners, and heavy water described as distinct zones within the reactor core (see Fig. 30), and (2) a spherical equal-volume model with the core materials homogenized (Fig. 31). For the model with the homogenized core, cell-weighted (flux- and volume-weighted) average cross sections were obtained for the central module of the core from infinite-cylinder, one-dimensional calculations. The averaged cross sections for the central module were then used for the entire homogenized core. All calculations were performed using neutron transport theory with S<sub>4</sub> angular quadrature (Ref. 16). Cross sections were generated in the manner described in Ref. 3. Fast group cross sections were calculated using the HRG code (Ref. 17), thermal group cross sections were calculated using TEMPEST-II (Ref. 18), and thermal-group up- and down-scattering probabilities were calculated using the SOPHIST code (Ref. 19). Twenty-five neutron energy groups were employed.

The experimentally measured critical mass, when corrected for insertion of a nozzle plug, removal of the end-reflector table gap, and foil-to-gas biasing was 7.82 kg (Ref. 15). As shown in the upper portion of Table X, critical masses calculated for the equal-volume detailed-core and homogenized-core spherical geometries were 6.93 and 6.52 kg, respectively. Thus, these calculated critical masses determined by two different approaches were within 11 to 16 percent of the experimentally measured fuel loading. These results also correlate to calculated critical masses for the reference nuclear light bulb engine for which two-dimensional transport theory results (Ref. 3) predicted a critical mass of 30.9 lb (14 kg) and the corresponding spherical equal-volume, detailed core model predicted 28.2 lb (12.8 kg), a difference of 10 percent.

Considering the geometric compromises involved in using spherical models of a basically cylindrical configuration, the comparisons of calculated and experimental fuel loadings are close enough to provide confidence in both spherical models for predicting critical masses for seven-module type cavity reactors such as the nuclear light bulb engine.

It is also desirable to predict reactivity changes produced by composition and configuration changes. Therefore, additional one-dimensional calculations were performed to compare measured and calculated material worths and to compare measured and calculated effects of variations in fuel region radius on critical fuel loading. Material worths for the nuclear fuel and simulated propellant were calculated using the homogenized-core spherical model. Comparisons of the calculated results to the measured values are shown in Table X. The agreement is within 15 to 20 percent.

Calculations of the effects of varying the fuel region radius were also performed using the homogenized-core spherical model. The results of these calculations are shown in Fig. 32 in which experimentally measured effects of fuel region radius changes are shown for the seven-module experiment and some single-cavity experiments (Refs. 15, 20, and 21). The calculated results for the seven-module experiment are in good agreement with the measurements. Also, the effects of variations in fuel region radius are less severe for the seven-module configuration than for single-cavity reactors.

## APPENDIX B

## SPACE RADIATOR PARAMETRIC STUDIES

A series of preliminary calculations was made to determine the effects of various parameters such as radiator materials, temperature levels, and dimensions on radiator weight and pressure loss in a space radiator designed to reject a portion of the moderator heat load. The method of analysis employed was similar to that described in Ref. 22 for the optimization of double surface radiators neglecting the effects of incident radiation from external sources. In this method, the radiator heat load, tube diameter, tube and fin thickness, inlet temperature, outlet temperature, and coolant weight flow are chosen for the desired radiator configuration. The fin width, tube length, total radiator weight and coolant pressure loss are then calculated for a series of assumed values of temperature at a point on the fin midway between the tubes. The variations in fin width and tube length will result in a minimum value of radiator weight for a specific combination of fin width and tube length. Calculations were performed to determine the effects of tube diameter and number of tubes in order to select optimum values of these variables. A specific tube diameter and number of tubes were selected and used in the calculation of radiator weight and pressure loss for aluminum, stainless steel, and tungsten radiators at various inlet and outlet temperatures.

It was determined that a variation in the number of tubes with a fixed inside diameter does not affect radiator weight but does affect pressure loss by reducing the required tube length. Reductions in tube diameter do decrease radiator weight but also increase pressure loss. The final values selected were a tube inside diameter of 0.24 in. with 6000 tubes.

The maximum allowable temperature in the radiator is determined by the radiator material. It was assumed that the maximum allowable temperatures in aluminum, stainless steel, and tungsten are 1500 R, 2500 R, and 3500 R, respectively. The required wall thickness of the tubes was based on the hoop stress associated with an internal pressure of approximately 100 atm. For a 0.24-in.-ID tube, this pressure requires a tube wall thickness of 0.03125 in. for aluminum or stainless steel (5000-psi design stress) and 0.01567 in. for tungsten (10,000-psi design stress). A series of calculations of radiator weight for the aforementioned geometry and inlet temperatures was performed for a radiator heat load of  $1.09 \times 10^5$  Btu/sec (2.5 percent of total engine power) with various values of radiator exit temperatures. The results of these studies are shown in Figs. 33 and 34.

In Fig. 33, the total radiator weight is very dependent upon the temperature range over which the radiator is operating. It is therefore not possible to determine a value of radiator weight for use with the engine without specifying the portion of the moderator heat load which is to be removed. Temperatures of 2500 R or higher are attained in the engine coolant circuits only in the solid moderator region, and the major cooling problems in the engine are at lower levels, such as those encountered in cooling the transparent structure (2000 R) or in cooling the beryllium structural components (1400 R). It appears that, if high-temperature heat is rejected (3500 R), the radiator weights are on the order of 1000-lb per percent of total engine power rejected, but if lower temperature heat is removed, the required radiator weight will increase.

It should be noted that the analysis does not include any consideration of the tube thickness which would be required to provide protection from meteroid penetration. Some preliminary investigations have indicated that the large areas of the radiators and thin walls would result in a high probability of meteroid damage. It has not been determined if it is more desirable to use thicker walls to eliminate the probability of meteroid penetration or to tolerate a small leakage rate of radiator coolant due to leaks caused by penetrations. If the radiator has on the order of 6000 tubes and a total coolant weight flow of 20 lb/sec, the loss of a single radiator tube by meteroid damage would cause a leak rate of 0.0033 lb/sec. Since the total running time anticipated for the engine is on the order of 1000 sec, this leak rate would result in the loss of 3.3 lb which is negligible relative to the primary hydrogen flow requirement of 42,300 lb for a 1000-sec run.

## APPENDIX C

## ALTERNATE CONFIGURATION FOR NUCLEAR LIGHT BULB ENGINE

Analyses were made for a nuclear light bulb engine in which the average inside diameter of the unit cells (hence, the number of cells per engine) was varied. The motivations for reducing unit cell size were to increase the allowable bursting and compressive pressure loads on the transparent walls and to bring the unit cell size into the range which could be tested full-scale in a nuclear reactor. Performance was calculated for a constant power level of 4600 megw and for constant coolant and propellant pressure drops throughout the system. It was found that for large numbers of cells in a hexagonal array (61 or more), engine performance deteriorated. This reduction in performance resulted from increases in flow rates, coolant passage sizes, and engine weight required as convective heat loads to the transparent walls and cavity liners increased. The increase in convective heat load as the number of cells increases is caused by an accompanying increase in surface-to-volume ratio for the propellant ducts.

Additional matters of concern with smaller unit cells are the divergence and effective length-to-diameter ratio of the propellant channels. These two factors should be chosen to minimize convective heat transfer to the transparent walls and cavity liners and to provide adequate stream divergence to minimize propellant seed coating on duct walls. An alternate configuration (Fig. 35) was conceived in which nearly rectangular propellant ducts are shared by adjacent cells. Each propellant channel subtends a 60-deg segment of transparent wall such that in a hexagonal array, each cell shares six propellant channels with its six surrounding neighbors. Interstitial moderator regions can be designed to contain the internally cooled transparent wall manifolding.

The advantages of this configuration are:

1. Each arc of transparent wall is 60-deg instead of 120-deg. This increases the allowable collapsing pressure load by approximately 4 times.
2. The transparent-wall manifolds can be imbedded in moderator material, thus doing away with the strut supports in the current reference engine.
3. The divergence of the propellant ducts is slightly larger and the ratio of propellant duct length to inlet width is much smaller for the alternate configuration than for the reference engine. This should reduce propellant seed coating on duct walls.

4. For fixed transparent-wall radius and propellant duct cross-sectional area, the propellant duct surface-to-volume ratio is smaller for the alternate configuration than for the reference engine, thus reducing the convective heat load to the duct walls.

Specific numerical comparisons of various properties of a 37-cell alternate configuration and the reference engine are contained in Table XI. Preliminary calculations indicate that a 37-cell engine employing the alternate propellant duct configurations could be designed with values of convective heat loads, propellant duct divergence, and a propellant duct length-to-inlet width ratio similar to those for the reference engine. At a power level of 4600 megw this configuration would have a specific impulse of 1760 sec, a hydrogen flow rate of 47.1 lb/sec, a total propellant flow rate (hydrogen, seed, transpiration coolant) of 56.8 lb/sec, and a thrust of 100,000 lb. Because of the increase in the number of cells, the transparent-wall diameter would be reduced to 7.4 in. The allowable bursting and collapsing pressures across the transparent walls would be 6.9 and 7.4 atm, respectively, compared with about 1.0 and 0.1 atm for the reference engine. Also, in-reactor tests of unit cells more nearly approaching the size of the full-scale engine cells could be performed.

TABLE I  
FULL-POWER, STEADY-STATE MODERATOR AND  
STRUCTURE HEAT DEPOSITION RATES

Fuel - U-233

Region	Mechanism of Heating	Heat Deposition Rate, Btu/sec**
Pressure Vessel	Neutron and Gamma	$0.1093 \times 10^5$ *
Nozzles	Neutron and Gamma	$0.0008 \times 10^5$
Flow Divider	Neutron and Gamma and Conduction	$0.0676 \times 10^5$
Tie Rods	Neutron and Gamma and Conduction	$0.0510 \times 10^5$
Cavity End Walls	Thermal Radiation and Conduction	$0.0606 \times 10^5$
Cavity Liner	Thermal Radiation and Conduction	$0.7661 \times 10^5$
Transparent Structure	Thermal Radiation and Conduction	$1.1290 \times 10^5$
Fuel Recycle System	Removal of Heat from Fuel	$0.605 \times 10^5$ ***
Upper and Lower End Moderator	Neutron and Gamma	$0.6640 \times 10^5$
Beryllium Oxide	Neutron and Gamma	$0.8457 \times 10^5$
Graphite	Neutron and Gamma	$0.4607 \times 10^5$
Direct Hydrogen Heating	Neutron and Gamma	$0.5564 \times 10^5$
	Total	$5.32 \times 10^5$
	Percent of Total Power	12.15 percent

\* Total heating in pressure vessel is  $0.165 \times 10^5$ . It is assumed that only 2/3 of the total will be removed by the closed secondary hydrogen coolant circuit and the remaining 1/3 will be removed by the hydrogen which is used for transpiration cooling of the exhaust nozzles.

\*\*  $10^5$  Btu/sec = 105.5 megw.

\*\*\*Includes  $0.305 \times 10^5$  Btu/sec from fission product heating (corresponds to 5-min run time).



TABLE II

FULL-POWER, STEADY-STATE TEMPERATURE, ENTHALPY, AND  
PRESSURE LEVELS IN PRIMARY HYDROGEN PROPELLANT CIRCUIT

Hydrogen Propellant Flow = 42.3 lb/sec  
Station Numbers Refer to Locations Shown in Fig. 2

Station	Location	Temperature, deg R	Enthalpy, Btu/lb	Pressure, atm
1000	Pump Inlet	36	120	1.0
1010	Fuel Cycle Heat Exchanger Inlet	90	550	713
1020	Secondary Heat Exchanger Inlet	640	1,979	712
1025	Secondary Heat Exchanger Outlet	2,095	7,143	710
1040	Turbine Outlet	1,889	6,600	507
1060*	Upper End Moderator Outlet	2,039	7,135	506.9
1070*	Axial Beryllium Oxide Outlet	2,608	9,134	500.64
1090*	Lower End Moderator Outlet	2,907	10,172	500.4
1110	Graphite Outlet	3,217	11,262	500
1115	Propellant, Including Direct H <sub>2</sub> Heating	12,157	103,500	500

\*Lumped in solid moderator region in Fig. 2

TABLE III

FULL-POWER, STEADY-STATE TEMPERATURE, ENTHALPY, AND  
PRESSURE LEVELS IN CLOSED SECONDARY HYDROGEN CIRCUIT

Hydrogen Coolant Circuit Flow = 42.3 lb/sec  
Station Numbers Refer to Locations Shown in Fig. 2

Station	Location	Temperature, deg R	Enthalpy, Btu/lb	Pressure, atm
2010	Pressure Vessel Liner Inlet	741	2250	510
2016	Nozzle Inlet	843	2508	508
2017	Lower End Wall Liner Inlet	843	2510	507.5
2020	Tie Rod, Flow Divider, and Cavity Liner Inlet	858	2582	507.5
2026	Upper End Wall Liner Inlet	1439	4673	502.4
2030	Transparent Wall Inlet	1454	4745	502.4
2040	Transparent Wall Outlet	2195	7414	500
2000	Heat Exchanger Outlet	739	2250	498

TABLE IV

FULL-POWER, STEADY-STATE TEMPERATURE AND  
ENTHALPY LEVELS IN NEON AND FUEL CIRCUIT

(Note: Station Numbers Refer to Locations Shown in Fig. 2)

Total Neon Flow Per Cavity\* = 21.1 lb/sec (147.7 lb/sec for 7 cavities)

Total Fuel Flow Per Cavity = 1.07 lb/sec (7.5 lb/sec for 7 cavities)

Station	Location	Temperature, deg R	Enthalpy, Btu/lb
3000	H-Ne Heat Exchanger Outlet	184	47
3010	Pump Outlet*	189	48
3020	Cavity Outlet	2663	457
3030	H-Ne Heat Exchanger Inlet	2663	457

\*The required neon flow rate into each cavity is 3.51 lb/sec (24.57 lb/sec for 7 cavities); 17.59 lb/sec (123.13 lb/sec for 7 cavities) of neon bypasses the cavity and is mixed with the flow which exits from the cavity to condense the fuel before the neon-fuel mixture enters the separator.

TABLE V

SEQUENCE OF EVENTS DURING START-UP FOR  
LINEAR TEMPERATURE RAMPS

Conditions After Event

Time	Event	Engine Pressure, $P_c$ - atm	Propellant Flow Rate, $W_p$ - lb/sec	Neon Flow Rate, $W_N$ - lb/sec	Fuel Flow Rate, $W_F$ - lb/sec	Fuel Mass, $M_F$ - lb	Engine Power, $Q$ - megw
------	-------	---------------------------------	---	-----------------------------------	-----------------------------------	--------------------------	-----------------------------

PHASE I

-80 sec to -55 sec	Bring turbo-pump up to 22000 rpm using external power source	0	0	0	0	0	0
-55 sec to -40 sec	Pressurize engine to 71 atm	71	0	0	0	0	0
-40 sec to -35 sec	Initiate flow in all circuits except fuel injection	71	0.423	21	0	0	0
-35 sec to -15 sec	Start fuel injection to obtain cold critical mass (27.1 lb)	71	0.423	21	6.775	27.1	0
-15 sec to 0 sec	Stabilize engine at 0.1 percent of full power	71	0.423	21	6.775	27.1	4.6

(Continued)

TABLE V (Concluded)

Time	Event	Engine Pressure, $P_c$ - atm	Propellant Flow Rate, $W_P$ - lb/sec	Neon Flow Rate, $W_N$ - lb/sec	Fuel Flow Rate, $W_F$ - lb/sec	Fuel Mass, $M_F$ - lb	Engine Power, $Q$ - megw
------	-------	---------------------------------	---	-----------------------------------	-----------------------------------	--------------------------	-----------------------------

## PHASE II

0	Begin start-up power ramp	71	0.423	21	6.775	27.1	4.6
0-6 sec or 0-60 sec	Variation during start-up power ramp	see Fig. 10	linear	linear	see Fig. 5	see Fig. 14	see Fig. 3
6 sec or 60 sec	End start-up power ramp	500	42.3	147.7	7.75	see Fig. 14	4600

TABLE VI

## ASSUMPTIONS EMPLOYED IN ENGINE DYNAMICS SIMULATION

1. Reactivity feedback coefficients and operating characteristics at nominal full-power were taken from Refs. 1 and 2, and have the following values:

Operating Power	= 4,600 megw
Chamber Pressure	= 500 atm
Fuel Radiating Temperature	= 15,000 deg R
Propellant Exit Temperature	= 12,000 deg R
Average Fuel Residence Time	= 4 sec
Critical Mass	= 30 lb
Prompt Neutron Lifetime	= 0.000516 sec
Fuel Radius	= 0.681 ft
Average Thermal Fission Cross Section	= 193 barns
Steady-State Fuel Injection Rate	= 7.5 lb/sec
Excess Reactivity Required to Offset Loss of Delayed Neutrons, $\delta k_0$	= 0.001480

## Reactivity Feedback Coefficients:

Fuel, $(\delta k/k)/(\Delta M_F/M_F)$	= +0.384
Moderator Temperature, $(\delta k/k)/(\Delta T_M/T_M)$	= +0.0083
Propellant Density, $(\delta k/k)/(\Delta \rho_H/\rho_{H_0})_{prop}$	= +0.0200
Moderator Coolant Density, $(\delta k/k)/(\Delta \rho_H/\rho_{H_0})_{mod}$	= -0.0155
Fuel Region Radius, $(\delta k/k)/(\Delta R_F/R_F)$	= +0.0520
Propellant Temperature, $(\delta k/k)/(\Delta T_P/T_{P_0})$	= +0.0100

2. Heat storage capacity is negligible in all components except the solid moderator region. The assumed values of  $mc_p$  in the solid moderator regions were 5124 Btu/deg R for the BeO and 6440 Btu/deg R for the graphite.
3. Choked flow conditions exist in the exit nozzle throat.
4. The turbopump characteristics used in the program are:
- |                                     |                              |
|-------------------------------------|------------------------------|
| Steady-state wheel speed            | = 22,000 rpm                 |
| Moment of inertia of turbopump unit | = 130 ft-lb-sec <sup>2</sup> |
5. The total flow rate in all circuits will vary directly with turbine wheel speed and the pump head rise will vary with the square of the wheel speed.

(Continued)

TABLE VI (Concluded)

6. Fission product heating in the fuel cycle circuit varies with time according to the expression  $Q_{FP} = 1890\sqrt{t}$ , where  $t$  is the total elapsed time of operation in seconds, and  $Q_{FP}$  is in Btu/sec.
7. Constant physical properties of the coolants are used in each region.
8. Constant transport lags and acoustic lags assumed for all regions and piping systems on the basis of reference coolant flow velocities and local temperature and pressure levels.
9. Fuel injection rate assumed to vary as the square root of the injection system pressure drop,  $W_F \propto \sqrt{P_F - P_C}$  where  $P_F$  regulated to be 500.25 atm.

TABLE VII

CHARACTERISTIC TIMES FOR SOUND TRANSMISSION THROUGH GASES  
IN ENGINE COMPONENTS AT FULL-POWER OPERATING CONDITIONS

Region	Volume, ft <sup>3</sup>	Charac- teristic Length, ft	Average Gas Density, lb/ft <sup>3</sup>	Total Gas Weight, lb	Sonic Velocity, ft/sec	Charac- teristic Time, 10 <sup>-3</sup> sec
--------	----------------------------	--------------------------------------	--	-------------------------------	------------------------------	--

Primary Hydrogen Propellant Circuit

Heat Exchanger, Turbopump and Manifolding	153	20	0.686	105	8,200	2.44
Solid Moderator	52.3	17.6	0.493	25.8	9,780	1.80
Cavity Region	85	6.0	0.171	14.5	14,000	0.43
Nozzle	20	2.4	0.075	1.5	21,000	0.12
Total Primary Propellant System	310	46.0	0.457	141.8	9,600	4.79

Neon and Fuel Circuit

Vortex Region	85	6.0	0.955	81	5,880	1.02
Piping, Manifolding, Heat Exchanger and Separator Region	92	20	1.96	180	2,860	7.00
Total Neon and Fuel Circuit	177	26.0	1.47	261	3,250	8.02



TABLE VIII

FACTORS AND ASSUMED INPUT VARIABLES USED IN TEMPERATURE VARIATION ANALYSIS

Symbol	Factor	Assumed Input Variation Limits
$\Delta Q/Q$	Heat Flux Deposition Rate, Btu/sec	$\pm 0.10$
$\Delta W/W$	Mass flow rate, lb/sec	$\pm 0.05$
$\Delta C_p/C_p$	Specific heat, Btu/lb-deg R	$\pm 0.01$
$\Delta \mu/\mu$	Viscosity of coolant, lb/ft-sec	$\pm 0.10$
$\Delta K_c/K_c$	Thermal conductivity of coolant, Btu/ft-sec-deg R	$\pm 0.10$
$\Delta K_m/K_m$	Thermal conductivity of structure, Btu/ft-sec-deg R	$\pm 0.10$
$\Delta T_{ci}/T_{ci}$	Coolant inlet temperature, deg R	$\pm 0.05$
$\Delta L/L$	Coolant passage length, ft	$\pm 0.01$
$\Delta d_i/d_i$	Coolant passage internal diameter, ft	see below
$\Delta X/X$	Coolant tube wall thickness, ft	see below
$\Delta s/s$	Coolant hole spacing	see below

## Region

Variable	Transparent Structure	Cavity Liner	Upper Graphite	Upper BeO	Axial BeO	Lower BeO	Lower Graphite	Axial Graphite
$\Delta d_i/d_i$	$\pm 0.20$	$\pm 0.10$	$\pm 0.01$	$\pm 0.10$	$\pm 0.10$	$\pm 0.10$	$\pm 0.05$	$\pm 0.025$
$\Delta X/X$	$\pm 0.40$	$\pm 0.40$	NA*	NA	NA	NA	NA	NA
$\Delta s/s$	NA	NA	$\pm 0.01$	$\pm 0.10$	$\pm 0.10$	$\pm 0.10$	$\pm 0.05$	$\pm 0.025$

\*not applicable

TABLE IX  
TEMPERATURE VARIATIONS IN SPECIFIC REGIONS OF NLB REACTOR

Region	Factors Which Lead to Greatest Variation in Material Temperature (see Table VIII)	Resulting Temperature Variation Extremes, deg R
Transparent Structure	$\Delta Q/Q$	$\pm 103.6$
	$\Delta W/W$	$\pm 41.25$
	$\Delta d_i/d_i$	$\pm 21.20$
	$\Delta X/X$	$\pm 76.00$
	$\Delta T_{ci}/T_{ci}$	$\pm 72.70$
Total Temperature Variation		$\pm 314.75$
Cavity Liner	$\Delta Q/Q$	$\pm 63.40$
	$\Delta W/W$	$\pm 30.89$
	$\Delta C_p/C_p$	$\pm 5.94$
	$\Delta L/L$	$\pm 6.34$
	$\Delta T_{ci}/T_{ci}$	$\pm 42.9$
Total Temperature Variation		$\pm 149.47$
Upper Graphite	$\Delta Q/Q$	$\pm 32.40$
	$\Delta K_c/K_c$	$\pm 6.66$
	$\Delta T_{ci}/T_{ci}$	$\pm 94.45$
	$\Delta K_m/K_m$	$\pm 20.70$
	$\Delta s/s$	$\pm 6.003$
Total Temperature Variation		$\pm 160.21$

(Continued)

TABLE IX (Continued)

Region	Factors Which Lead to Greatest Variation in Material Temperatures (see Table VIII)	Resulting Temperature Variation Extremes, deg R
Upper BeO	$\Delta Q/Q$	$\pm 25.60$
	$\Delta W/W$	$\pm 10.6$
	$\Delta K_c/K_c$	$\pm 6.66$
	$\Delta T_{ci}/T_{ci}$	$\pm 95.3$
	$\Delta s/s$	$\pm 6.67$
Total Temperature Variation		$\pm 144.83$
Axial BeO	$\Delta Q/Q$	$\pm 102.60$
	$\Delta W/W$	$\pm 32.45$
	$\Delta T_{ci}/T_{ci}$	$\pm 101.45$
	$\Delta K_m/K_m$	$\pm 35.70$
	$\Delta s/s$	$\pm 103.53$
Total Temperature Variation		$\pm 375.73$
Lower BeO	$\Delta Q/Q$	$\pm 43.50$
	$\Delta W/W$	$\pm 13.50$
	$\Delta T_{ci}/T_{ci}$	$\pm 130.4$
	$\Delta s/s$	$\pm 42.05$
	$\Delta d_i/d_i$	$\pm 13.05$
Total Temperature Variation		$\pm 242.50$

(Continued)

TABLE IX (Concluded)

Region	Factors Which Lead to Greatest Variation in Material Temperatures (see Table VIII)	Resulting Temperature Variation Extremes, deg R
Lower Graphite	$\Delta Q/Q$	$\pm 23.44$
	$\Delta W/W$	$\pm 13.50$
	$\Delta \mu/\mu$	$\pm 4.33$
	$\Delta K_c/K_c$	$\pm 6.66$
	$\Delta T_{ci}/T_{ci}$	$\pm 139.9$
Total Temperature Variation		$\pm 183.78$
Axial Graphite	$\Delta Q/Q$	$\pm 65.00$
	$\Delta W/W$	$\pm 19.50$
	$\Delta T_{ci}/T_{ci}$	$\pm 145.35$
	$\Delta K_m/K_m$	$\pm 24.00$
	$\Delta s/s$	$\pm 17.40$
Total Temperature Variation		$\pm 271.25$

TABLE X

COMPARISON OF EXPERIMENTAL AND CALCULATED CRITICAL MASSES  
AND NUCLEAR FUEL WORTHS FOR SEVEN-CAVITY CONFIGURATIONS

Calculations Performed Using One-Dimensional Neutron Transport Theory  
(Description of Seven-Module Cavity Reactor Experiment Given in Ref. 15 and Fig. 31)

	Experiment	Calculation Detailed Spherical Model	Calculation Homogenized-Core Spherical Model
Critical Mass of Uranium, $M_c$ , kg	7.82	6.93	6.52
Fuel Worth, $(\Delta k/k)/(\Delta M/M_c)$	0.338	0.282	0.270
Hydrogen Worth, $(\Delta k/k)/(\Delta M/M_H)$	-0.0374	-	-0.0425

NUCLEAR LIGHT BULB CRITICAL MASS CALCULATIONS

(See Ref. 3 for Description of Reactor Configuration and Calculation Techniques)

	Two-Dimensional Neutron Transport Theory	One-Dimensional Neutron Transport Theory Detailed Spherical Model
Critical Mass of U-233 $M_c$ , kg	14.0	12.8

TABLE XI

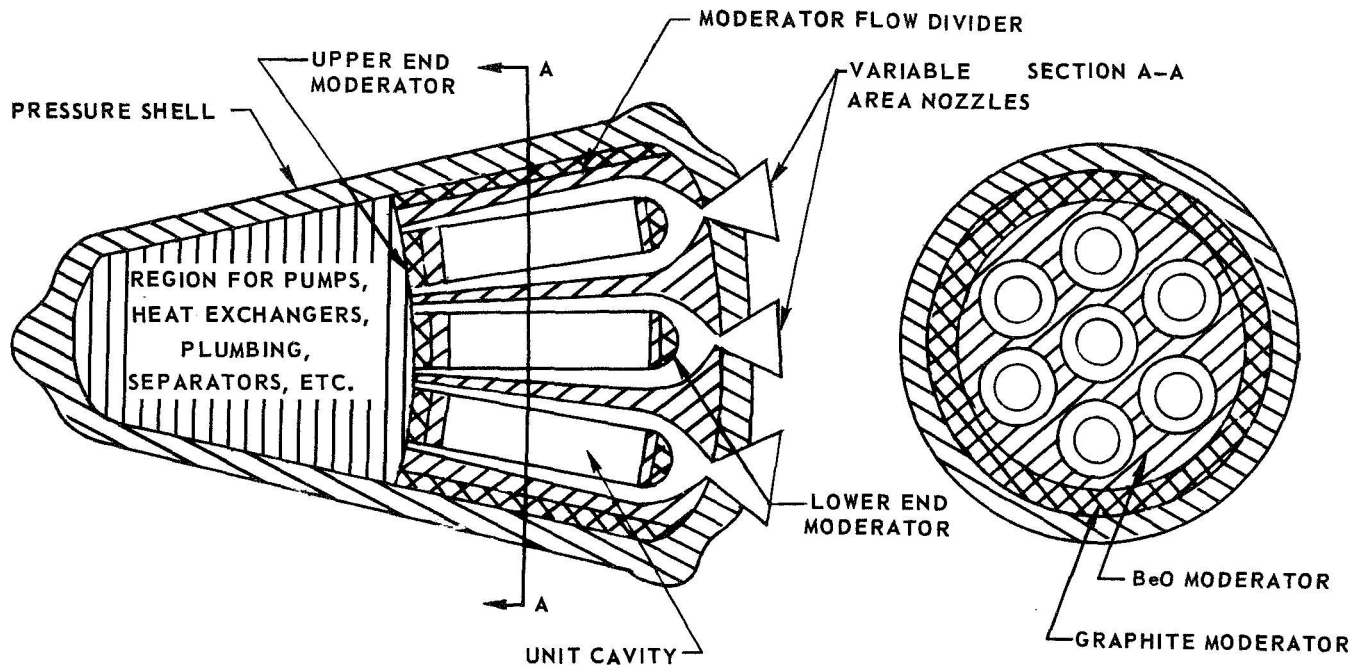
COMPARISON OF GEOMETRIC AND PERFORMANCE CHARACTERISTICS FOR A  
37-CELL ALTERNATE CONFIGURATION AND THE 7-CELL NUCLEAR LIGHT BULB ENGINE  
(See APPENDIX C and Fig. 35)

Power = 4600 megw

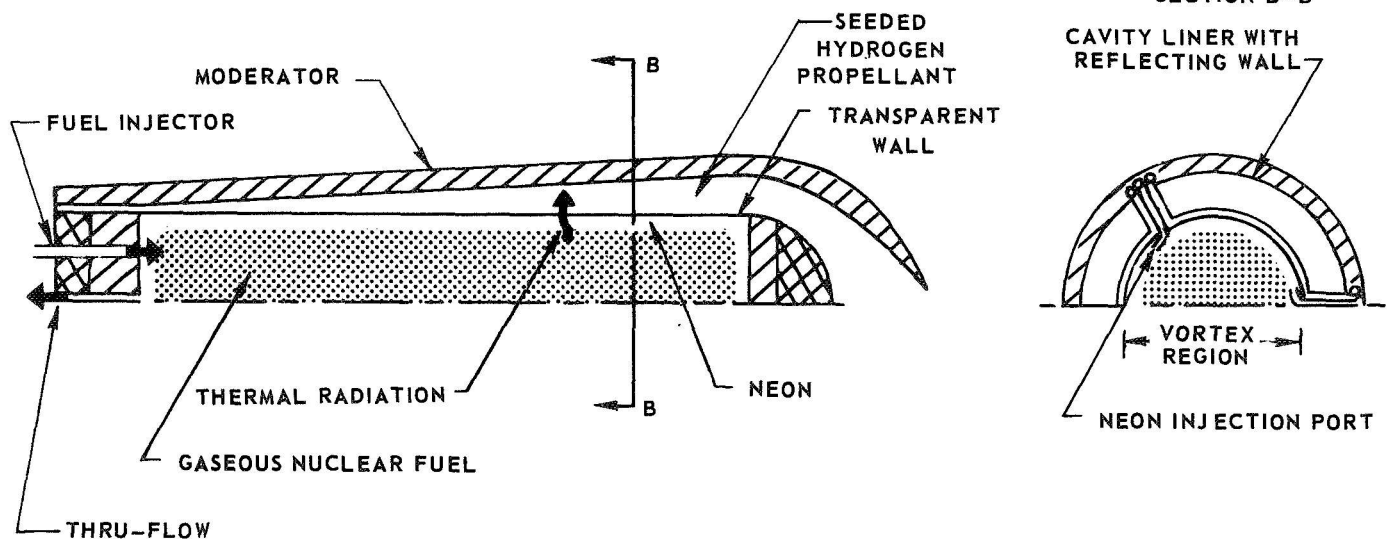
Compared Characteristic	37-Cell Alternate Configuration	Reference Engine
Propellant Duct Length/Inlet Width	42.5	64.5
Transparent-Wall Bursting Pressure	6.9 atm	1.0 atm
Transparent-Wall Collapsing Pressure	7.4 atm	0.1 atm
Power Convected to Liners	79.8 megw	81.0 megw
Power Convected to Transparent Walls	80.9 megw	59.5 megw
Hydrogen Flow Rate	47.0 lb/sec	42.3 lb/sec
Total Propellant Flow Rate	56.8 lb/sec	49.5 lb/sec
Specific Impulse	1760 sec	1870 sec
Thrust	100,000 lb	92,000 lb

# SKETCHES ILLUSTRATING PRINCIPLE OF OPERATION OF NUCLEAR LIGHT BULB ENGINE

## (a) OVERALL CONFIGURATION



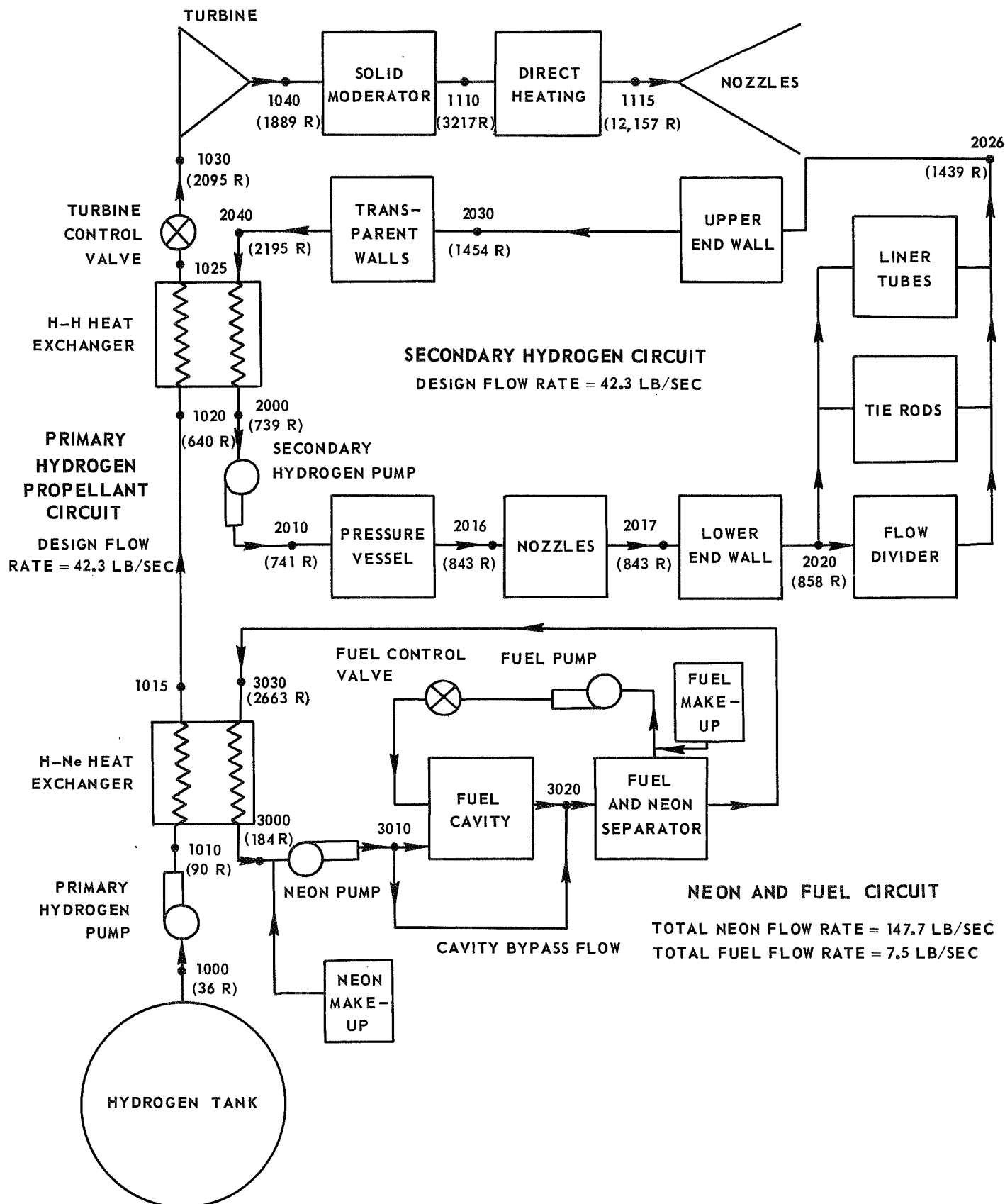
## (b) CONFIGURATION OF UNIT CAVITY



# NUCLEAR LIGHT BULB FLOW DIAGRAM

STATIONS DENOTED BY FOUR-DIGIT NUMBERS NOT IN PARENTHESES

DESIGN TEMPERATURE LEVELS DENOTED BY NUMBERS IN PARENTHESES

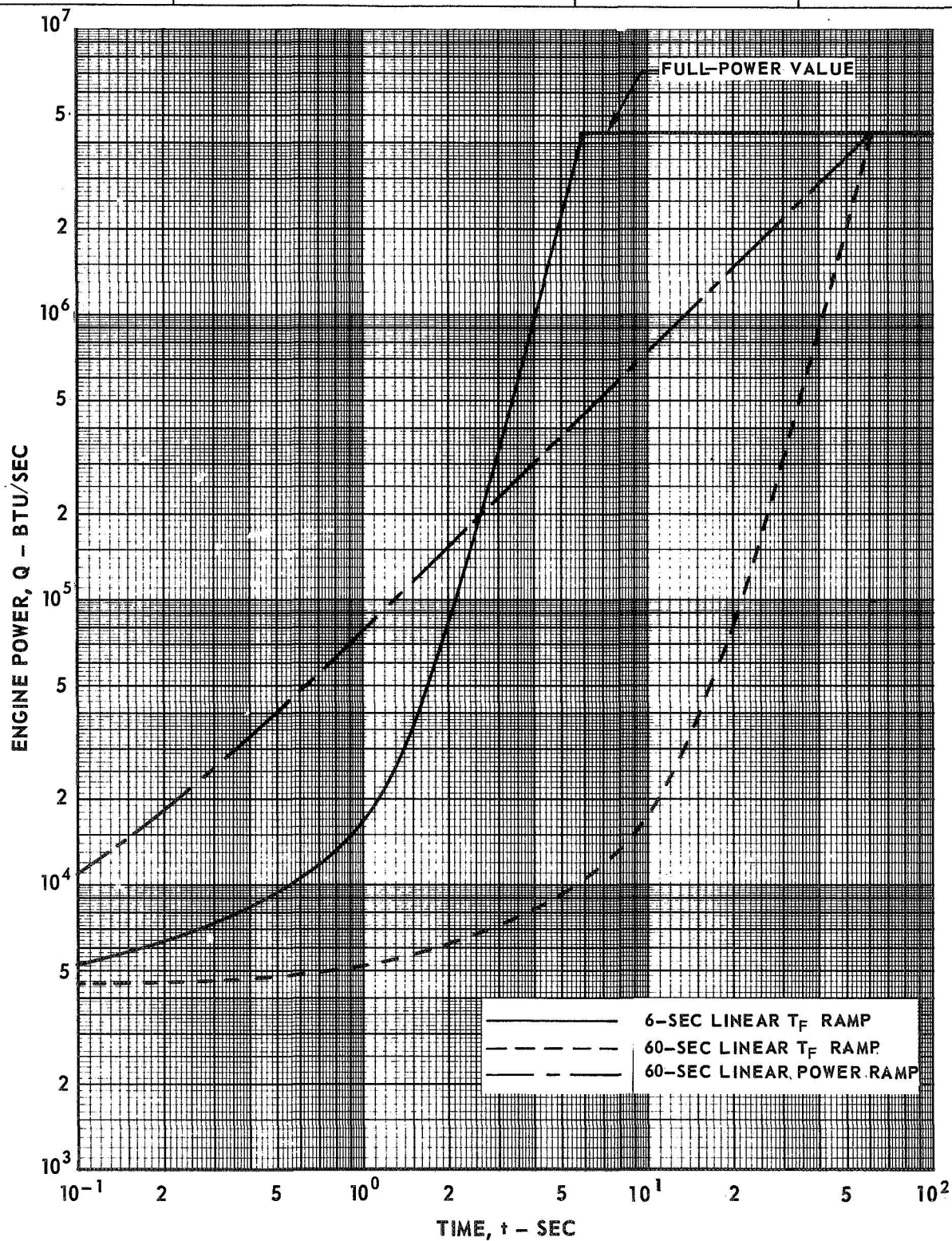




## ENGINE POWER DURING START-UP

HYDROGEN PROPELLANT FLOW RATE INCREASED LINEARLY WITH TIME DURING START-UP

TYPE OF RAMP	INITIAL HYDROGEN FLOW RATE	FUEL RESIDENCE TIME	INITIAL PRESSURE
LINEAR $T_F$	0.42 LB/SEC	4 SEC	71 ATM
LINEAR POWER	4.23 LB/SEC	20 SEC	20 ATM

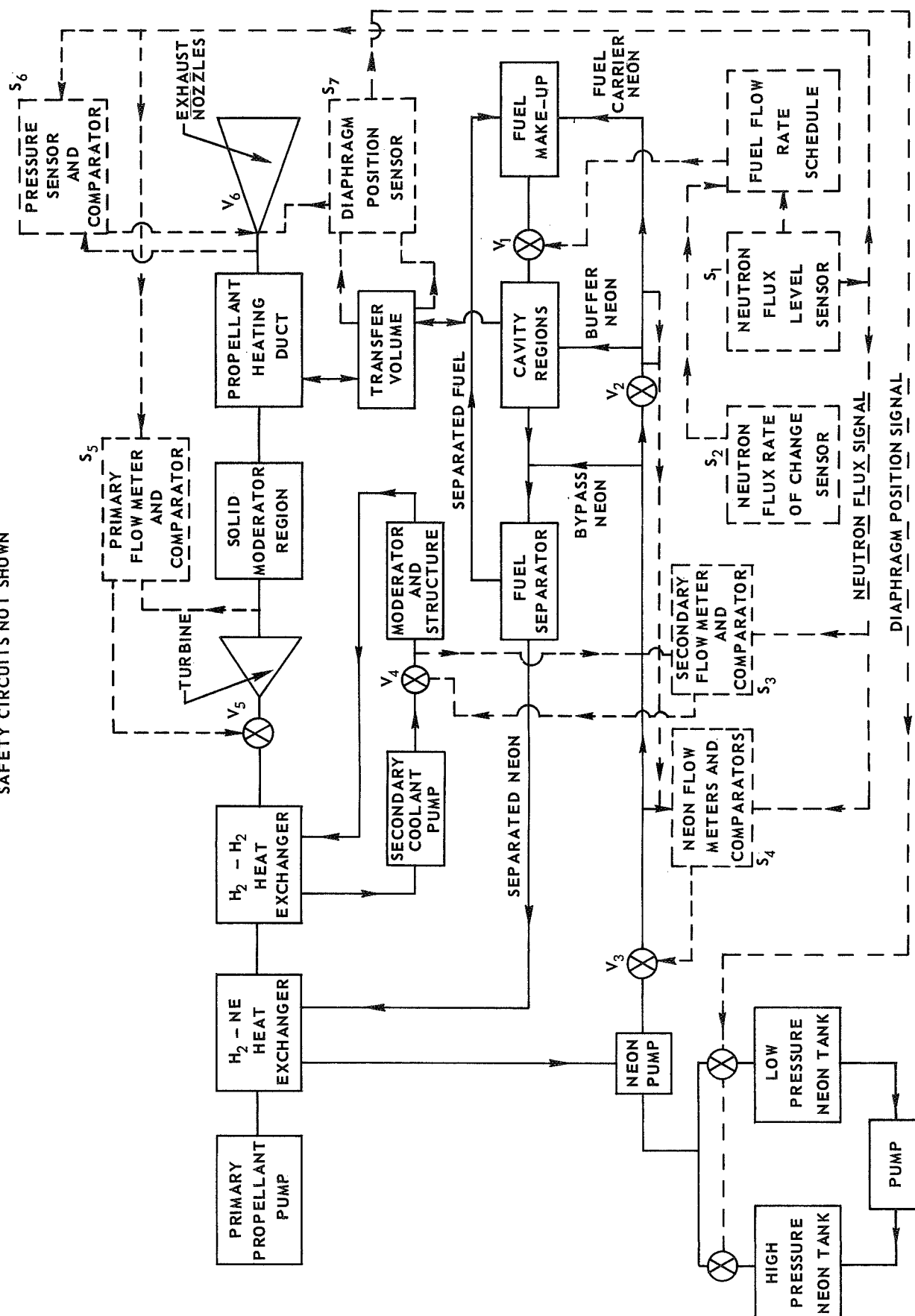


## BLOCK DIAGRAM OF START UP CONTROL SYSTEM

## FLOW CIRCUITS

--- SENSING AND CONTROL CIRCUITS

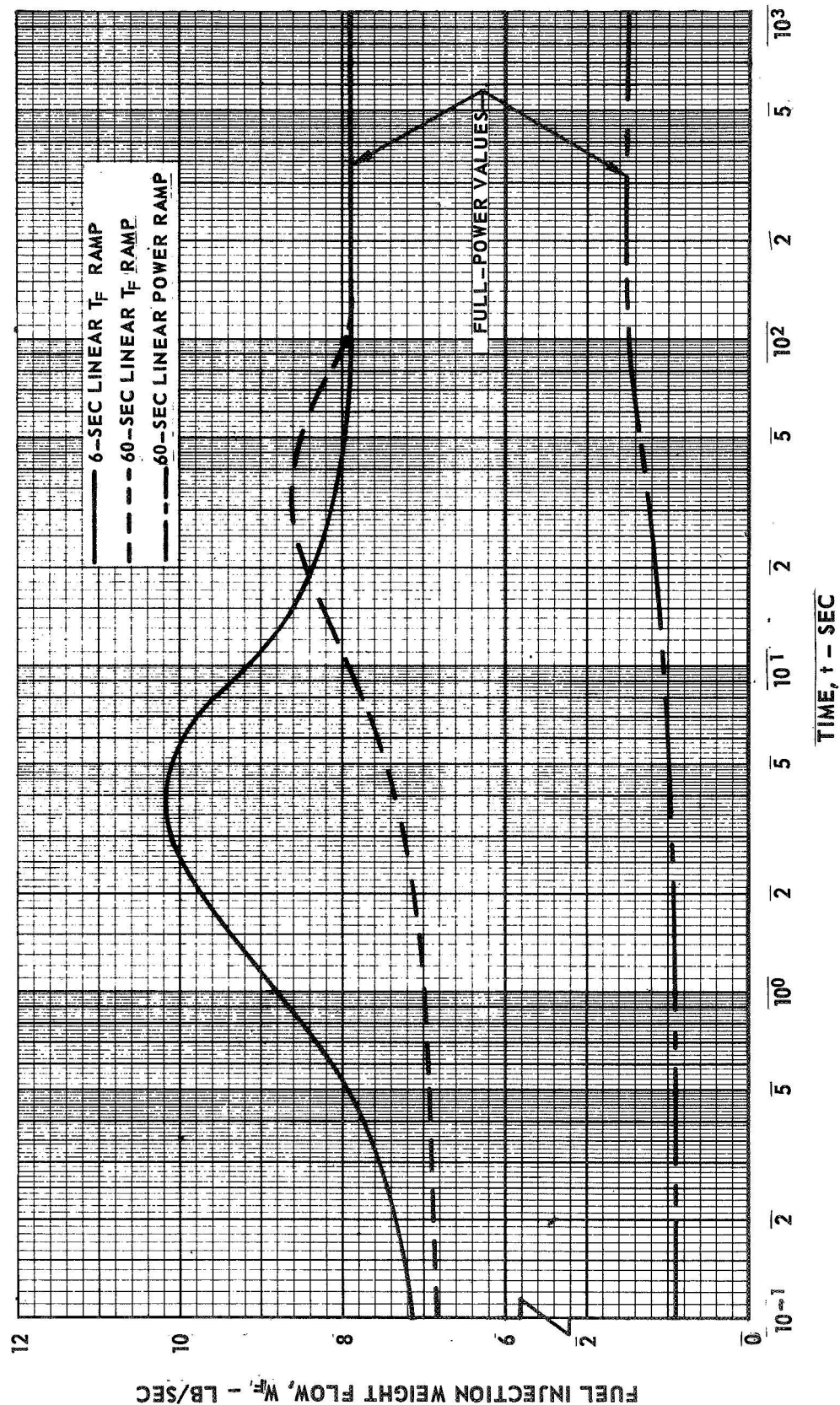
**SAFETY CIRCUITS NOT SHOWN**



# FUEL INJECTION WEIGHT FLOW DURING START - UP

WEIGHT FLOW IS TOTAL REQUIRED FOR ALL SEVEN CAVITIES

TYPE OF RAMP	INITIAL HYDROGEN FLOW RATE	FUEL RESIDENCE TIME	INITIAL PRESSURE
LINEAR $T_F$	0.42 LB/SEC	4 SEC	71 ATM
LINEAR POWER	4.23 LB/SEC	20 SEC	20 ATM

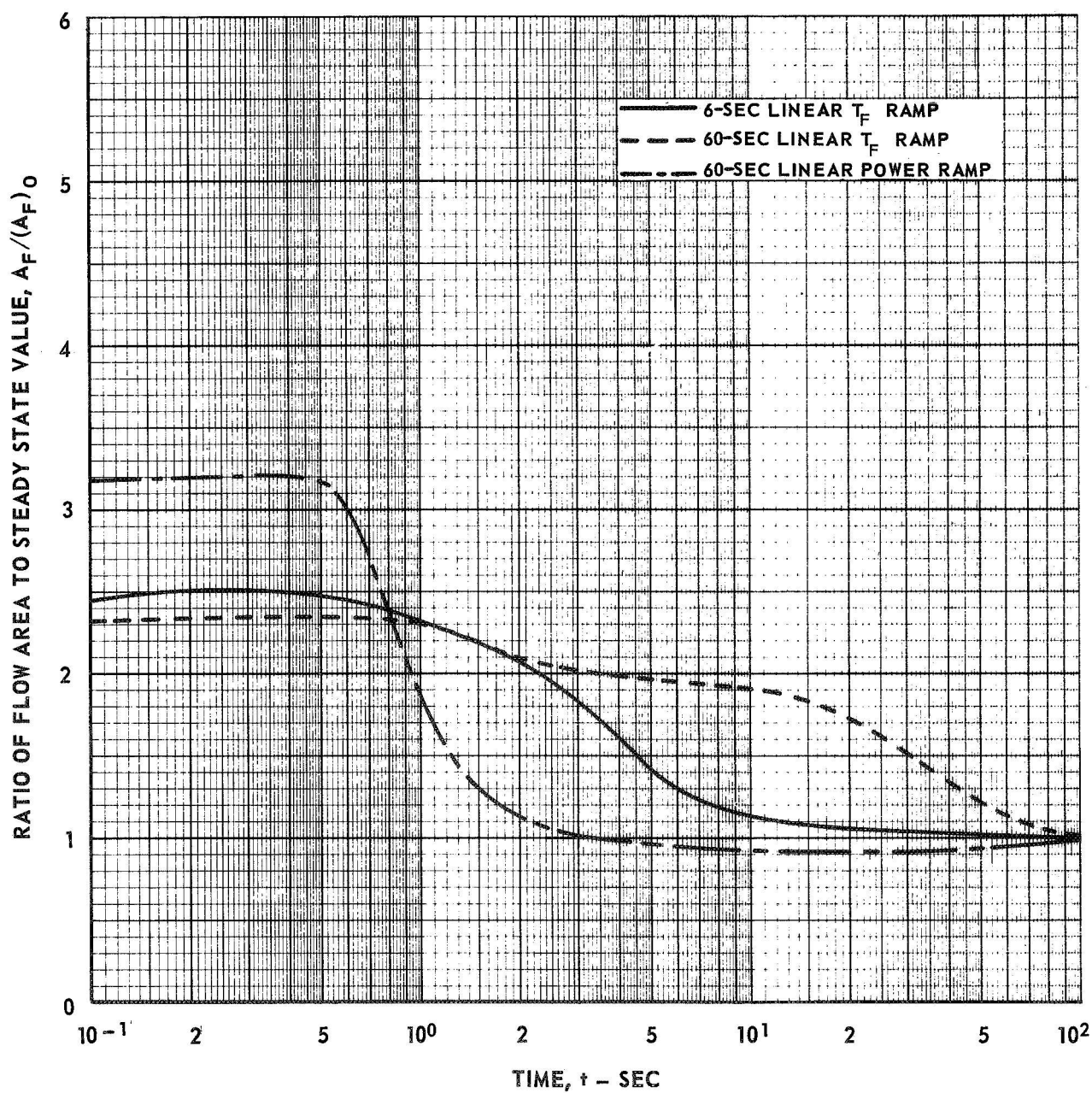


# VARIATION OF FUEL CONTROL VALVE FLOW AREA DURING START - UP

$(A_F)_0$  = STEADY STATE VALUE OF CONTROL VALVE AREA

$$A_F / (A_F)_0 = \sqrt{\frac{W_F^2}{(W_F)_0^2} \cdot \frac{(P_C)_0}{P_C}}$$

TYPE OF RAMP	INITIAL HYDROGEN FLOW RATE	FUEL RESIDENCE TIME	INITIAL PRESSURE
LINEAR $T_F$	0.42 LB/SEC	4 SEC	71 ATM
LINEAR POWER	4.23 LB/SEC	20 SEC	20 ATM





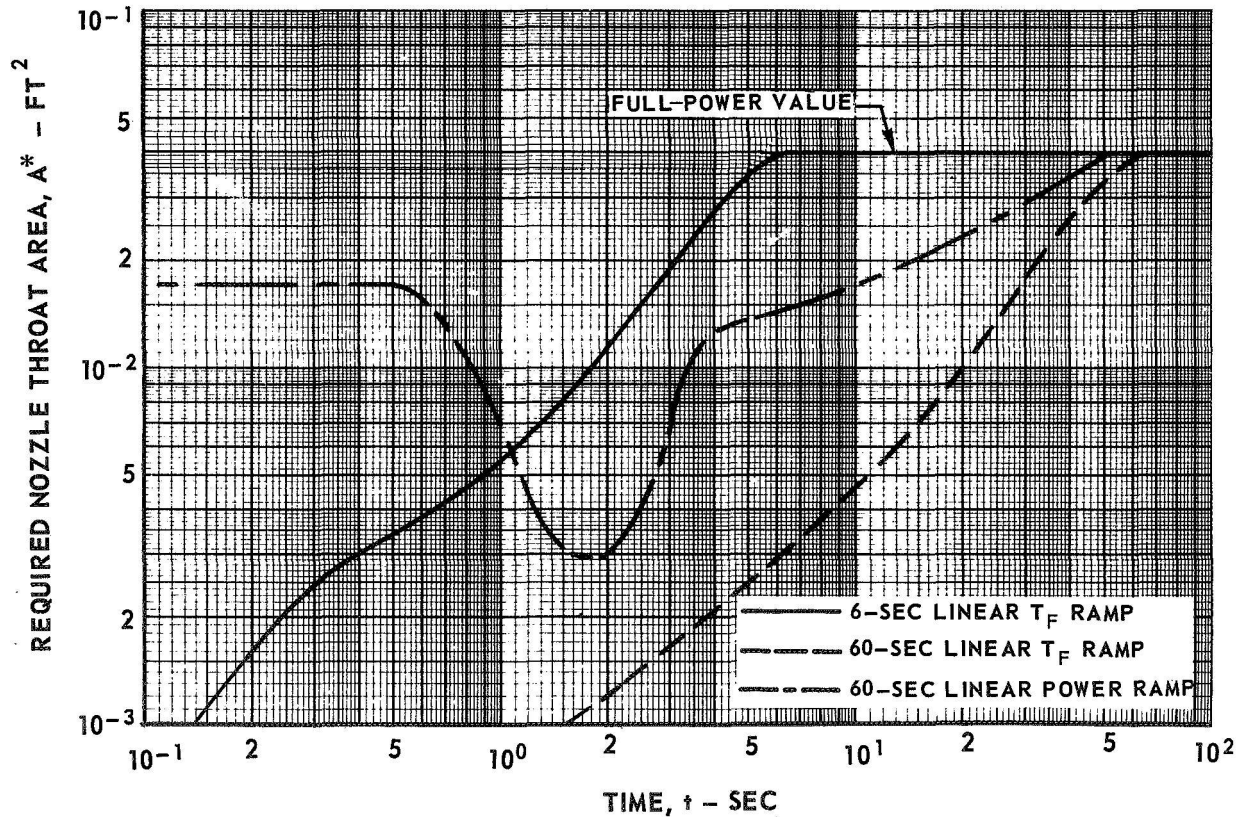
## REQUIRED NOZZLE THROAT AREA DURING START-UP

NOZZLE AREA SHOWN IS TOTAL REQUIRED FOR ALL NOZZLES

NOZZLE AREAS BASED ON THROAT FLOW PARAMETERS OF REF. 12

HYDROGEN PROPELLANT FLOW RATE INCREASED LINEARLY  
WITH TIME DURING START-UP

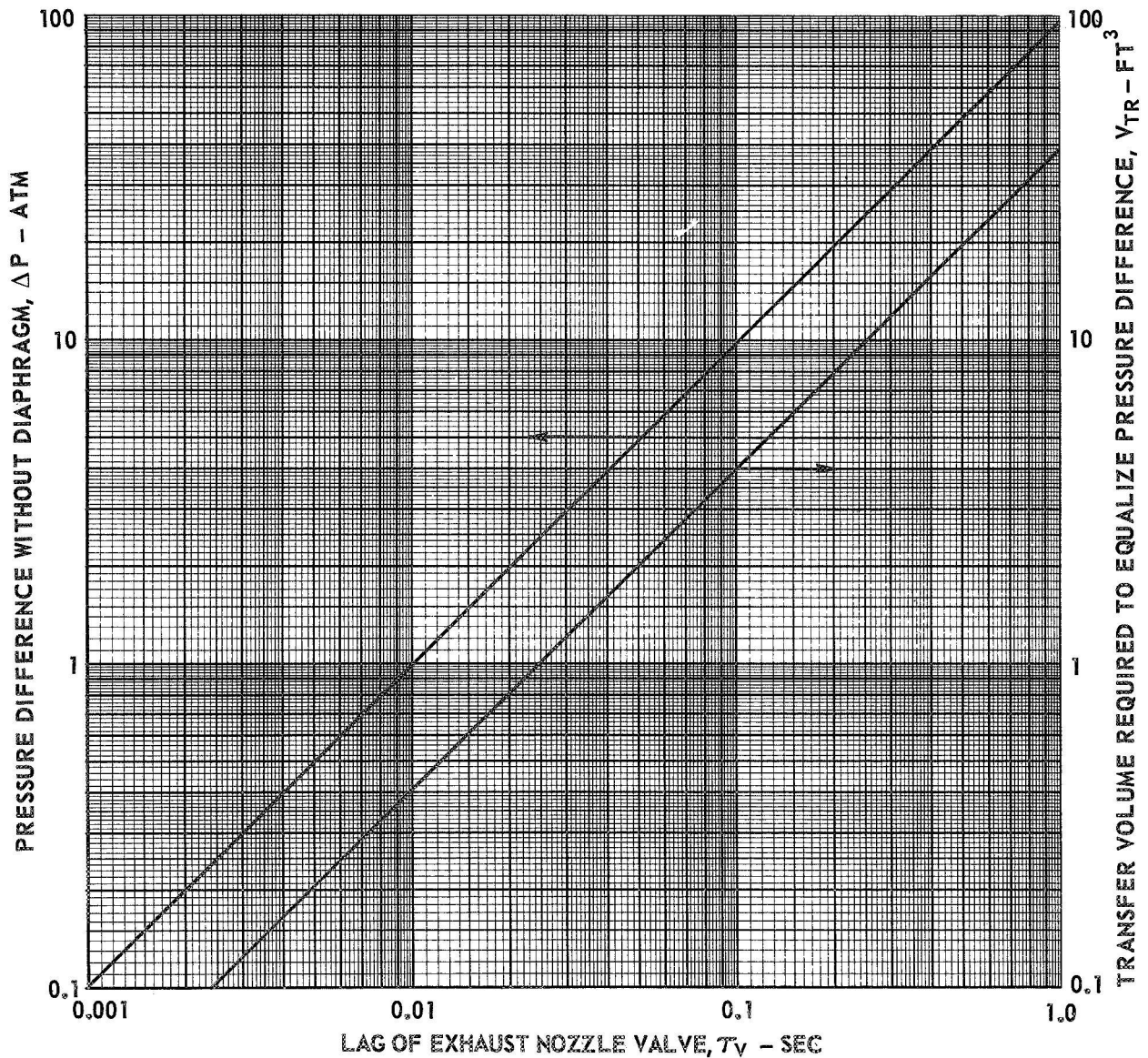
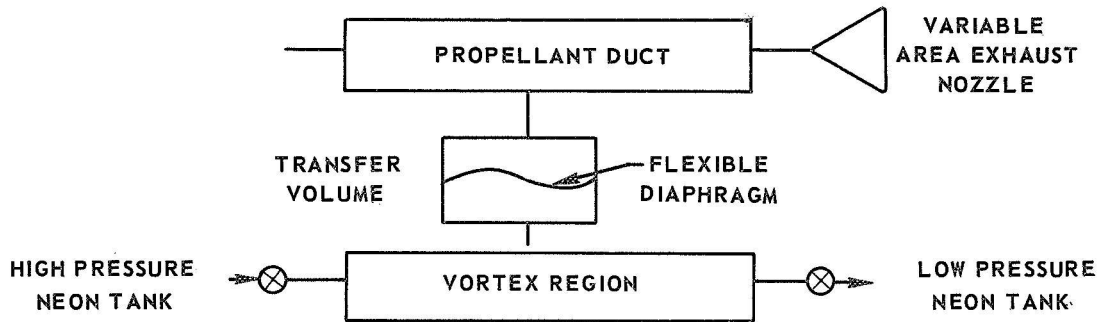
TYPE OF RAMP	INITIAL HYDROGEN FLOW RATE	FUEL RESIDENCE TIME	INITIAL PRESSURE
LINEAR $T_F$	0.42 LB/SEC	4 SEC	71 ATM
LINEAR POWER	4.23 LB/SEC	20 SEC	20 ATM



## TRANSFER VOLUME PRESSURE EQUALIZATION CONCEPT DURING START-UP

MAXIMUM VALUE OF  $dp/dt = 100 \text{ ATM/SEC}$ 

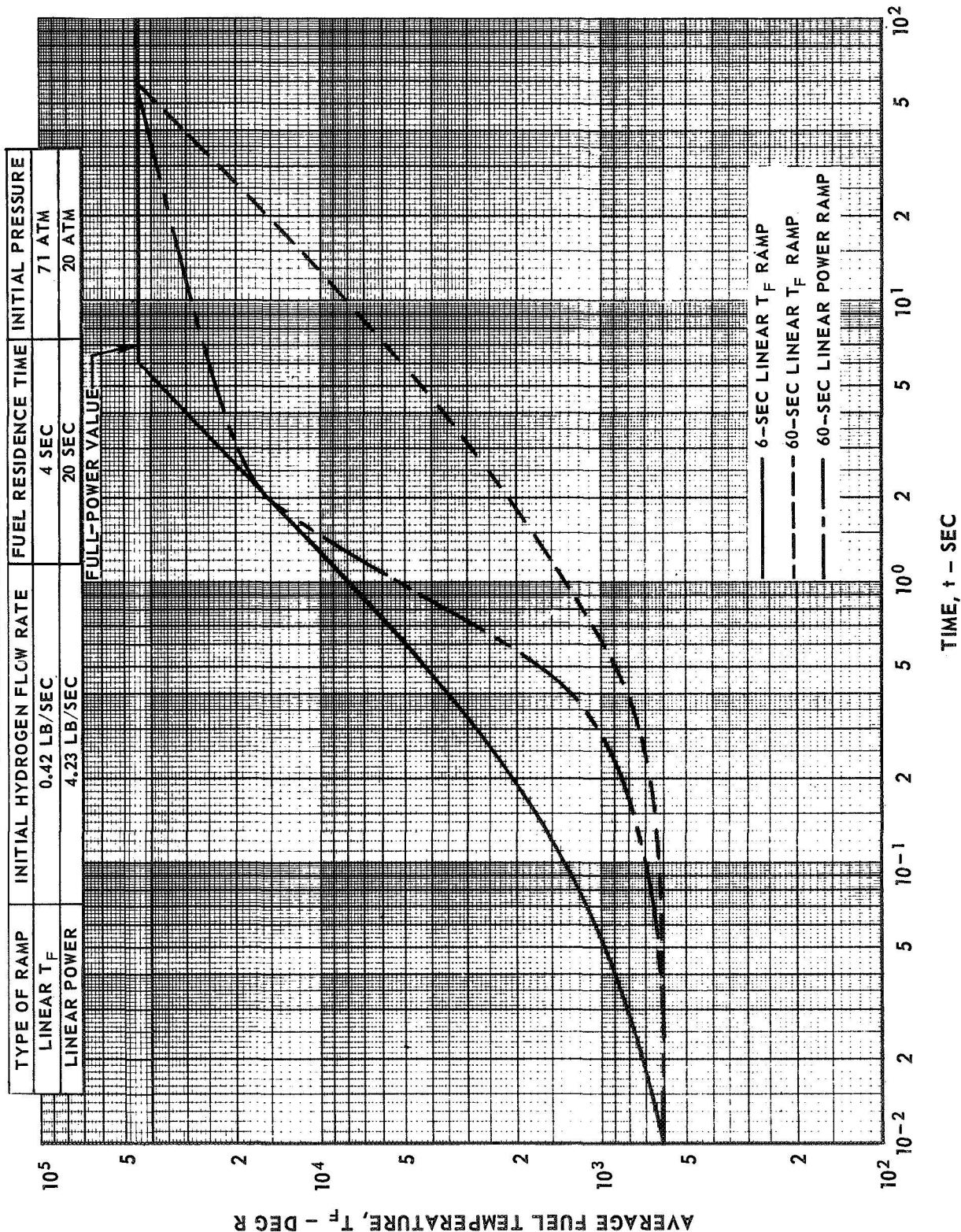
EXHAUST NOZZLE AREA VARIED TO CONTROL PRIMARY PROPELLANT PRESSURE



# AVERAGE FUEL TEMPERATURE DURING START-UP

$$T^* = T_F / 3.0$$

HYDROGEN PROPELLANT FLOW RATE INCREASED LINEARLY  
WITH TIME DURING START-UP

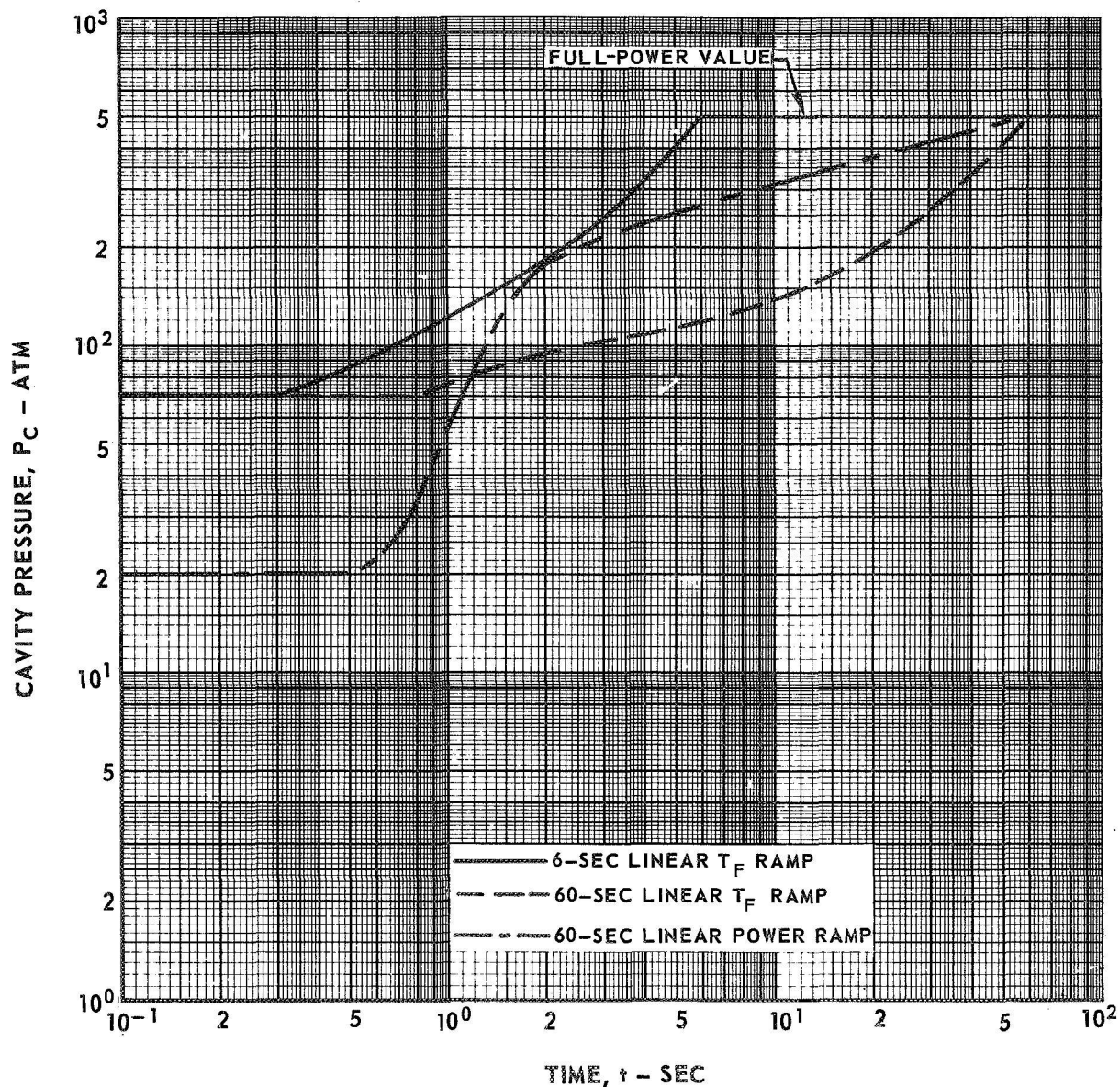


## CAVITY PRESSURE DURING START-UP

PRESSURES BASED ON NEON TEMPERATURE AND DENSITY AT EDGE OF FUEL

HYDROGEN PROPELLANT FLOW RATE INCREASED LINEARLY  
WITH TIME DURING START-UP

TYPE OF RAMP	INITIAL HYDROGEN FLOW RATE	FUEL RESIDENCE TIME	INITIAL PRESSURE
LINEAR $T_F$	0.42 LB/SEC	4 SEC	71 ATM
LINEAR POWER	4.23 LB/SEC	20 SEC	20 ATM





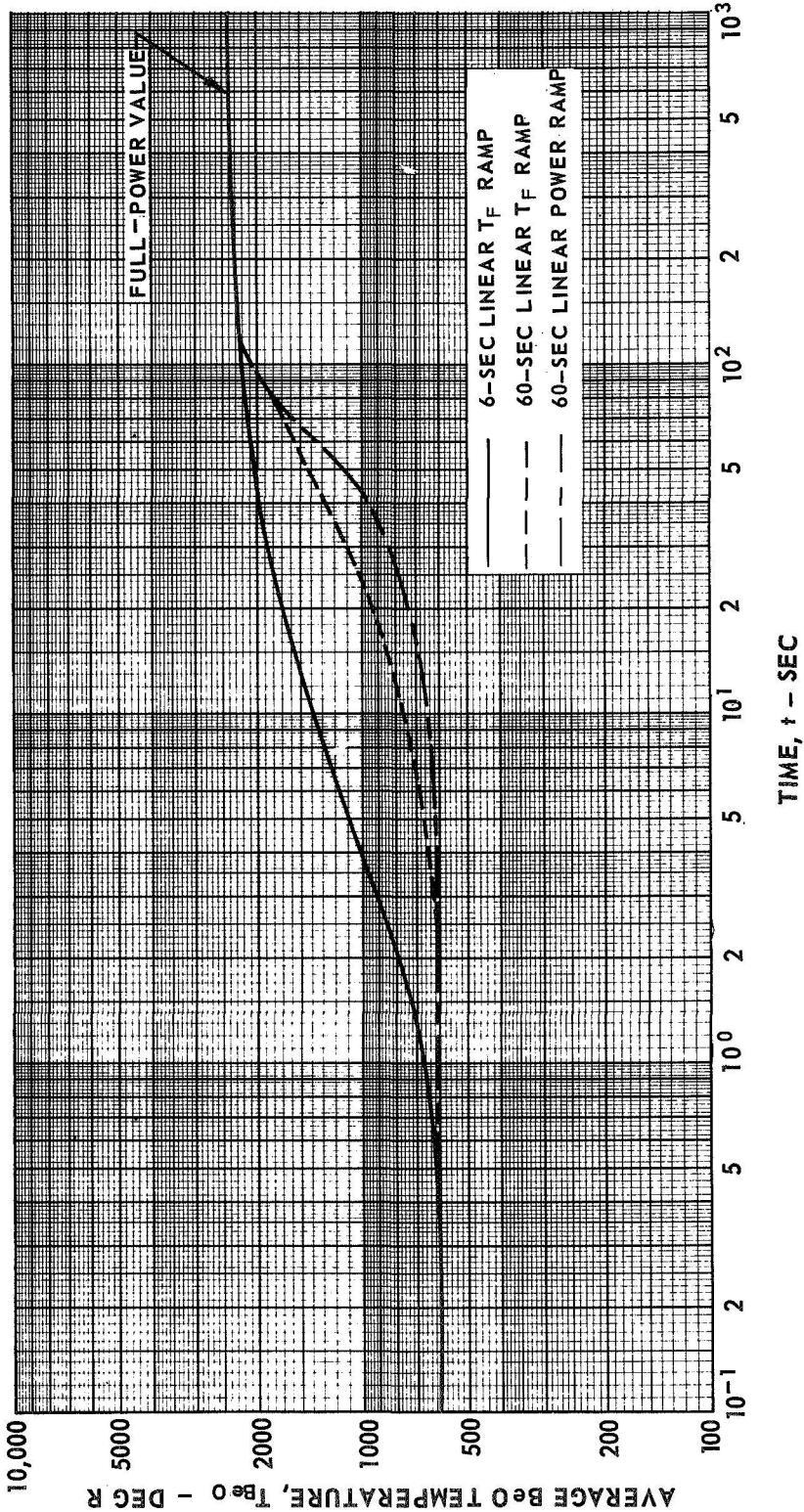
AVERAGE BeO TEMPERATURE DURING START-UP

TOTAL BeO MASS = 12,200 LB

ASSUMED VALUE OF BeO SPECIFIC HEAT = 0.42 BTU/(LB-DEG R)

HYDROGEN PROPELLANT FLOW RATE INCREASED LINEARLY WITH TIME DURING START-UP

TYPE OF RAMP	INITIAL HYDROGEN FLOW RATE	FUEL RESIDENCE TIME	INITIAL PRESSURE
LINEAR $T_F$	0.42 LB/SEC	4 SEC	71 ATM
LINEAR POWER	4.23 LB/SEC	20 SEC	20 ATM



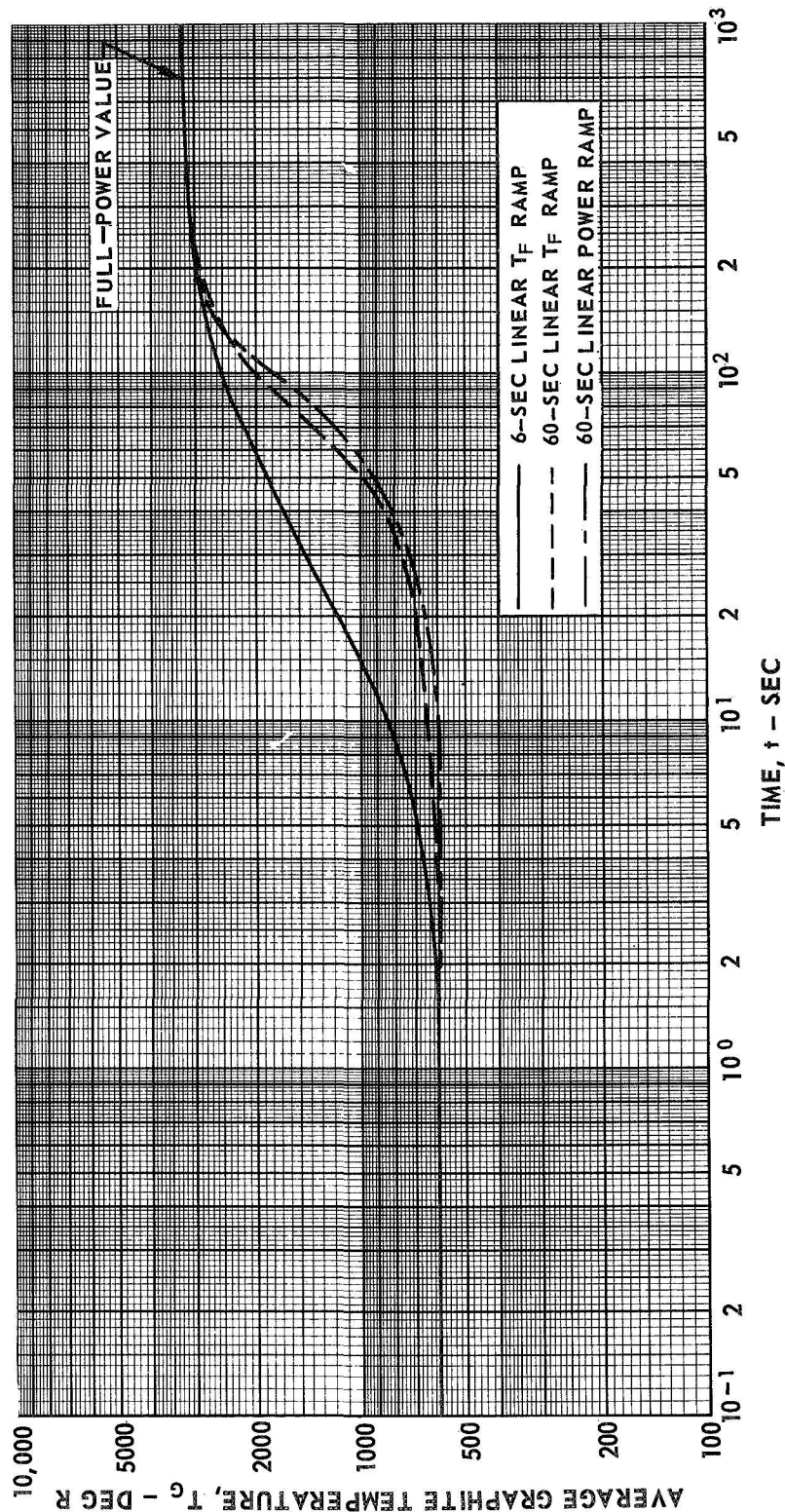
# AVERAGE GRAPHITE TEMPERATURE DURING START-UP

TOTAL GRAPHITE MASS = 26,800 LB

ASSUMED VALUE OF GRAPHITE SPECIFIC HEAT = 0.24 BTU/(LB-DEG R)

HYDROGEN PROPELLANT FLOW RATE INCREASED LINEARLY WITH TIME DURING START-UP

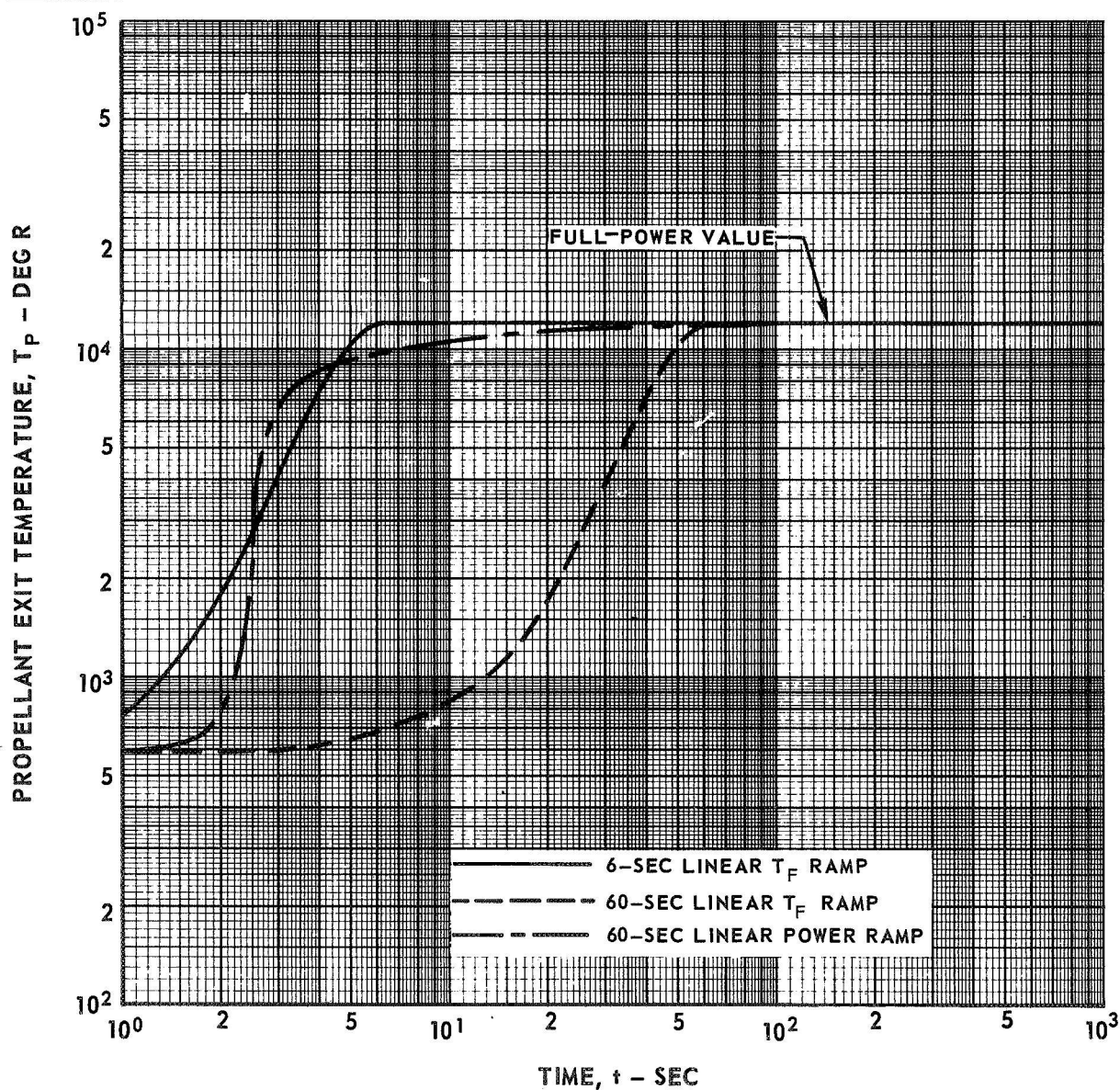
TYPE OF RAMP	INITIAL HYDROGEN FLOW RATE	FUEL RESIDENCE TIME	INITIAL PRESSURE
LINEAR $T_F$	0.42 LB/SEC	4 SEC	71 ATM
LINEAR POWER	4.23 LB/SEC	20 SEC	20 ATM



# PROPELLANT EXIT TEMPERATURE DURING START-UP

HYDROGEN PROPELLANT FLOW RATE INCREASED LINEARLY  
WITH TIME DURING START-UP

TYPE OF RAMP	INITIAL HYDROGEN FLOW RATE	FUEL RESIDENCE TIME	INITIAL PRESSURE
LINEAR $T_F$	0.42 LB/SEC	4 SEC	71 ATM
LINEAR POWER	4.23 LB/SEC	20 SEC	20 ATM



U - 233 CRITICAL MASS DURING START - UP

SEE TEXT FOR DESCRIPTION OF MODEL USED IN CALCULATIONS

TYPE OF RAMP	INITIAL HYDROGEN FLOW RATE	FUEL RESIDENCE TIME	INITIAL PRESSURE
LINEAR $T_F$	0.42 LB/SEC	4 SEC	71 ATM
LINEAR POWER	4.23 LB/SEC	20 SEC	20 ATM

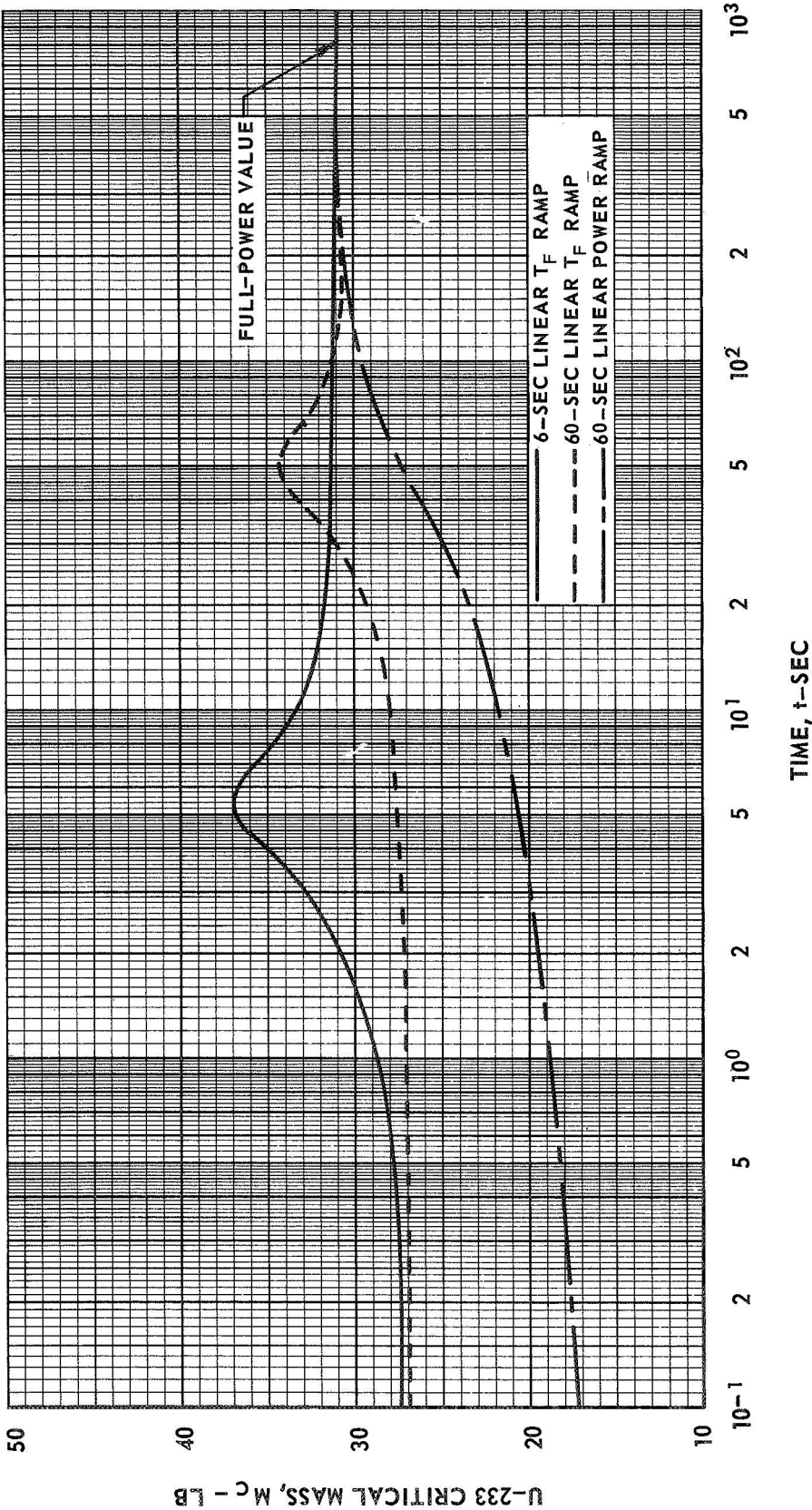
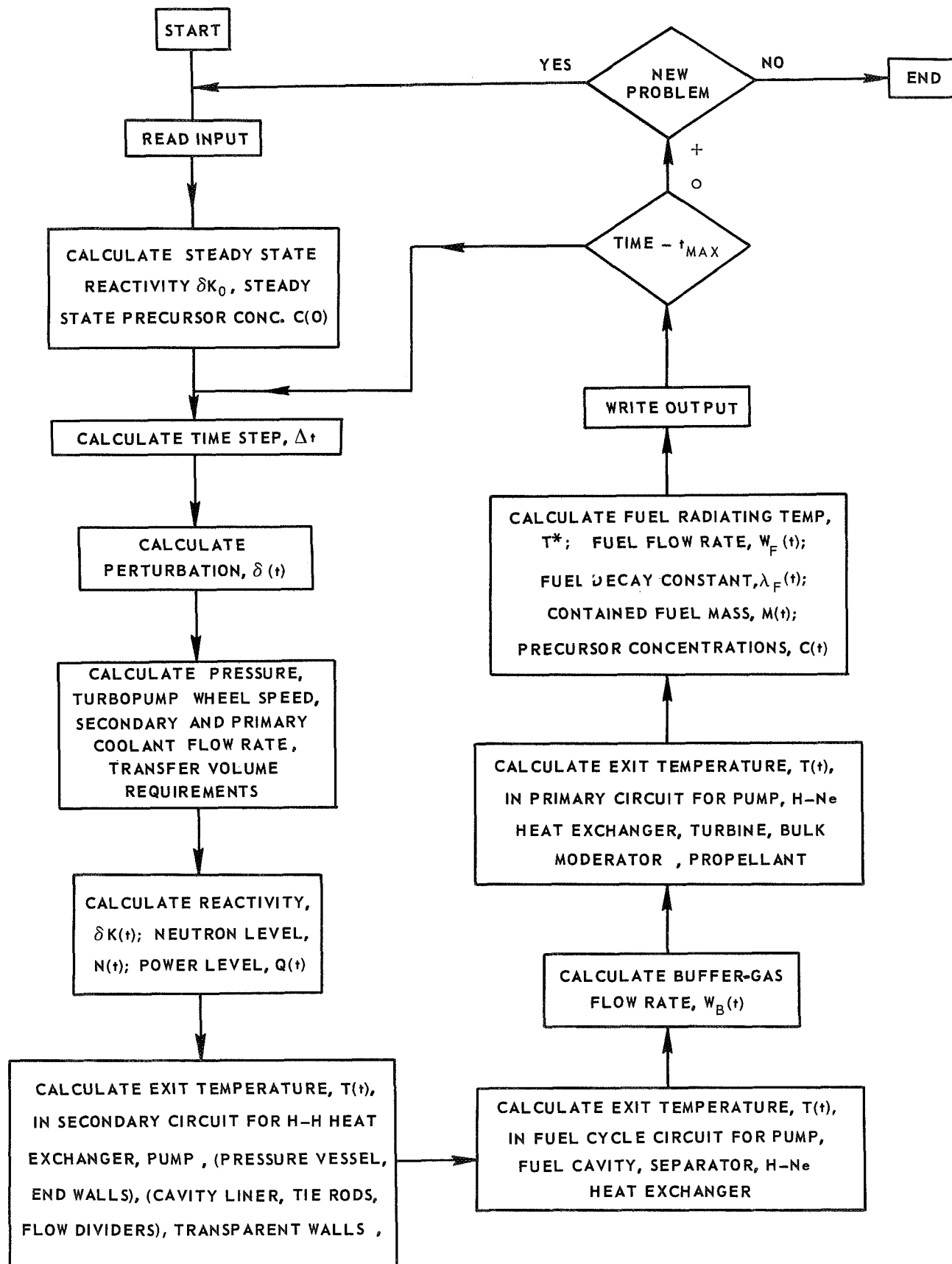


FIG. 14

## NUCLEAR LIGHT BULB SIMULATION FLOW DIAGRAM

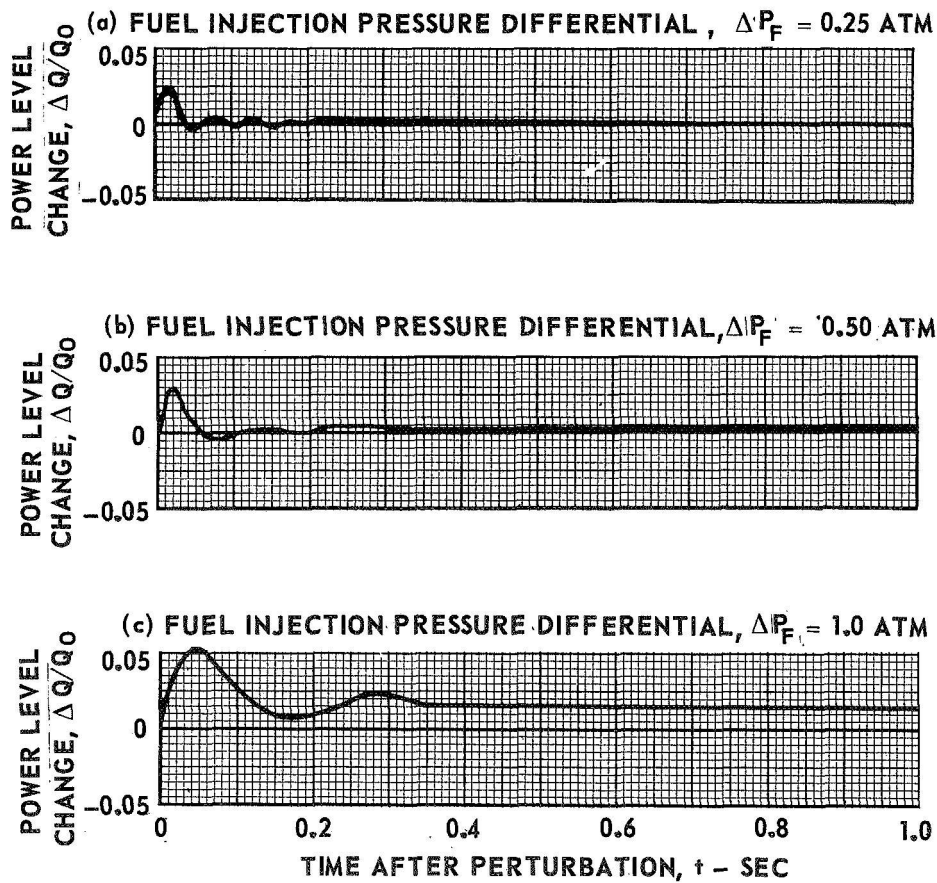
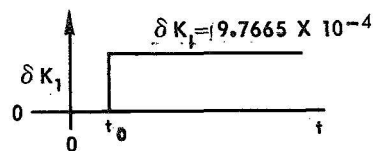




# POWER LEVEL RESPONSE OF UNCONTROLLED ENGINE TO STEP CHANGE IN IMPOSED REACTIVITY FOR DIFFERENT FUEL INJECTION PRESSURE DIFFERENTIALS

CONSTANT FUEL RADIUS

$$W_F = K_F A_F \left( \frac{P_F - P_C}{\Delta P_F} \right)^{1/2}$$

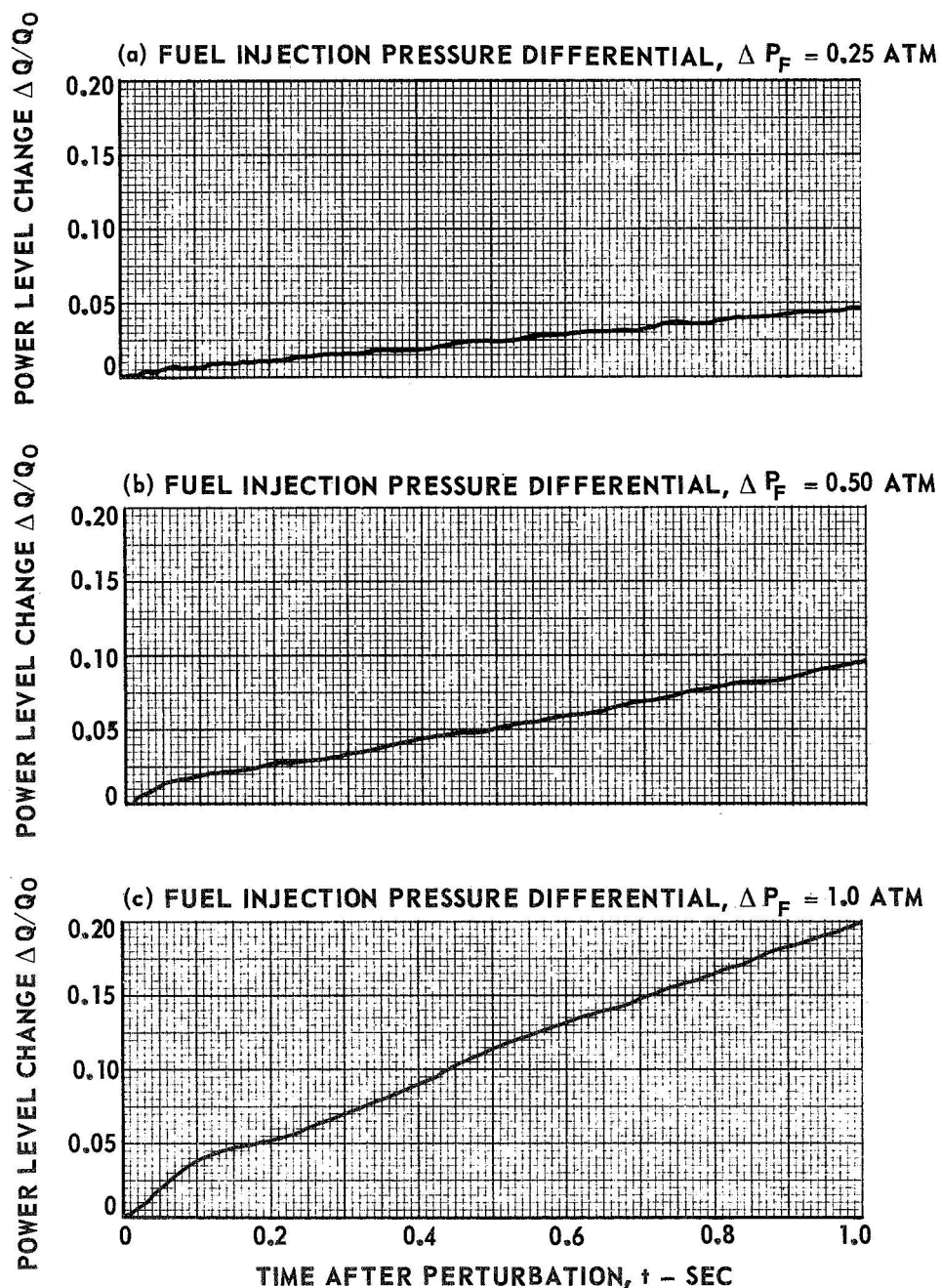
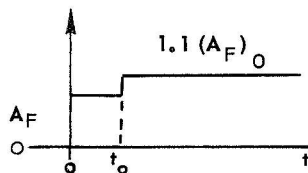


# POWER LEVEL RESPONSE OF UNCONTROLLED ENGINE TO STEP CHANGE IN FUEL CONTROL VALVE AREA FOR DIFFERENT FUEL INJECTION PRESSURE DIFFERENTIALS

CONSTANT FUEL RADIUS

$$A_F = 1.10 (A_F)_0$$

$$W_F = K_F A_F \left( \frac{P_F - P_C}{\Delta P_F} \right)^{1/2}$$

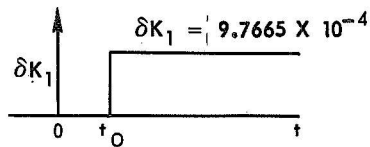


# VARIATION IN FUEL INJECTION PRESSURE DIFFERENTIAL IN UNCONTROLLED ENGINE WITH STEP CHANGES IN IMPOSED REACTIVITY AND FUEL CONTROL VALVE AREA

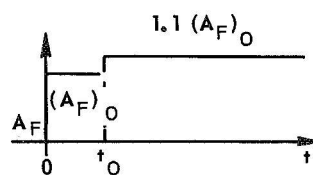
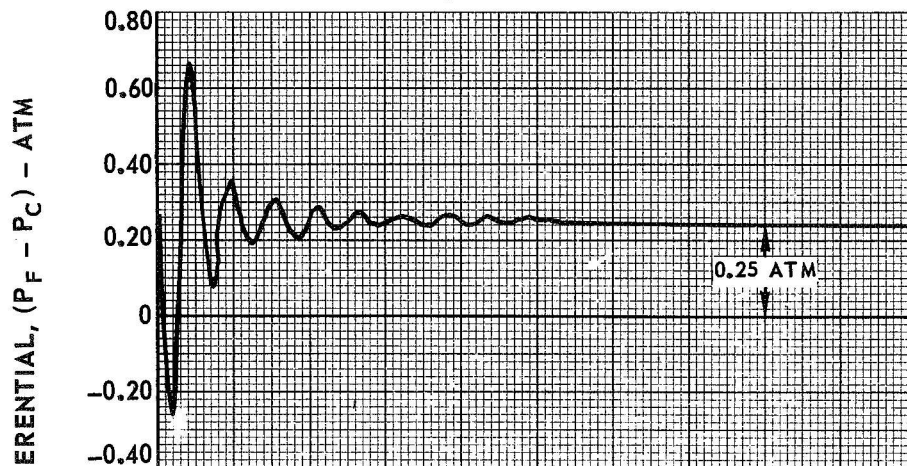
CONSTANT FUEL RADIUS

$$\Delta P_F = 0.25 \text{ ATM}$$

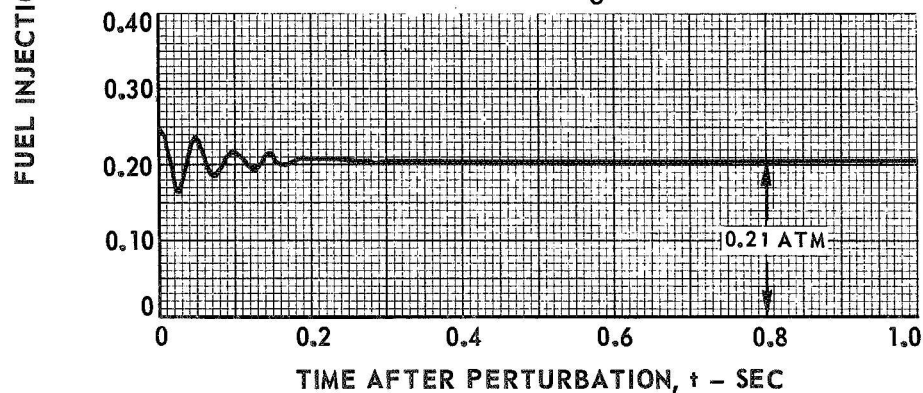
$$W_F = K_F A_F \left[ \frac{P_F - P_C}{\Delta P_F} \right]^{1/2}$$



(a) RESPONSE TO  $\delta K_1 = 9.7665 \times 10^{-4}$



(b) RESPONSE FOR  $A_F = 1.10 (A_F)_0$

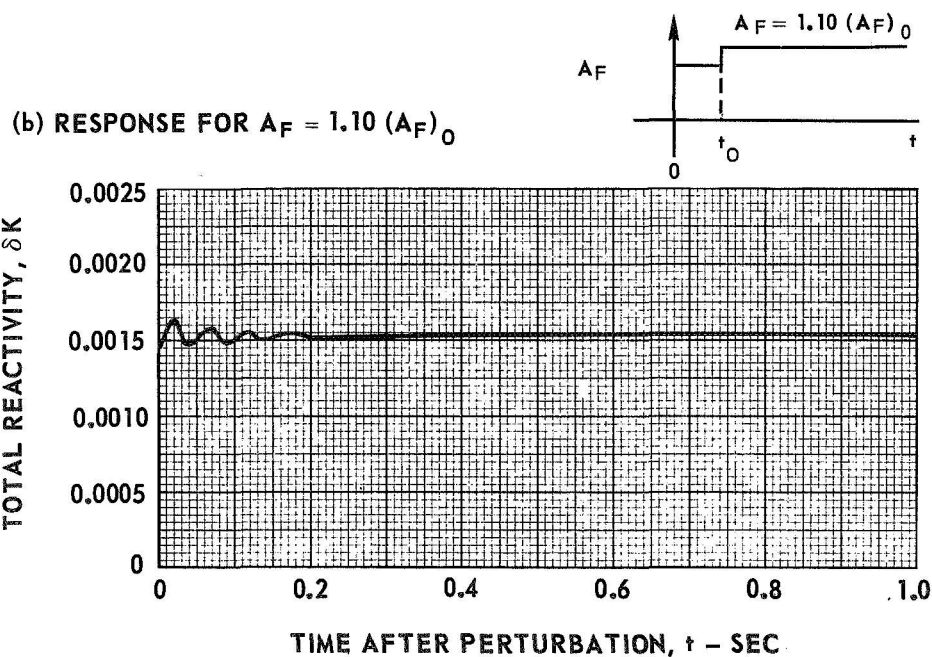
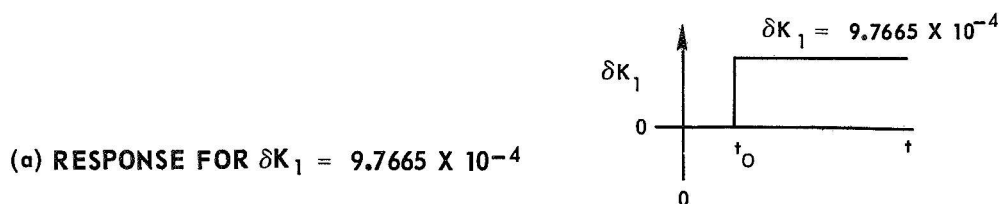




# REACTIVITY RESPONSE OF UNCONTROLLED ENGINE TO STEP CHANGE IN IMPOSED REACTIVITY AND FUEL CONTROL VALVE AREA

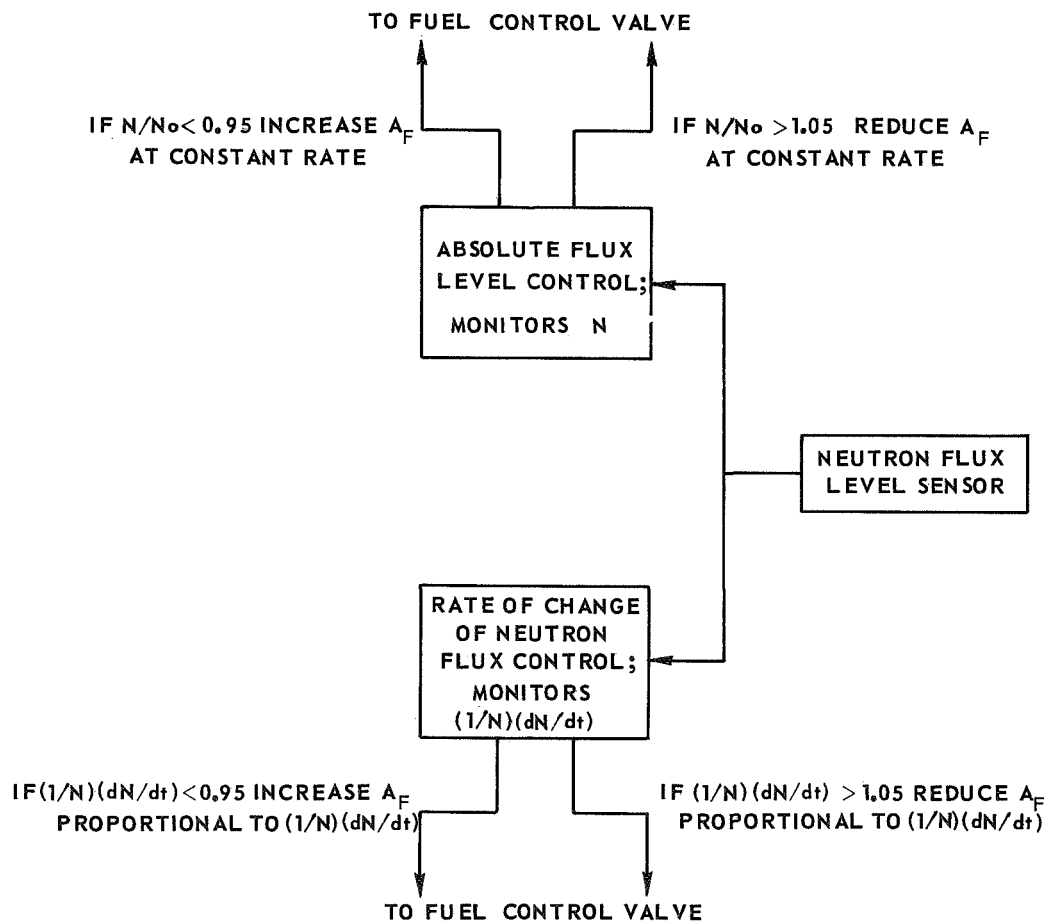
CONSTANT FUEL RADIUS

$$\Delta P_F = 0.25 \text{ ATM}$$



# BLOCK DIAGRAM OF CONTROL SYSTEM EMPLOYED AT FULL- POWER OPERATING CONDITIONS

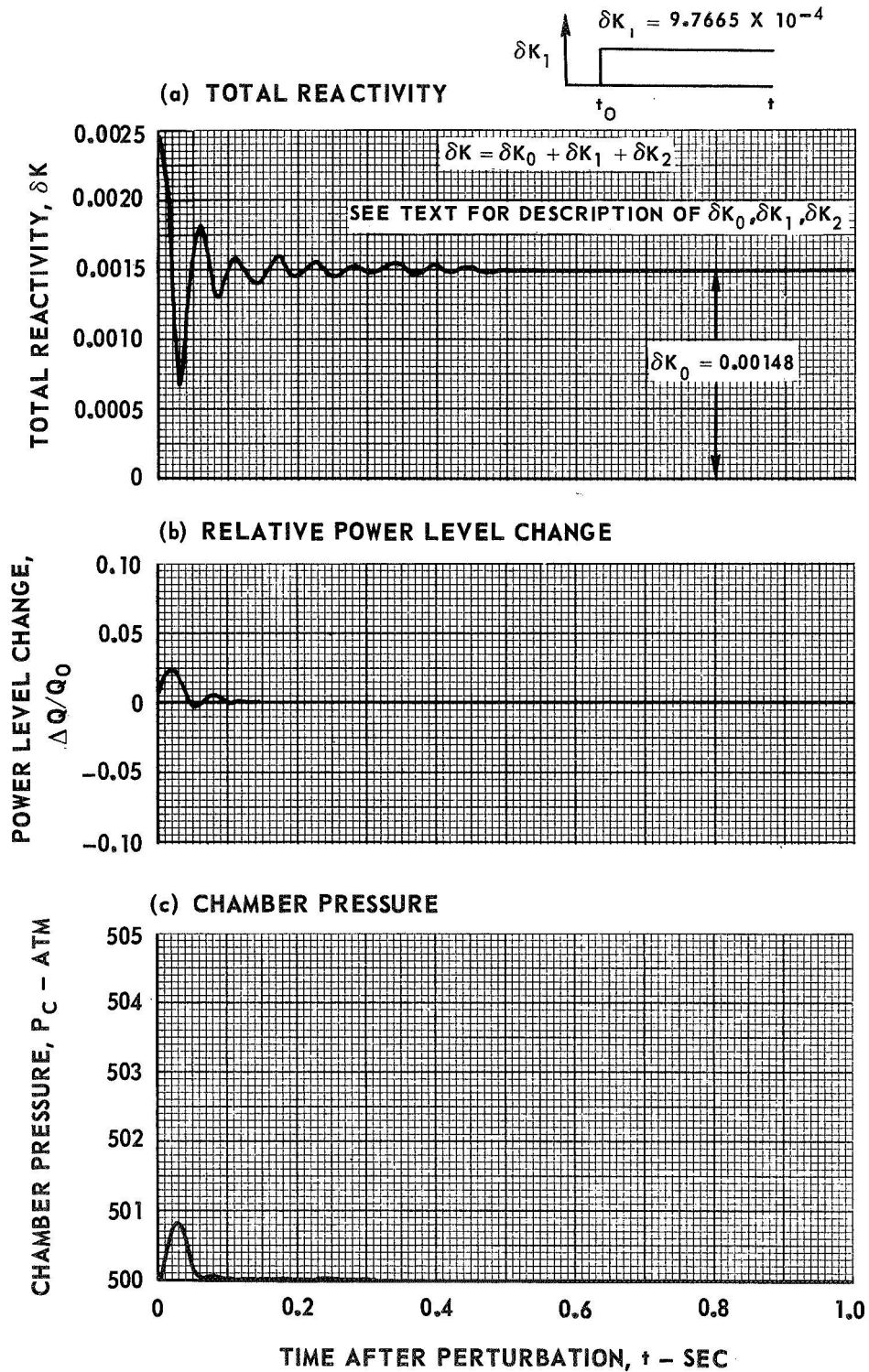
CONTROL ACHIEVED BY VARYING AREA OF FUEL  
CONTROL VALVE SHOWN IN FIGS. 2 AND 4



# RESPONSE OF CONTROLLED ENGINE TO POSITIVE STEP CHANGE IN IMPOSED REACTIVITY

CONSTANT FUEL RADIUS

$$\Delta P_F = 0.25 \text{ ATM}$$



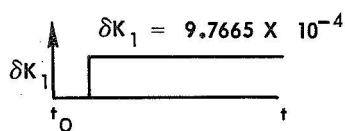
(CONTINUED)

# RESPONSE OF CONTROLLED ENGINE TO POSITIVE STEP CHANGE IN IMPOSED REACTIVITY

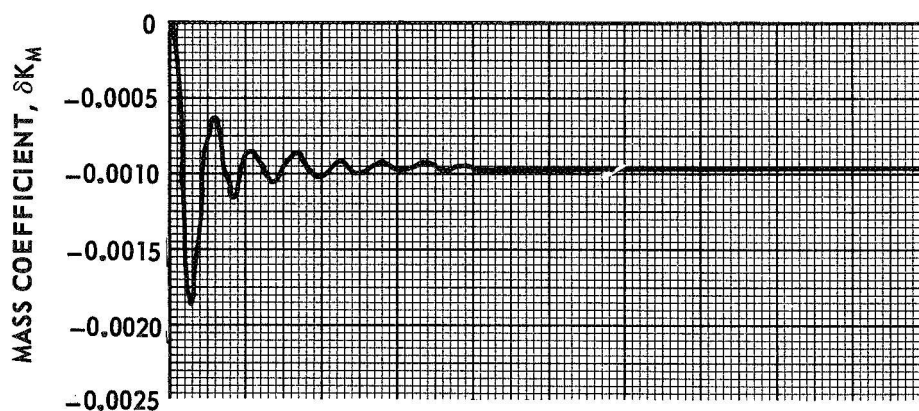
(CONTINUED)

CONSTANT FUEL RADIUS

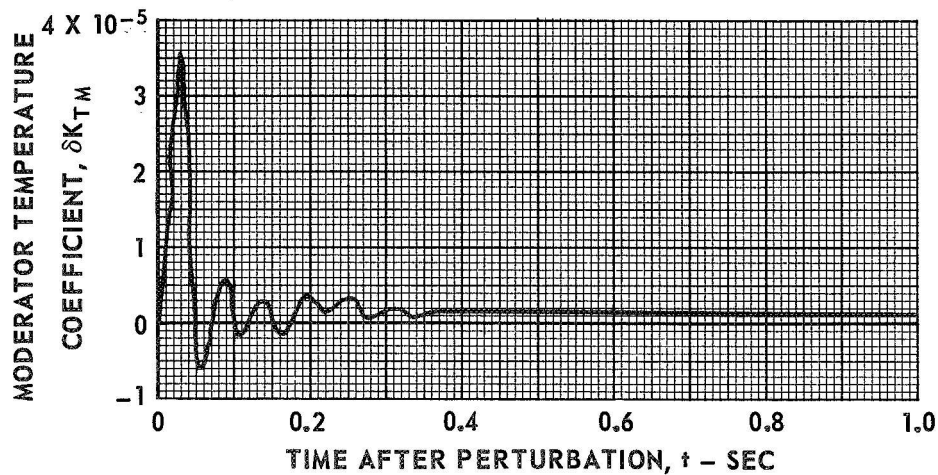
$$\Delta P_F = 0.25 \text{ ATM}$$



(d) REACTIVITY COEFFICIENT DUE TO FUEL MASS VARIATION



(e) REACTIVITY COEFFICIENT DUE TO MODERATOR TEMPERATURE VARIATION



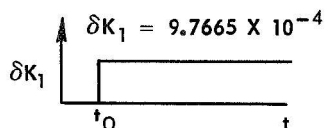
(CONTINUED)

# RESPONSE OF CONTROLLED ENGINE TO POSITIVE STEP CHANGE IN IMPOSED REACTIVITY

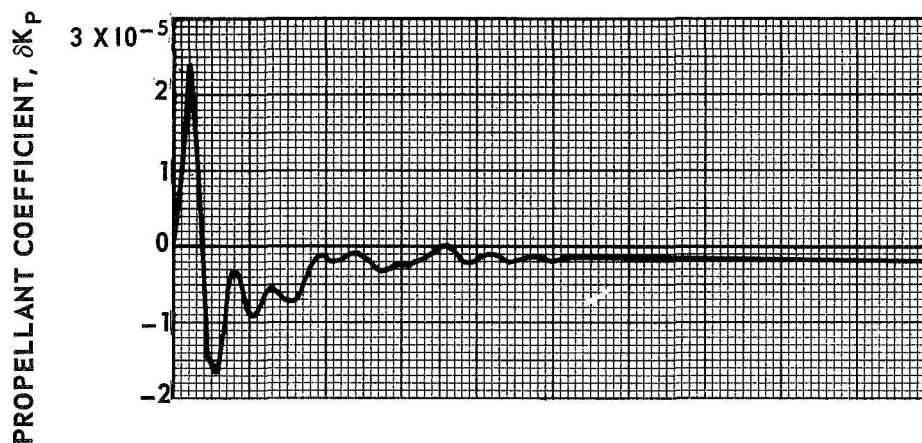
(CONTINUED)

CONSTANT FUEL RADIUS

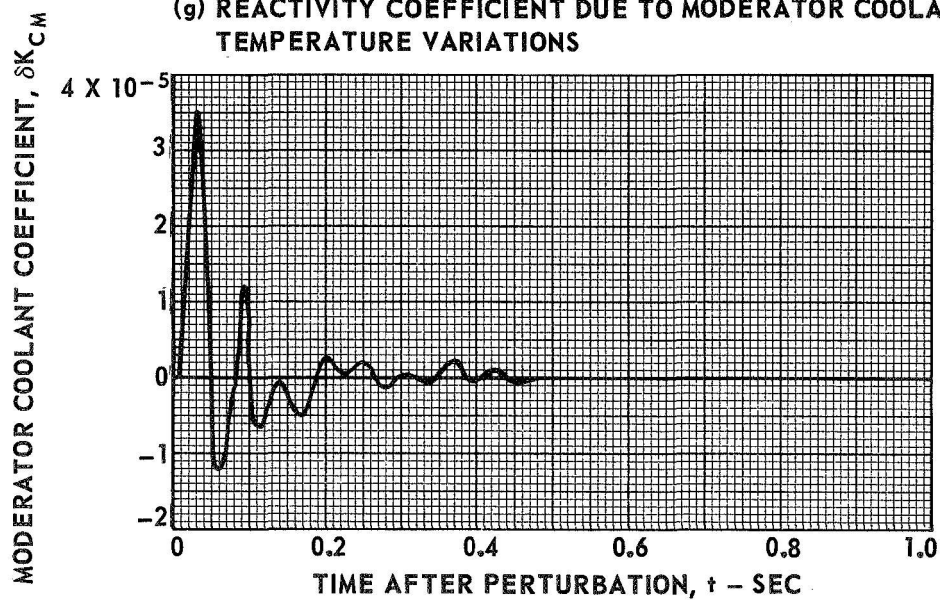
$$\Delta P_F = 0.25 \text{ ATM}$$



(f) REACTIVITY COEFFICIENT DUE TO PROPELLANT DENSITY  
AND TEMPERATURE VARIATIONS



(g) REACTIVITY COEFFICIENT DUE TO MODERATOR COOLANT  
TEMPERATURE VARIATIONS



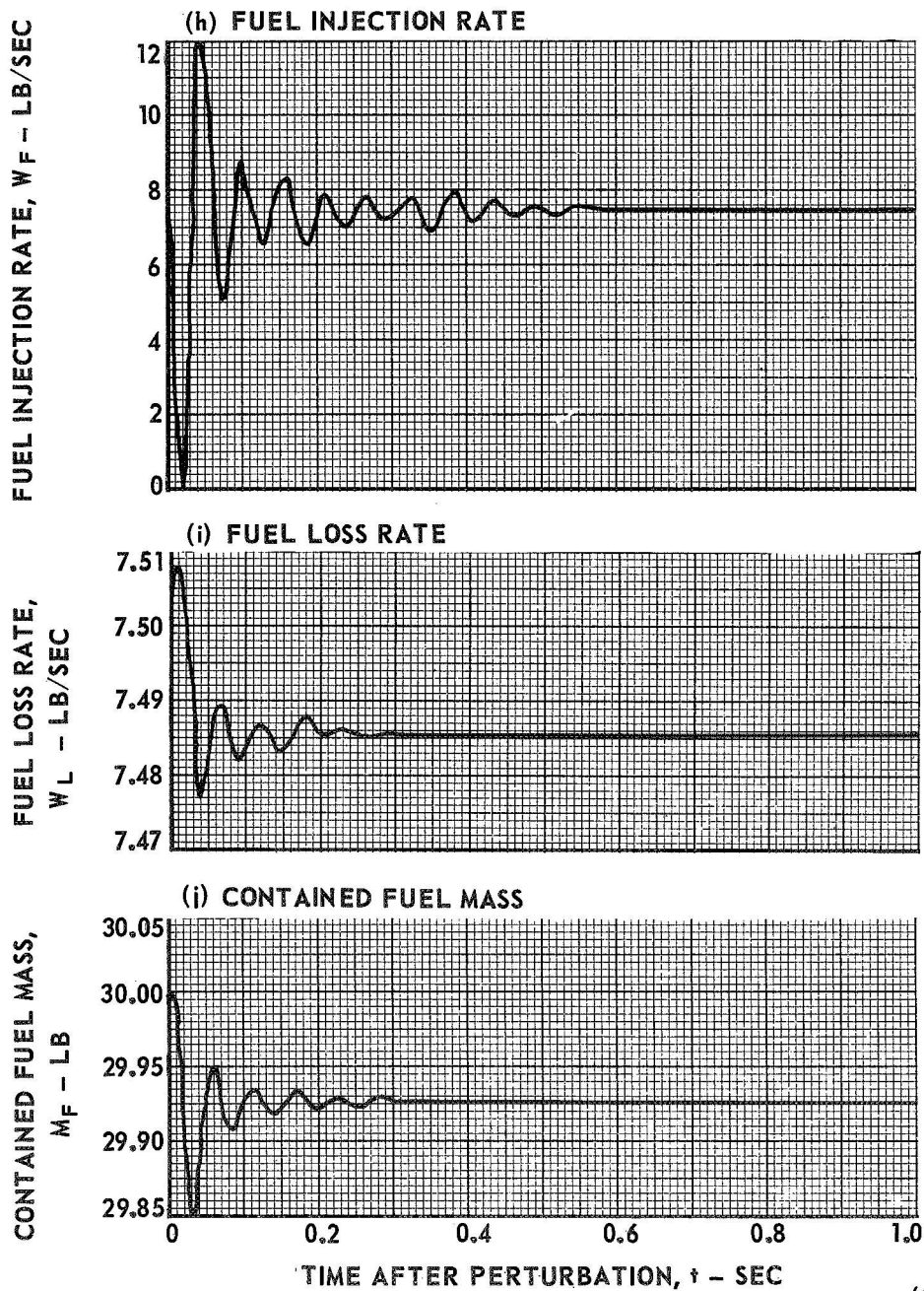
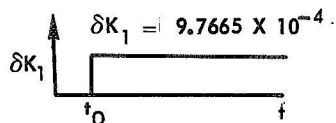
(CONTINUED)

# RESPONSE OF CONTROLLED ENGINE TO POSITIVE STEP CHANGE IN IMPOSED REACTIVITY

(CONTINUED)

CONSTANT FUEL RADIUS

$$\Delta P_F = 0.25 \text{ ATM}$$



(CONTINUED)

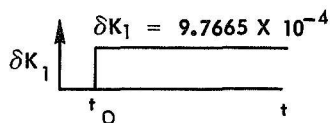


# RESPONSE OF CONTROLLED ENGINE TO POSITIVE STEP CHANGE IN IMPOSED REACTIVITY

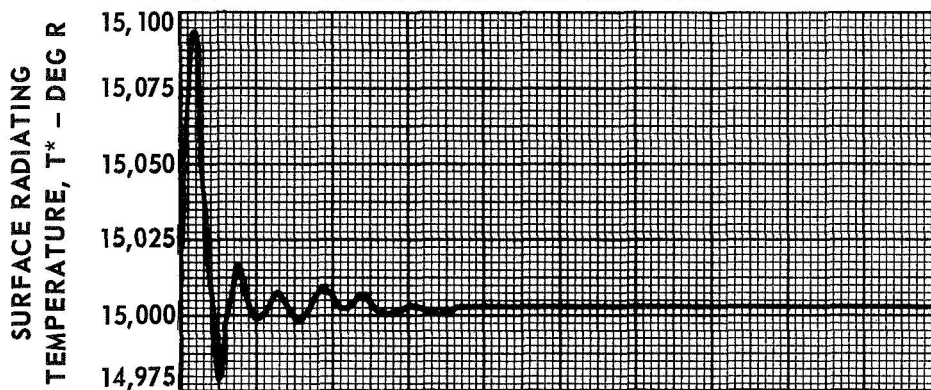
(CONCLUDED)

CONSTANT FUEL RADIUS

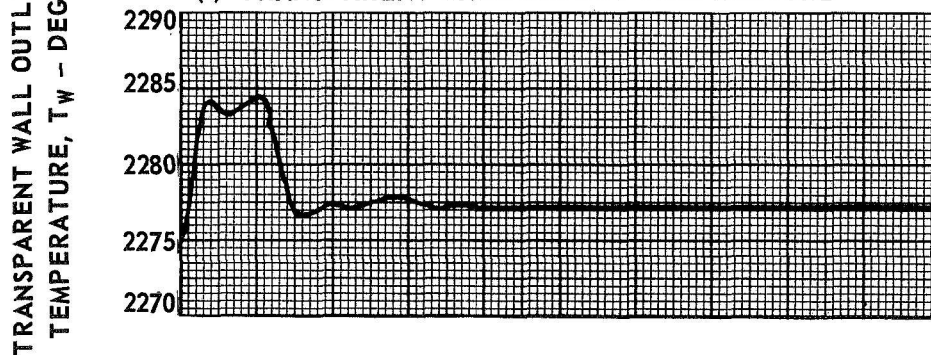
$$\Delta P_F = 0.25 \text{ ATM}$$



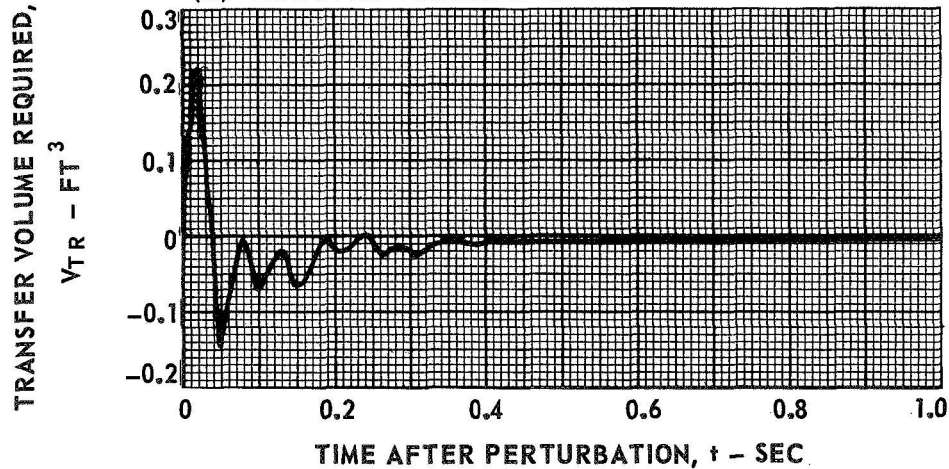
(k) SURFACE RADIATING TEMPERATURE



(l) TRANSPARENT-WALL OUTLET TEMPERATURE



(m) TRANSFER VOLUME REQUIRED



# RESPONSE OF CONTROLLED ENGINE TO POSITIVE INITIAL STEP CHANGE IN FUEL INJECTION CONTROL VALVE AREA

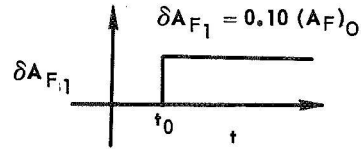
CONSTANT FUEL RADIUS

$$\Delta P_{Fi} = 0.25 \text{ ATM}$$

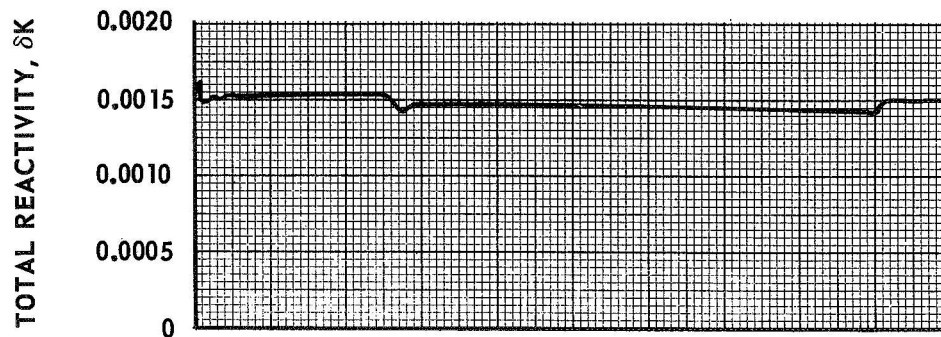
$$A_F = (A_F)_0 + \delta A_{F1} + \delta A_{F2}$$

SEE TEXT FOR DESCRIPTION OF  $\delta A_{F1}$  AND  $\delta A_{F2}$

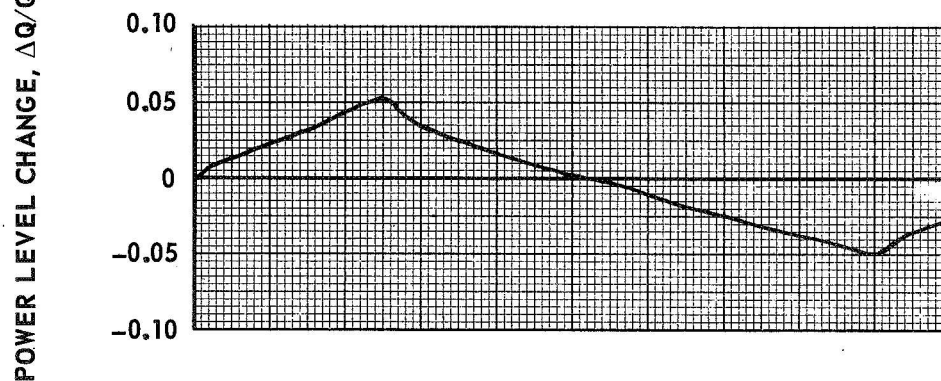
$$W_F = K_F A_F \left( \frac{P_F - P_C}{0.25} \right)^{1/2}$$



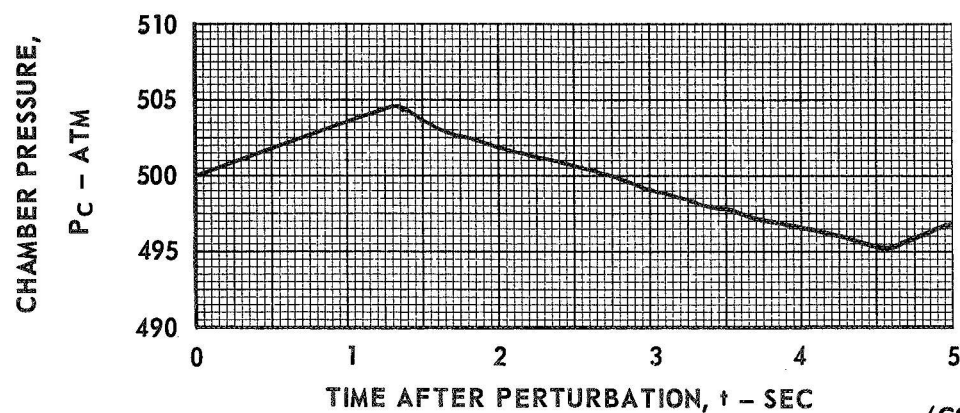
(a) TOTAL REACTIVITY



(b) RELATIVE POWER LEVEL CHANGE



(c) CHAMBER PRESSURE



(CONTINUED)



# RESPONSE OF CONTROLLED ENGINE TO POSITIVE INITIAL STEP CHANGE IN FUEL INJECTION CONTROL VALVE AREA

(CONTINUED)

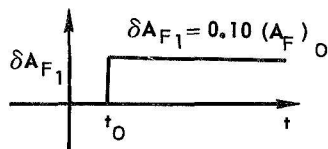
CONSTANT FUEL RADIUS

$$\Delta P_F = 0.25 \text{ ATM}$$

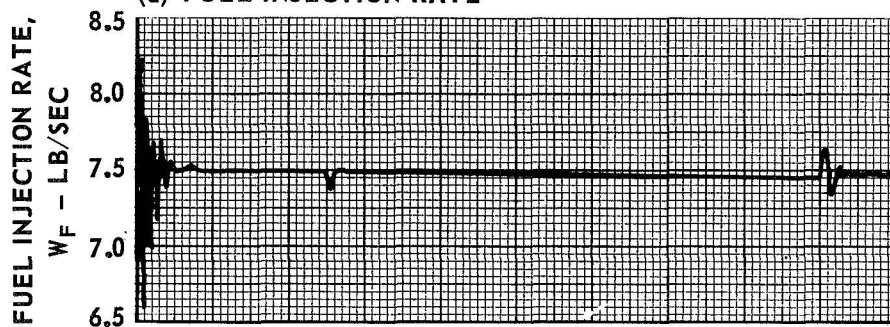
$$A_F = (A_F)_0 + \delta A_{F1} + \delta A_{F2}$$

SEE TEXT FOR DESCRIPTION OF  $\delta A_{F1}$  AND  $\delta A_{F2}$ 

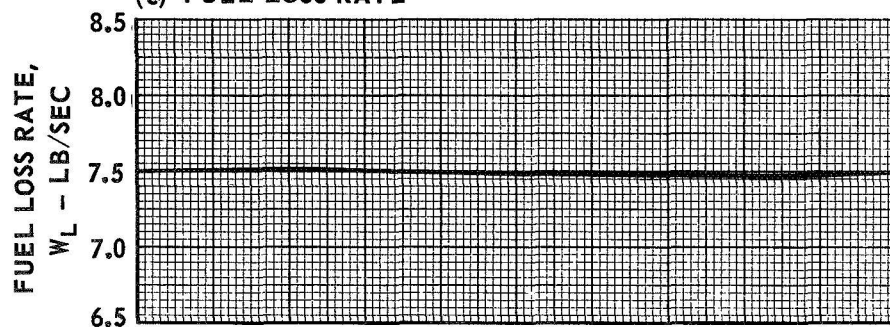
$$W_F = K_F A_F \left( \frac{P_F - P_C}{0.25} \right)^{1/2}$$



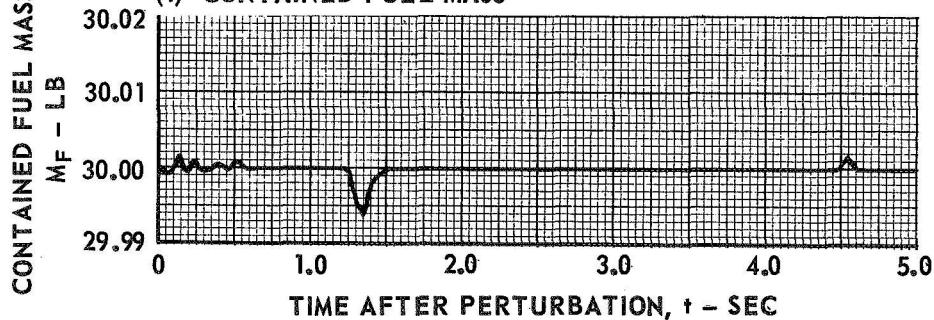
(d) FUEL INJECTION RATE



(e) FUEL LOSS RATE



(f) CONTAINED FUEL MASS



(CONTINUED)

# RESPONSE OF CONTROLLED ENGINE TO POSITIVE INITIAL STEP CHANGE IN FUEL INJECTION CONTROL VALVE AREA

(CONCLUDED)

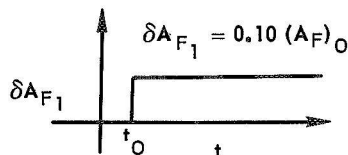
CONSTANT FUEL RADIUS

$$\Delta P_F = 0.25 \text{ ATM}$$

$$A_F = (A_F)_O + \delta A_{F1} + \delta A_{F2}$$

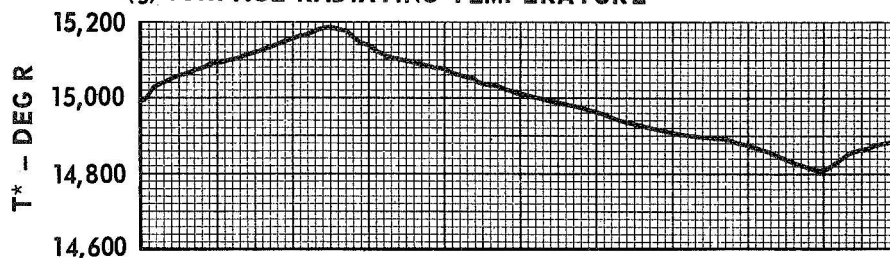
SEE TEXT FOR DESCRIPTION OF  $\delta A_{F1}$  AND  $\delta A_{F2}$

$$W_F = K_F A_F \left( \frac{P_F - P_C}{0.25} \right)^{1/2}$$



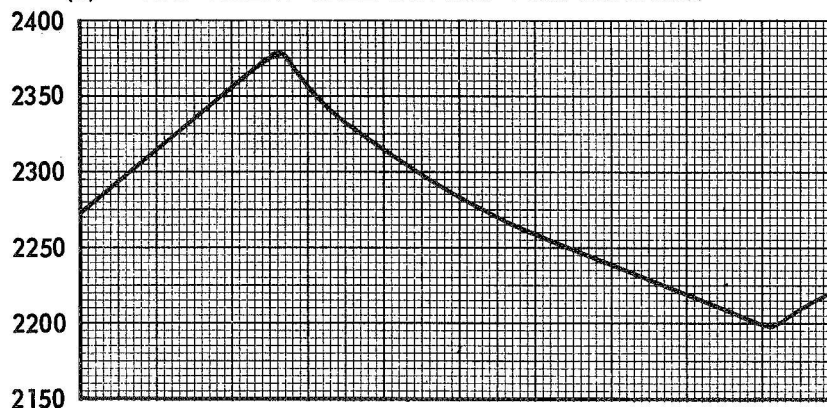
SURFACE RADIATING  
TEMPERATURE,  
 $T^* - \text{DEG R}$

(g) SURFACE RADIATING TEMPERATURE



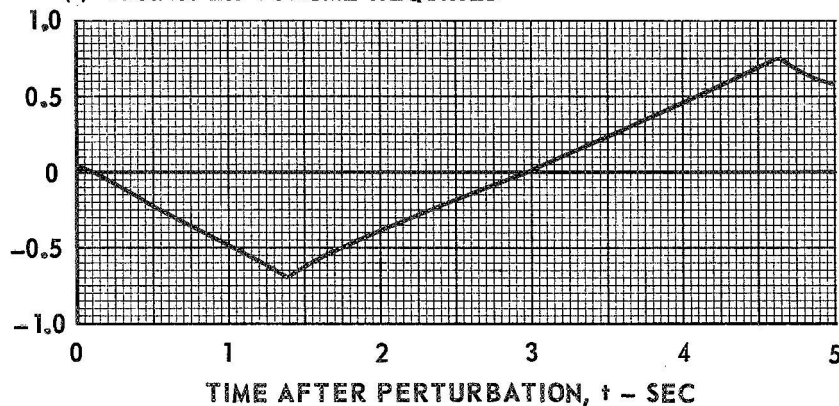
TRANSPARENT WALL OUTLET  
TEMPERATURE,  $T_w - \text{DEG R}$

(h) TRANSPARENT-WALL OUTLET TEMPERATURE



TRANSFER VOLUME  
REQUIRED,  $V_{TR} - \text{FT}^3$

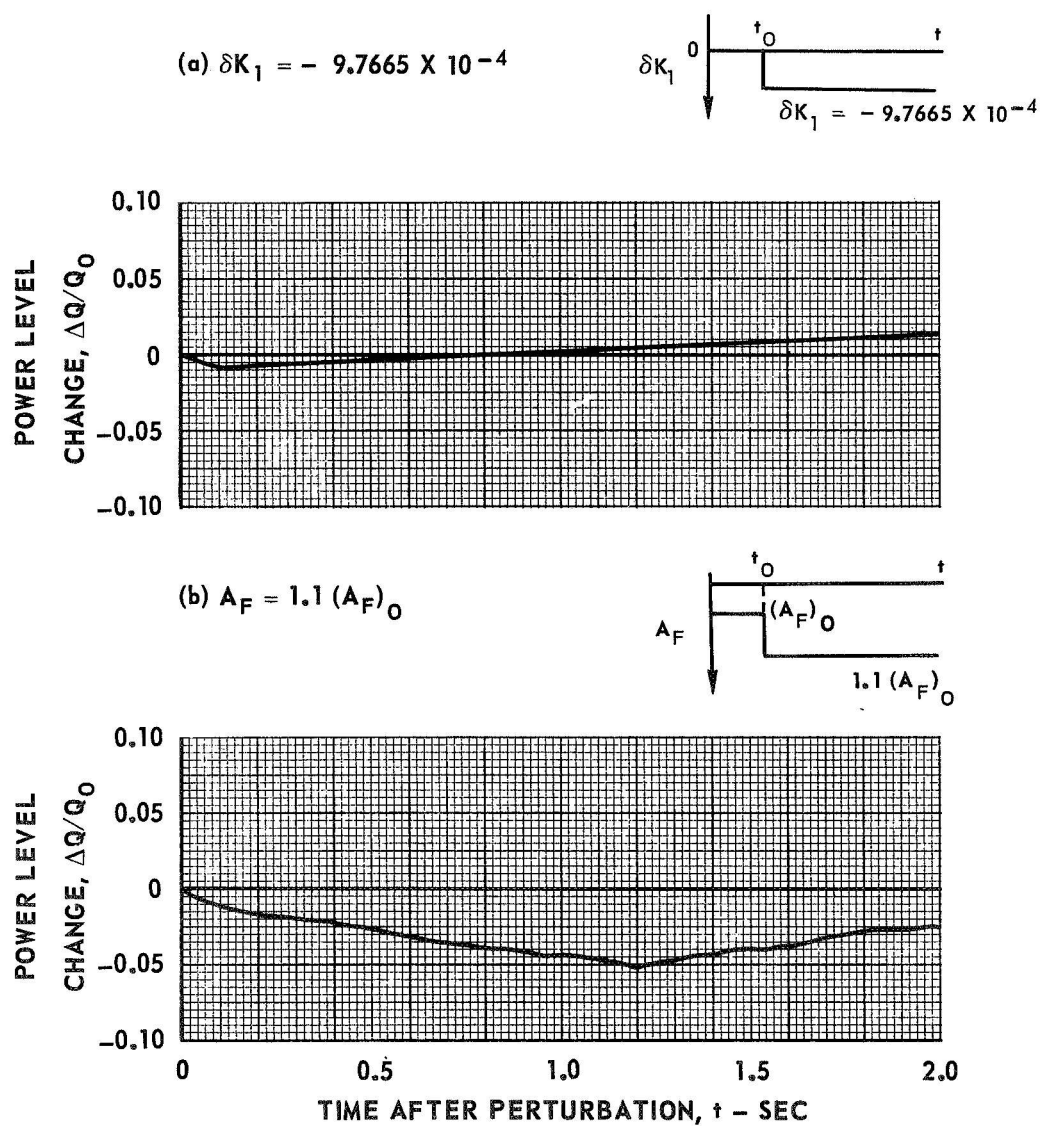
(i) TRANSFER VOLUME REQUIRED



# POWER LEVEL RESPONSES OF CONTROLLED ENGINE TO NEGATIVE STEP CHANGES IN IMPOSED REACTIVITY AND FUEL INJECTION CONTROL VALVE AREA

CONSTANT FUEL RADIUS

$$\Delta P_F = 0.25 \text{ ATM}$$



# POWER LEVEL RESPONSE OF CONTROLLED ENGINE TO TERMINATING RAMP CHANGES IN TURBOPUMP WHEEL SPEED

CONSTANT FUEL RADIUS

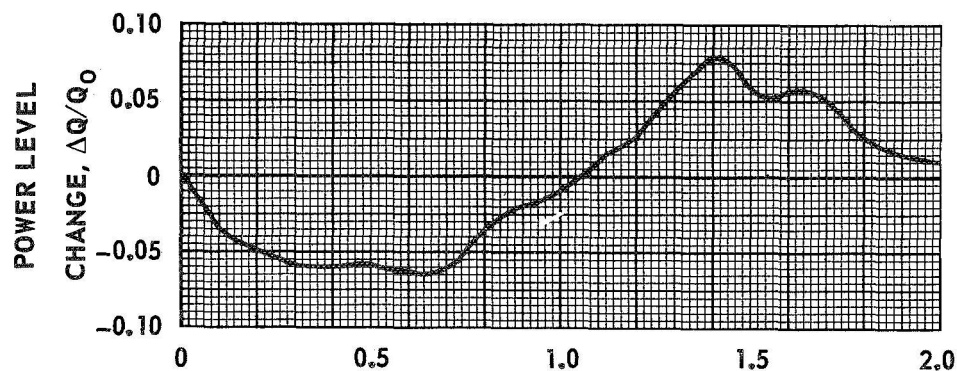
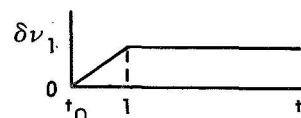
$$\Delta P_F = 0.25 \text{ ATM}$$

$$\nu_0 = 22,000 \text{ RPM}$$

$\delta \nu_1 = \text{IMPOSED WHEEL SPEED CHANGE}$

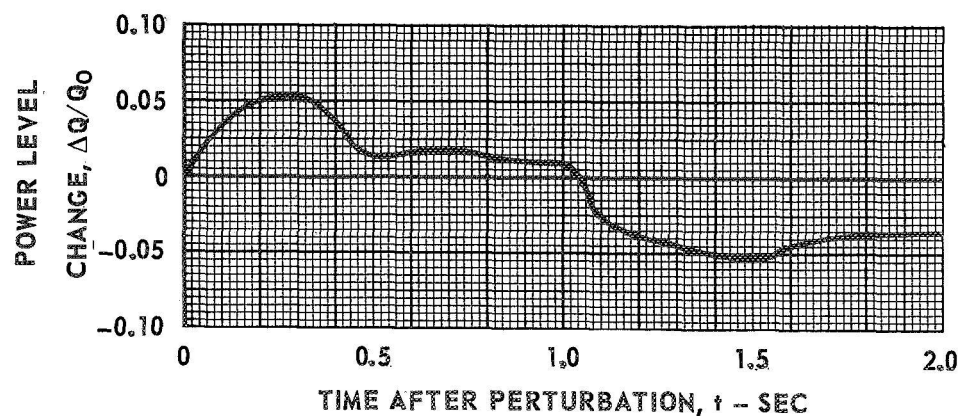
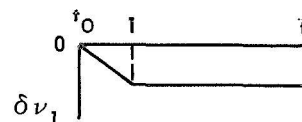
(a)  $\delta \nu_1 = 0.02 \nu / \text{SEC}$  FOR  $t = 0.0$  TO  $1.0 \text{ SEC}$ ;

$\delta \nu_1 = 0.02 \nu_0$  FOR  $t > 1.0$



(b)  $\delta \nu_1 = -0.02 \nu_0 / \text{SEC}$  FOR  $t = 0.0$  TO  $1.0 \text{ SEC}$ ;

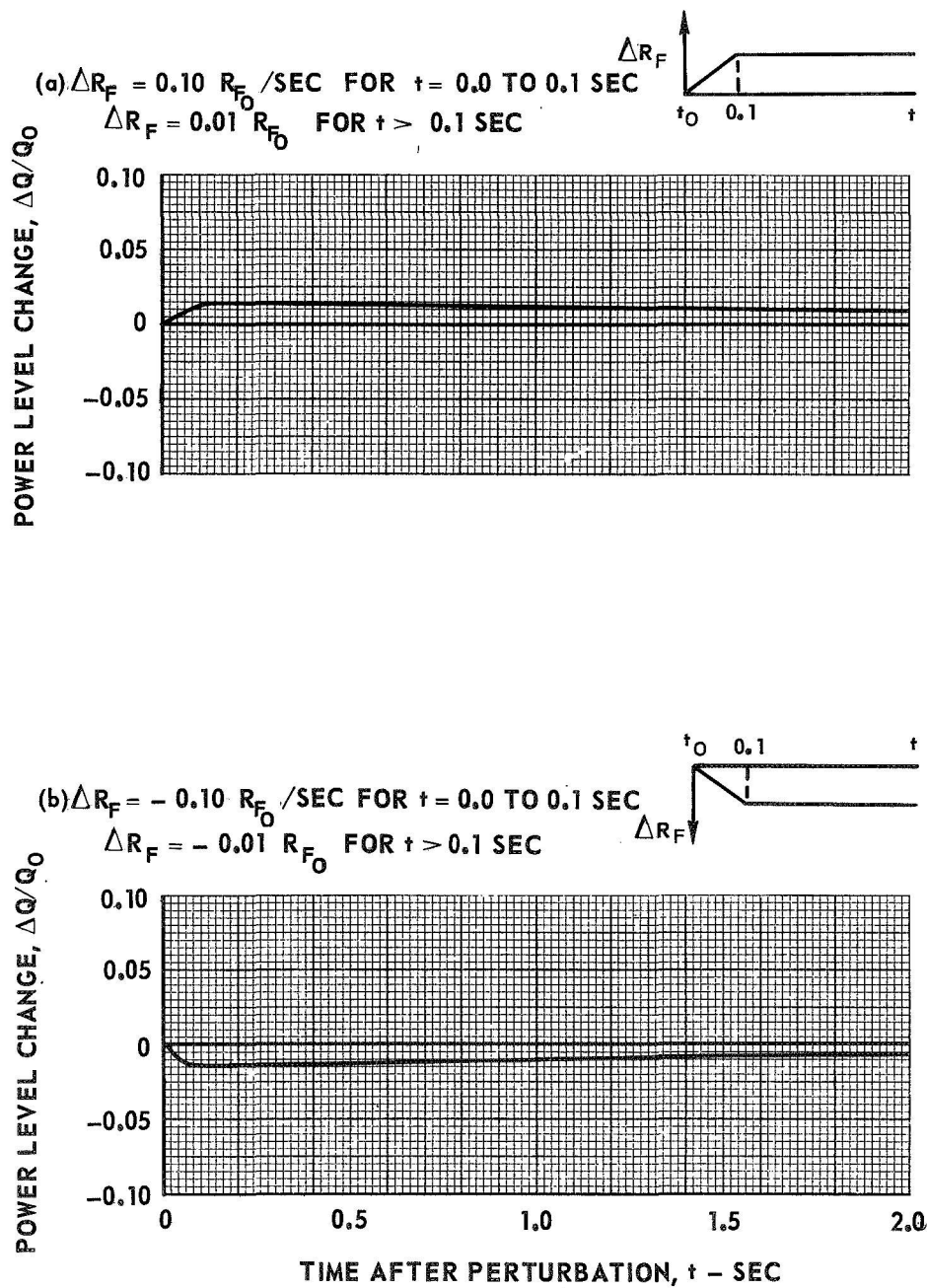
$\delta \nu_1 = -0.02 \nu_0$  FOR  $t > 1.0$



# POWER LEVEL RESPONSE OF CONTROLLED ENGINE TO TERMINATING RAMP CHANGES IN FUEL CLOUD RADIUS

$$\Delta P_F = 0.25 \text{ ATM}$$

$$R_F = R_{F0} + \Delta R_F$$



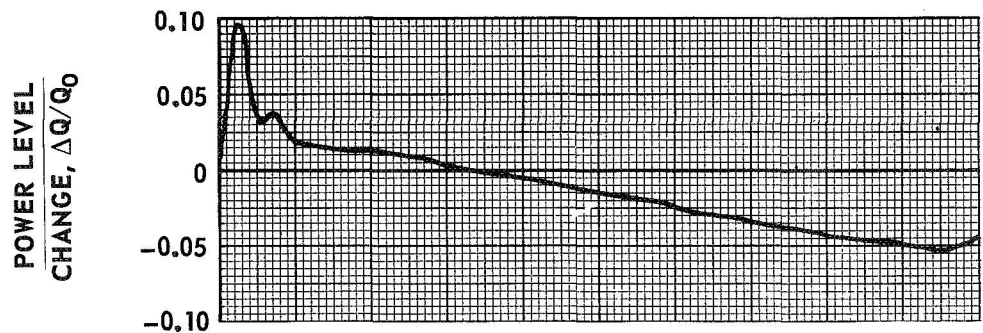
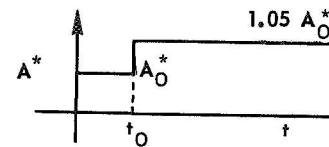
# POWER LEVEL RESPONSE OF CONTROLLED ENGINE TO STEP CHANGES IN EXHAUST NOZZLE AREA

CONSTANT FUEL RADIUS

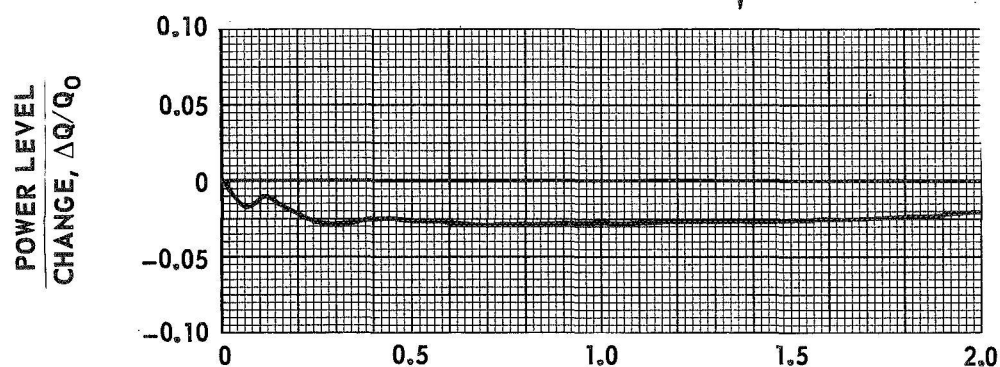
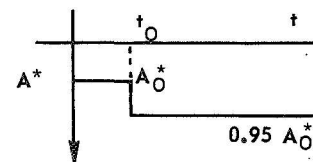
$$\Delta P_F = 0.25 \text{ ATM}$$

$$A_O^* = 4.004 \times 10^{-2} \text{ FT}^2$$

(a)  $A^* = 1.05 A_O^*$



(b)  $A^* = 0.95 A_O^*$



TIME AFTER PERTURBATION,  $t$  - SEC

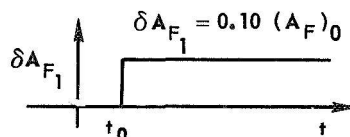


# RESPONSE OF CONTROLLED ENGINE TO POSITIVE INITIAL STEP CHANGE IN FUEL CONTROL VALVE AREA FOR VARIOUS VALUES OF CONTROL GAIN

CONSTANT FUEL RADIUS

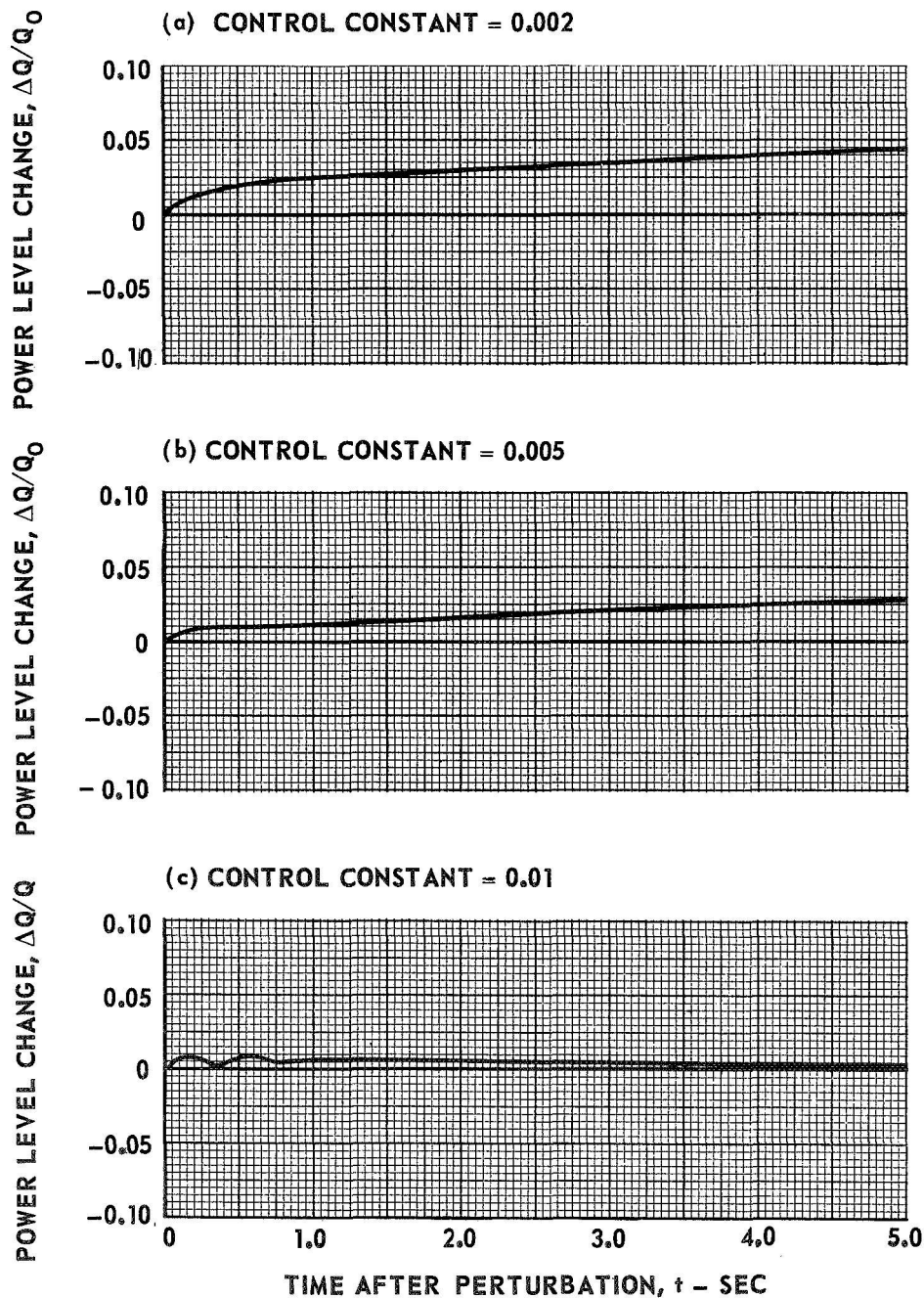
$$\Delta P_F = 0.25 \text{ ATM}$$

$$W_F = K_F A_F \left( \frac{P_F - P_C}{0.25} \right)^{1/2}$$



CONTROL RESPONDS TO VALUES OF  $(1/N) (dN/dt)$  GREATER THAN 1.005

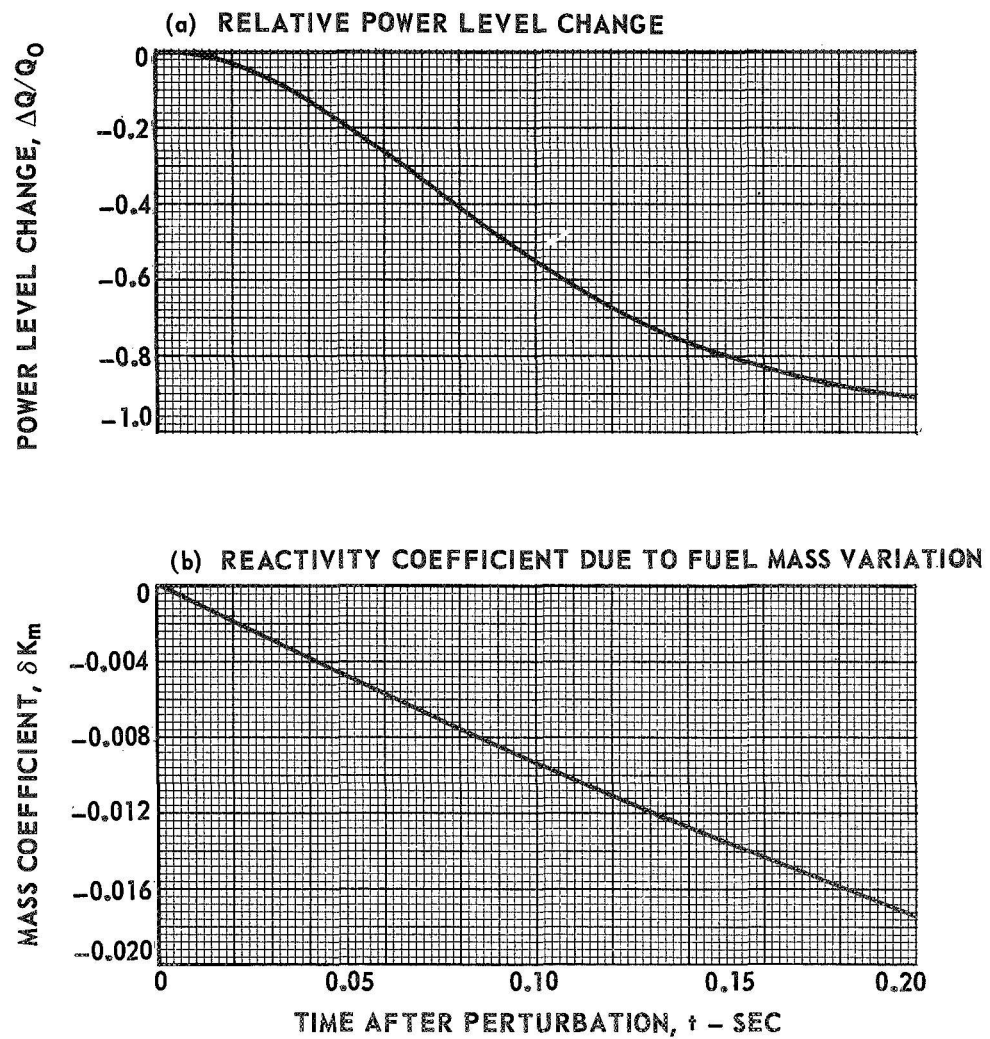
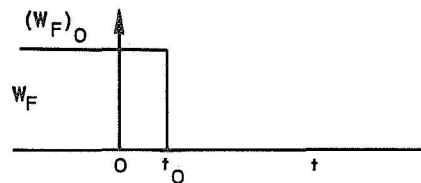
GAIN: VALVE AREA CHANGE =  $(A_F)_0 \left[ (1/N) (dN/dt) \right] \times \text{CONTROL CONSTANT}$



# RESPONSE OF ENGINE TO ACTIVATED SHUTDOWN

FUEL INJECTION RATE,  $w_F = 0$  AT  $t = t_0$

$Q_0 = 4600$  MEGW





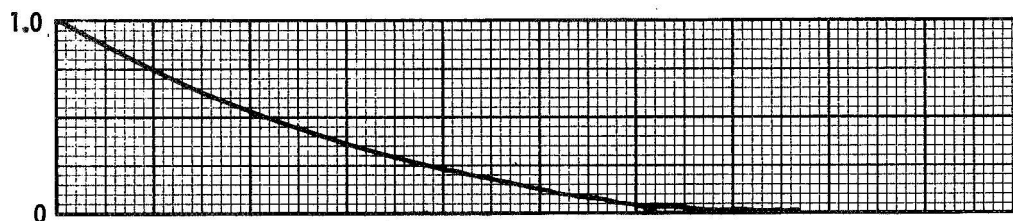
# RESULTS OF STATISTICAL ANALYSIS OF TEMPERATURE VARIATIONS WHICH RESULT FROM DIMENSIONAL TOLERANCES AND UNCERTAINTIES IN HEAT DEPOSITION AND FLOW RATES IN SELECTED ENGINE COMPONENTS

SEE TABLE VIII AND IX FOR DESCRIPTION OF VARIABLE FACTORS CONSIDERED IN EACH COMPONENT

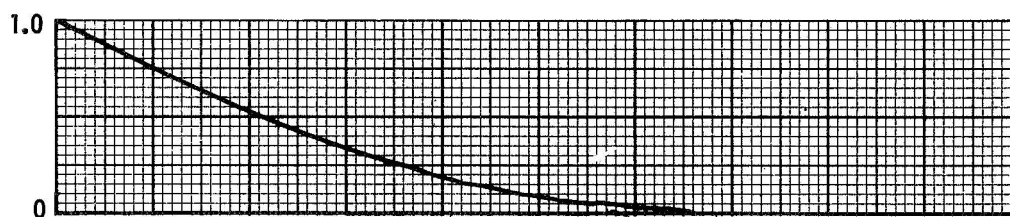
$\Delta T_V$  = TEMPERATURE VARIATION FROM NOMINAL VALUE

$(\Delta T_V)_{MAX}$  = MAXIMUM TEMPERATURE VARIATION FROM NOMINAL VALUE

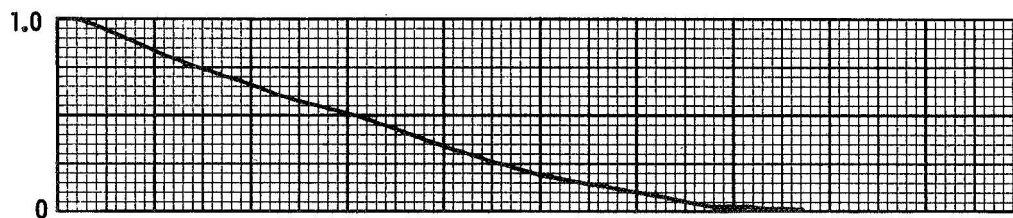
(a) CAVITY LINER TUBES,  $(\Delta T_V)_{MAX} = 149.7 R$



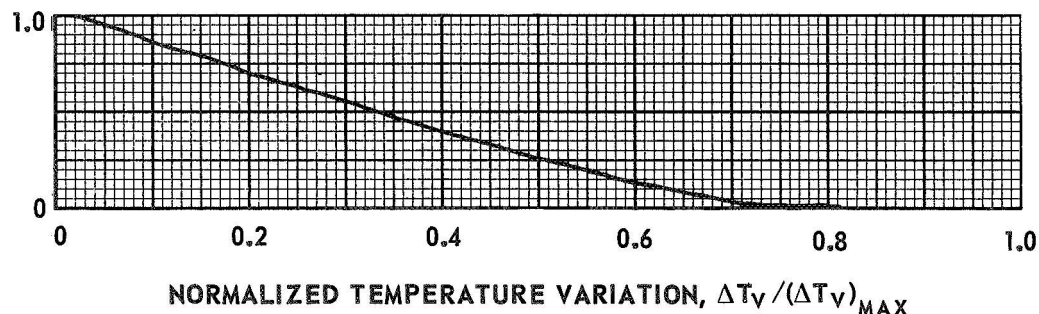
(b) TRANSPARENT WALL TUBES,  $(\Delta T_V)_{MAX} = 314.7 R$



(c) UPPER GRAPHITE MODERATOR,  $(\Delta T_V)_{MAX} = 160.2 R$



(d) UPPER BeO MODERATOR,  $(\Delta T_V)_{MAX} = 144.8 R$



CONTINUED

# RESULTS OF STATISTICAL ANALYSIS OF TEMPERATURE VARIATIONS WHICH RESULT FROM DIMENSIONAL TOLERANCES AND UNCERTAINTIES IN HEAT DEPOSITION AND FLOW RATES IN SELECTED ENGINE COMPONENTS

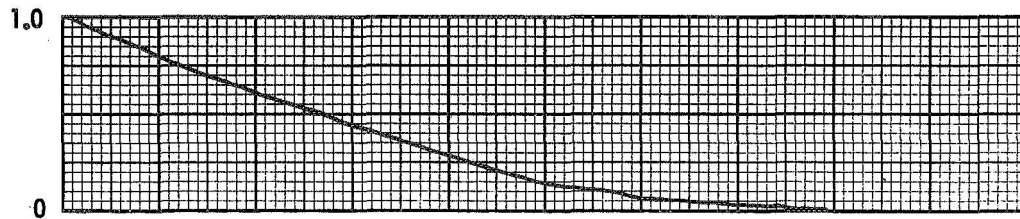
(CONCLUDED)

SEE TABLES VIII AND IX FOR DESCRIPTION OF VARIABLE FACTORS CONSIDERED IN EACH COMPONENT

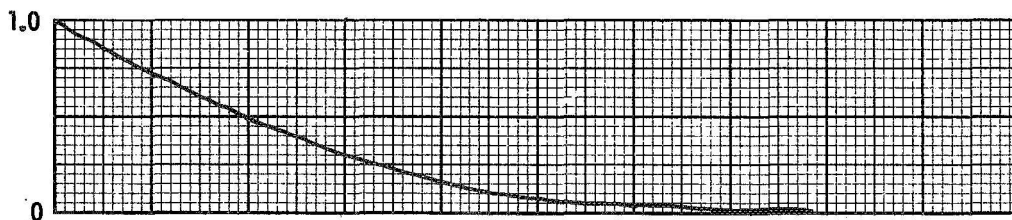
$\Delta T_V$  = TEMPERATURE VARIATION FROM NOMINAL VALUE

$(\Delta T_V)_{MAX}$  = MAXIMUM TEMPERATURE VARIATION FROM NOMINAL VALUE

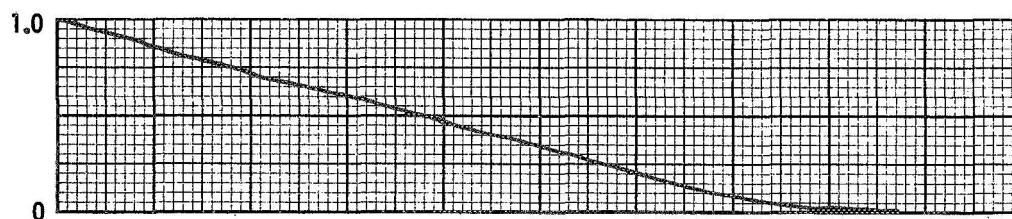
(e) AXIAL BeO MODERATOR,  $(\Delta T_V)_{MAX} = 375.7 R$



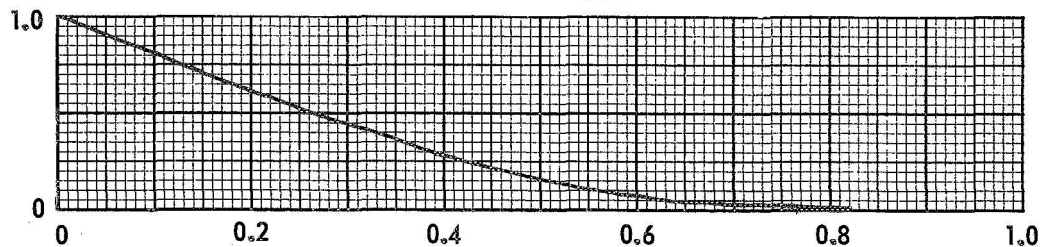
(f) LOWER BeO MODERATOR,  $(\Delta T_V)_{MAX} = 242.5 R$



(g) LOWER GRAPHITE MODERATOR,  $(\Delta T_V)_{MAX} = 183.8 R$



(h) AXIAL GRAPHITE MODERATOR,  $(\Delta T_V)_{MAX} = 271.2 R$

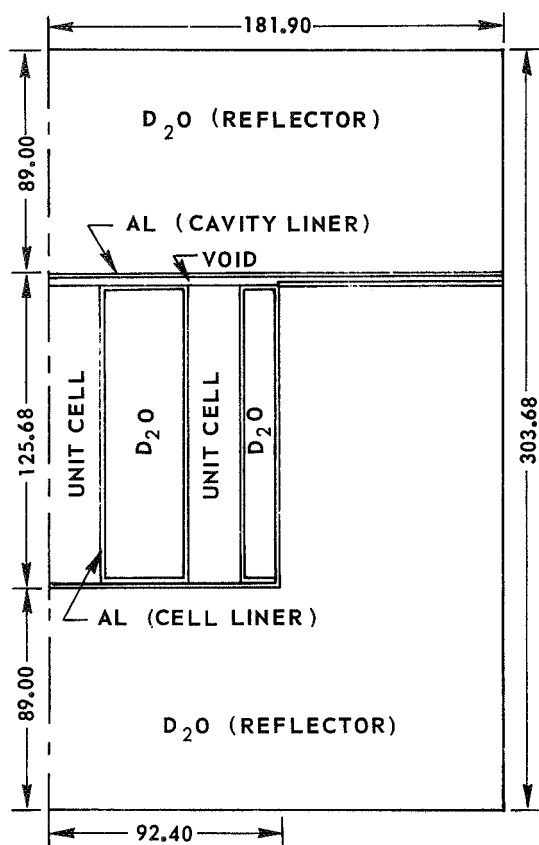


NORMALIZED TEMPERATURE VARIATION,  $\Delta T_V/(\Delta T_V)_{MAX}$

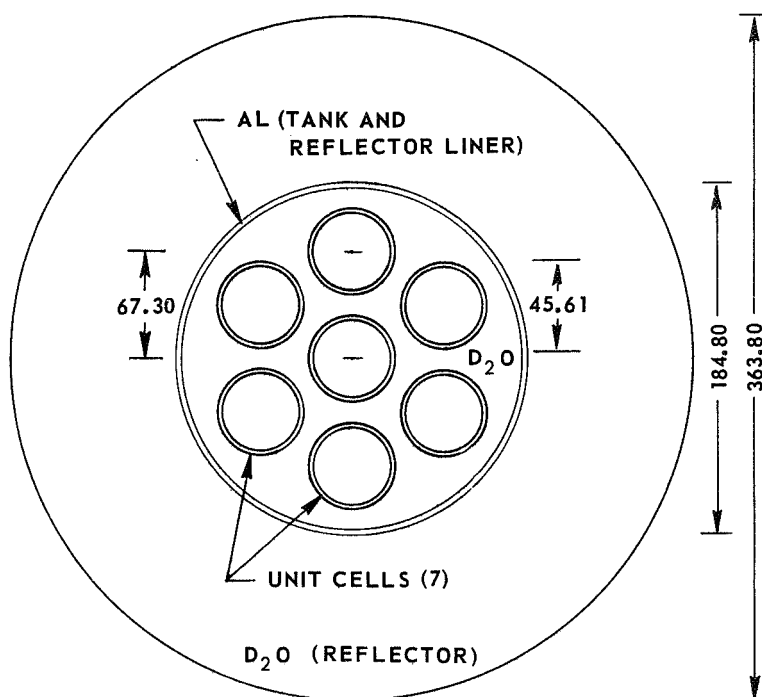
## SEVEN-MODULE CAVITY REACTOR CONFIGURATION USED IN TESTS OF REF.15

ALL DIMENSIONS IN CM

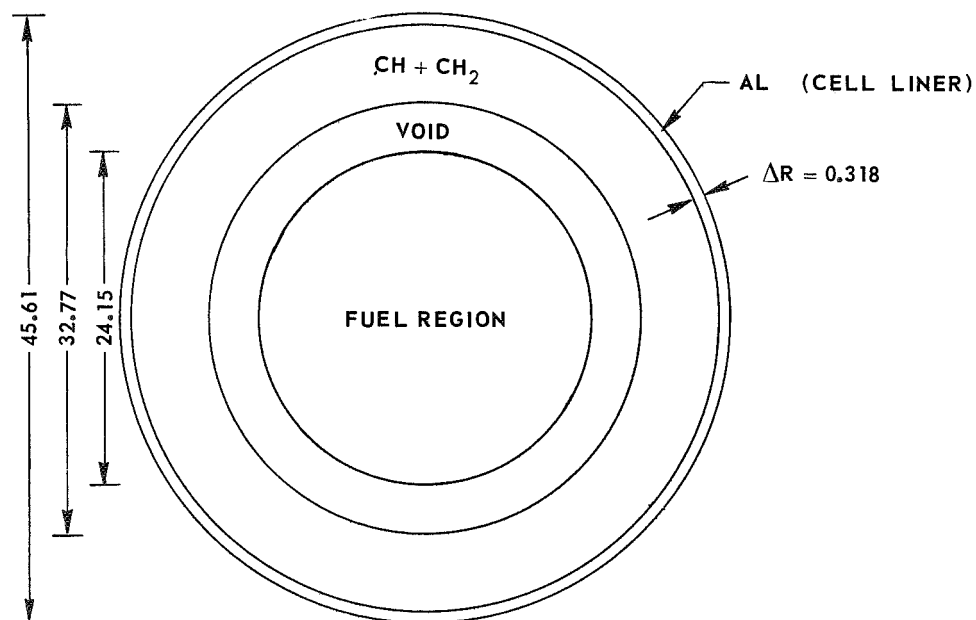
(a) AXIAL CROSS-SECTION OF REACTOR



(b) RADIAL CROSS-SECTION OF REACTOR



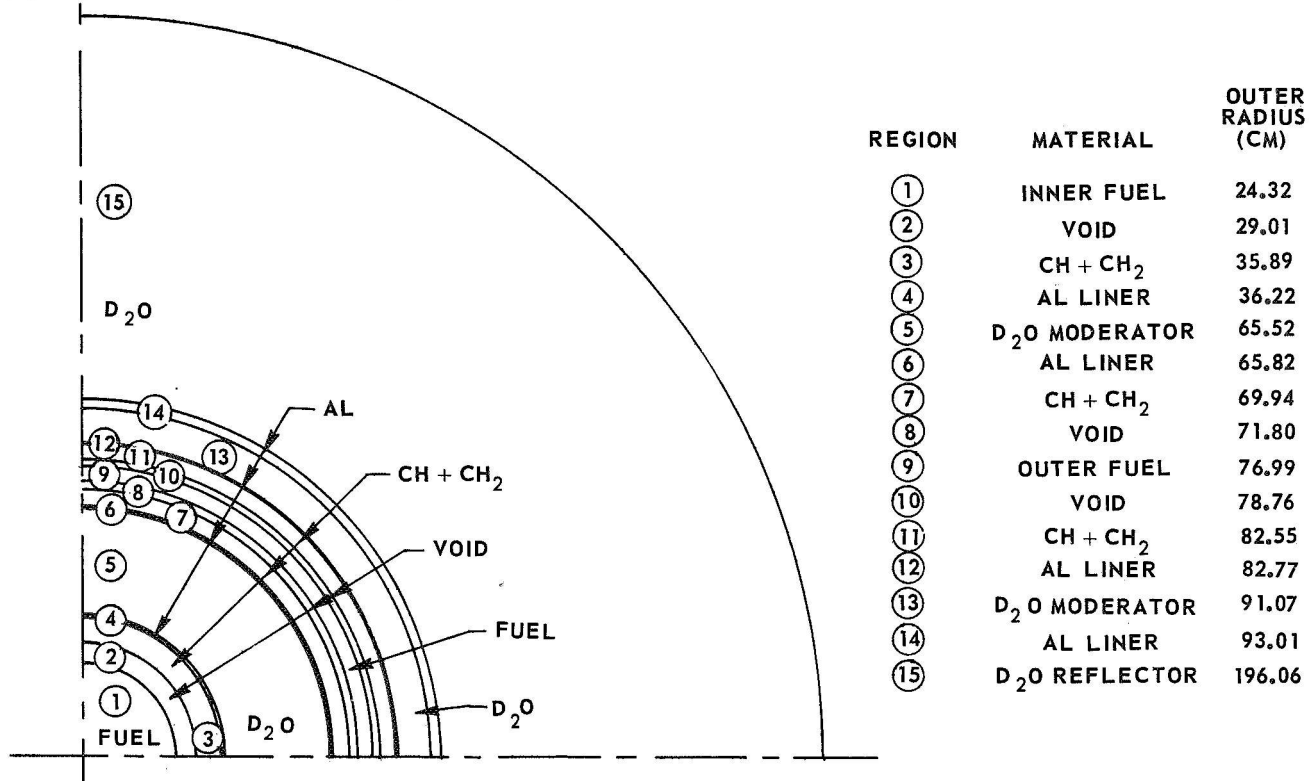
(c) RADIAL CROSS-SECTION OF UNIT CELL



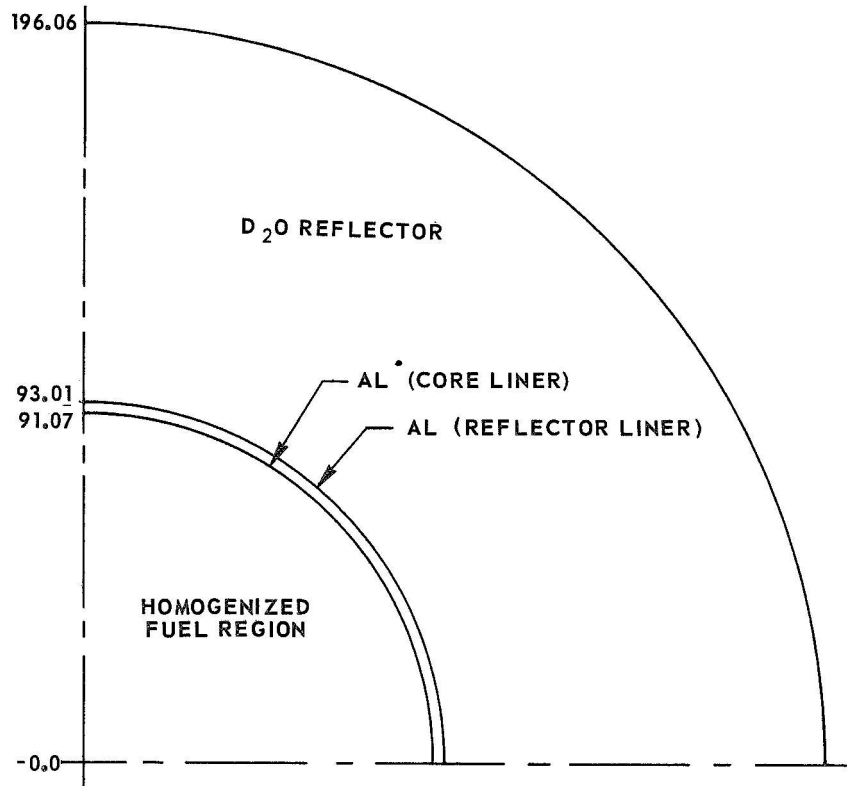
## SPHERICAL MODELS OF SEVEN-MODULE CAVITY REACTOR CONFIGURATION

ALL DIMENSIONS IN CM

(a) EQUAL-VOLUME MODEL, DETAILED CORE

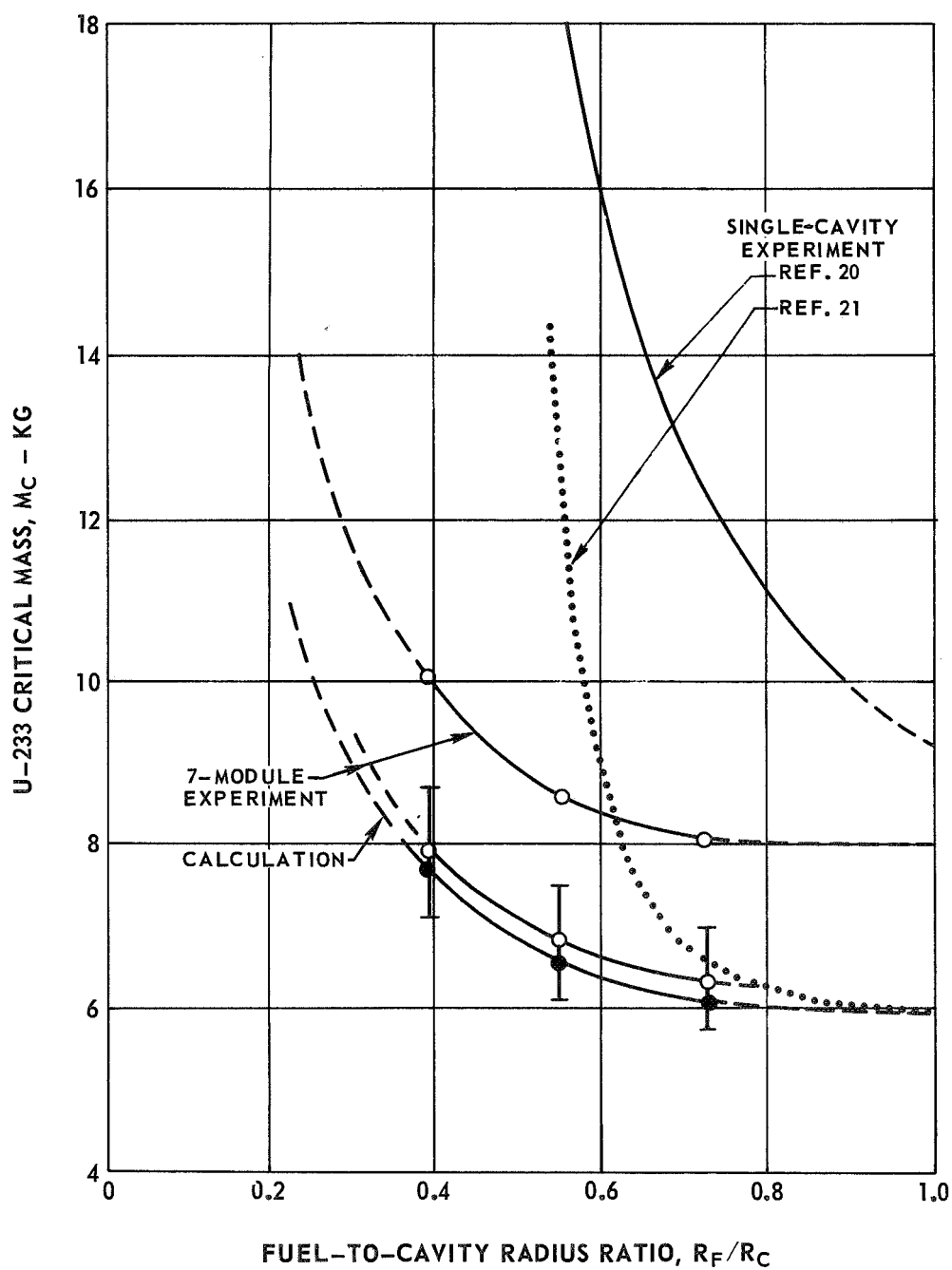


(b) EQUAL-VOLUME MODEL, HOMOGENIZED CORE



## EFFECT OF CHANGING FUEL RADIUS ON CRITICAL MASS

- 7-MODULE, HOMOGENIZED-CORE CALCULATION
- 7-MODULE EXPERIMENT, REF. 15
- SINGLE-CAVITY EXPERIMENT, REF. 20
- ..... SINGLE-CAVITY EXPERIMENT, REF. 21
- |  
|  
| 7-MODULE EXPERIMENT CORRECTED FOR NOZZLE PLUG,  
TABLE GAP AND FOIL-TO-GAS BIAS FACTOR;  
SEE TEXT AND REF. 15



## EFFECT OF RADIATOR COOLANT OUTLET TEMPERATURE ON SPACE RADIATOR WEIGHT

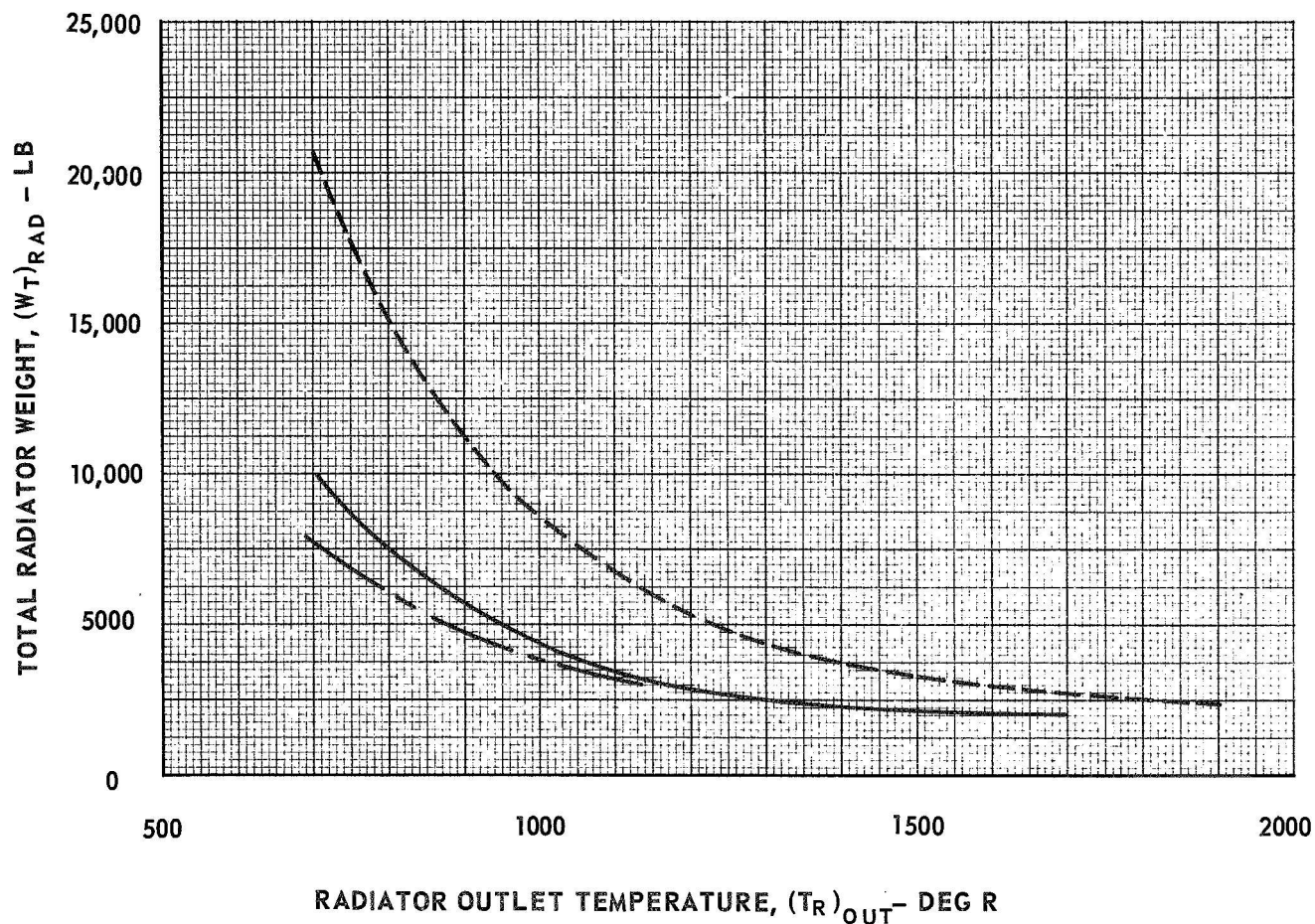
SEE APPENDIX B FOR DESCRIPTION OF RADIATOR CONFIGURATION

HYDROGEN COOLANT

TOTAL HEAT REJECTED BY RADIATOR = 115 MEGW (2.5 PERCENT OF TOTAL ENGINE POWER)

TUBE ID = 0.24 IN, NUMBER OF TUBES = 6000

SYMBOL	RADIATOR MATERIAL	RADIATOR INLET TEMPERATURE, $(T_R)_{IN}$ DEG R	TUBE WALL AND FIN THICKNESS, IN	MATERIAL DENSITY, LB/FT <sup>3</sup>
————	STEEL	2500	0.03125	490
-----	ALUMINUM	1500	0.03125	170
- - - -	TUNGSTEN	3500	0.01567	1180



# **EFFECT OF RADIATOR COOLANT OUTLET TEMPERATURE ON PRESSURE LOSS IN SPACE RADIATOR**




SEE APPENDIX B FOR DESCRIPTION OF RADIATOR CONFIGURATION

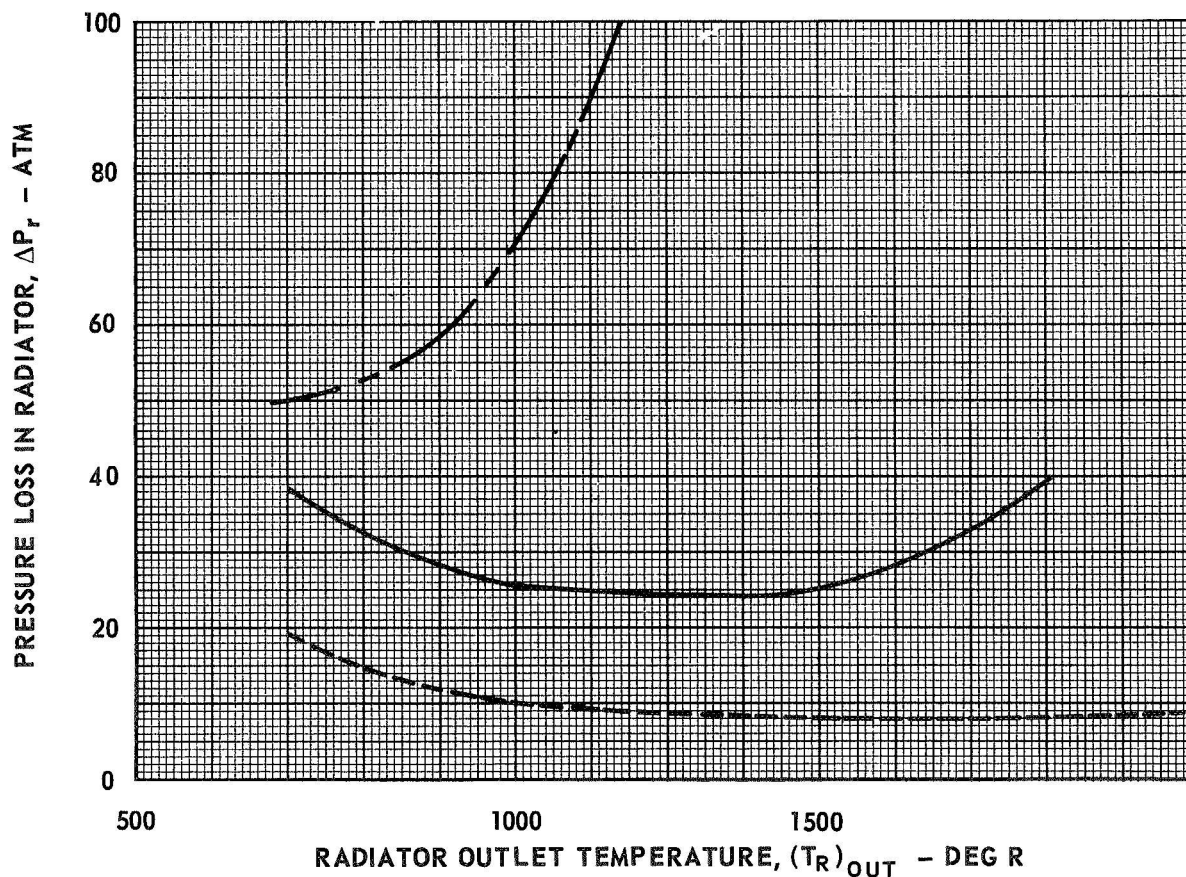
HYDROGEN COOLANT

TOTAL HEAT REJECTED BY RADIATOR = 115 MEGW (2.5 PERCENT OF TOTAL ENGINE POWER)

TUBE ID = 0.24 IN., NUMBER OF TUBES = 6000

MAXIMUM OPERATING PRESSURE = 100 ATM

SYMBOL	RADIATOR MATERIAL	RADIATOR INLET TEMPERATURE, $(T_R)_{IN}$ DEG R	TUBE WALL AND FIN THICKNESS, IN	MATERIAL DENSITY, LB/FT <sup>3</sup>
	STEEL	2500	0.03125	490
	ALUMINUM	1500	0.03125	170
	TUNGSTEN	3500	0.01567	1180





# SKETCH OF ALTERNATE GEOMETRIC CONFIGURATION FOR NUCLEAR LIGHT BULB ENGINE

SEE APPENDIX C FOR DESCRIPTION OF CONFIGURATION

CELLS IN ARRAYS OF 7, 19, OR 37 UNITS

